12-2014

Stability Analysis of the Rotary Drill-String

Liangming Pan
University of Tennessee - Knoxville, lpan3@vols.utk.edu

To the Graduate Council:

I am submitting herewith a dissertation written by Liangming Pan entitled "Stability Analysis of the Rotary Drill-String." I have examined the final electronic copy of this dissertation for form and content and recommend that it be accepted in partial fulfillment of the requirements for the degree of Doctor of Philosophy, with a major in Mechanical Engineering.

J. A. M. Boulet, Major Professor

We have read this dissertation and recommend its acceptance:

Hans DeSmidt, Subhadeep Chakraborty, Yulong Xing

Accepted for the Council:

Carolyn R. Hodges

Vice Provost and Dean of the Graduate School

(Original signatures are on file with official student records.)

Stability Analysis

of the Rotary Drill-String

A Dissertation Presented for the

Doctor of Philosophy

Degree

The University of Tennessee, Knoxville

Liangming Pan

December 2014

DEDICATION

This dissertation is dedicated to my wife. A special feeling of gratitude to my brilliant and outrageously loving and supportive wife, Ning Zhong, who took care of me throughout the entire doctorate program. I will always appreciate all she has done for me.

I dedicate this work and give special thanks to my parents, Wenhu Pan and Miaoying Gong, and my parents-in-law, Meizuo Zhong and Laizhong Ning. They are there for me all these years and always encouraging me and stay faithful to me.

ACKNOWLEDGEMENTS

I would like to thank my major advisor Dr. J. A. M. Boulet for his moral support, encouragement and guidance throughout the whole study. Also, each committee member has been wonderful in their support and patience throughout my research. I would like to thank the committee members: Dr. Hans A. Desmidt, Dr. Subhadeep Chakraborty and Dr. Yulong Xing for giving me so many insightful suggestions.

Finally, heartfelt thanks go to all of my family for their love and encouragement.

ABSTRACT

Oil and natural gas are major energy sources for modern society. A rotary drilling system is the best known technology to extract them from underground. The vibration and stability of drilling systems have been studied for decades to improve drilling efficiency and protect expensive down-hole components. It is well known that severe drill-string vibrations are caused by many different loads: axial loads such as the hook load and the self-weight of the drill-string, end torques applied by the surface motor and restrained at the bit, the inertial load caused by whirling, the fluid drag force, and the contact force between the borehole wall and the drill-string. The drill-string is usually subjected to a complex combination of these loads.

The motivation for this dissertation is the need to understand the complex vibration states and the stability of the drill-string in order to better control its constructive and destructive potential. A mathematical model is proposed to describe the steady-state stability of a long, vertical, rectilinear drill-string. The model accounts for a complex combination of constant and variable loads that affect the behavior of drill-strings. The first critical values of these loads and the corresponding mode shape are obtained by the analytical method and the Rayleigh-Ritz method. COMSOL and ABAQUS are used to validate the numerical results for the cases without analytical solutions. With these results, we see that the Rayleigh-Ritz method gives accurate results and is a good way for us to understand more deeply the dynamics of the drilling process and predict the instability of the drilling system.

TABLE OF CONTENTS

LIST OF TABLES

LIST OF FIGURES

CHAPTER 1

INTRODUCTION AND GENERAL INFORMATION

The introduction briefly discusses the drilling system and the mechanical behaviors of the drill-string. It also provides a short motivation for the thesis and an outline of the organization of the Chapters.

1.1 Drilling System

Oil and natural gas are the major energy sources for the modern society. How to extract underground oil and gas efficiently and economically has been studied for decades. The best known technique used mostly in the oil industry is the rotary drilling system. The system can drill a well very deep underground and the world's longest and deepest well is longer than 10 kilometers now. The main process during a deep well drilling is to create a borehole by means of a rock-cutting tool, called a bit. The rotary drilling relies on a combined mechanical/hydraulic system to support the drilling process. There are two flows in this process: energy transport from surface to the bit, and material transport from the bit to surface.

A typical land-based drilling rig is shown in Figure 1.1. The mechanical part of the drilling system is composed of a bit, a drill-string, and a rotary drive system. A rotating bit consists of a steel body with or without rotating parts to generate the borehole. Bits can have a diameter between 0.1 and 0.9 m, where the smaller diameter bits are used for the deeper sections of the well. A drill-string consists

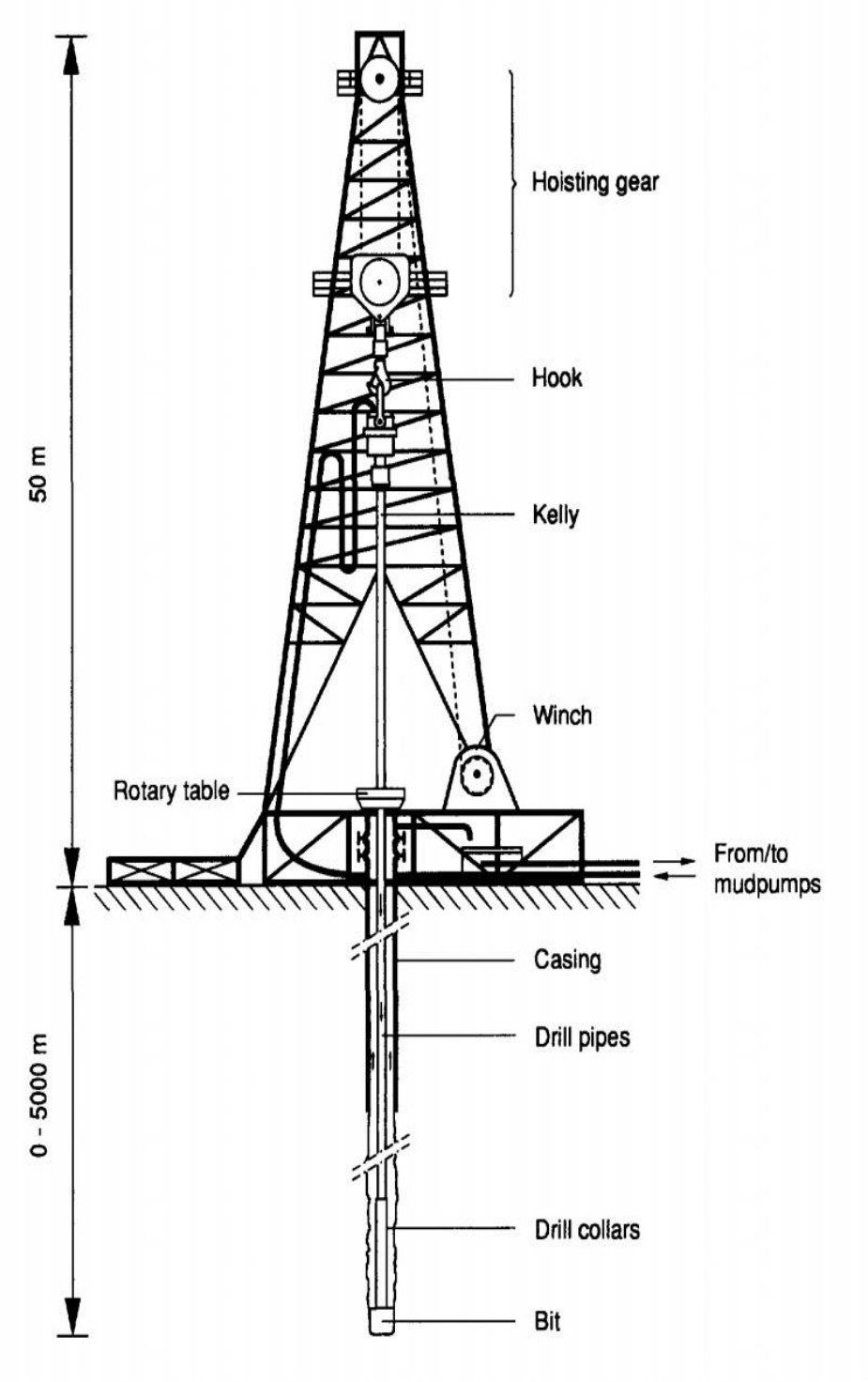

Figure 1.1 Components of a Rotary Drilling System

mainly of drill pipes to rotate the bit. The lowest part of the drill-string is called the bottom-hole assembly (BHA), which consists of drill collars with larger stiffness than the drill-pipe, stabilizers to stabilize the BHA and the bit to crush rocks. The length of the BHA is typically several hundred meters. Typical drill collars have an outside diameter up to 250 mm and a wall thickness up to 85 mm. Stabilizers have a blade length up to 1 m and a diameter that is 5 to 50 mm less than the diameter of the borehole [1]. The rotary drive system at the surface usually consists of an electric motor, a gearbox, and a right-angle reduction gear with a large horizontal disc-shaped gear wheel: the rotary table. The rotary table is located directly above the borehole and connected to the drill-string. Torque is transmitted from the rotary table to the drill-string via the Kelly to control the vertical motion of the drill-string. The hydraulic part consists of the drilling fluid (mud), pumps, and a transport channel: the drilling fluid is pumped down through the hollow drill-string and flows back through the annulus between the drill-pipe and the borehole wall. The drilling fluid aids the cutting process by jetting action: it cools and lubricates the bit and transports the cuttings from the hole bottom to the surface.

1.2 Mechanics of the Drill-string

The drilling industry has a common problem of severe drill-string vibrations during the drilling process. Field observations, in the form of down-hole and surface vibration measurements, have clearly indicated that the drill-string, particularly the BHA, generally is subjected to severe vibrations in several ways: lateral (bending), torsional (rotational), and axial (longitudinal) vibration, or more often, as combinations of these three basic modes. A drill-string is an extremely slender structure with a ratio between length and

diameter larger than a human hair. Because the drill-string has a smaller diameter than the borehole, it is free to vibrate laterally. Torsional vibration is caused by the input torque at the top end and the resisting torque at the bottom end because of the cutting. Axial vibration is caused by the self-weight of the drill-string, the input hook load at the top and the varying support load at the bit. These vibrations are especially important in the lower part of the drill-string. Typical frequencies of lateral vibration are from 0.5 to tens of Hz. The torsional vibration has a typical frequency of 0.05 to 0.5 Hz. The typical frequency of axial vibrations is between 1 and 10 Hz [1].

These different vibrations of the drill-string are caused by the complex loads applied to it. The primary functions of the drill-string are to transmit torque and to transport drilling fluid, and as a result a drill-string is loaded by torque and pressure. Torque values at the bit are usually between 0.5 and 10 kNm, but due to friction along the borehole wall the torque required to rotate the string at the surface may be between 0.5 and 50 kNm [1]. Another large load acting on the drill-string is the self-weight of the drill-string. The drill-string is supported from the surface and hung down in the borehole. In the upper part of the drill-string, the state of stress is tension which may be several thousands of kN. In the lower part of the drill-string (the lowest few hundred meters of the drill-string), the state of the stress is compression due to the weight on the bit (WOB) and the axial reaction force at the bottom end of the drill-string. The hook load is the axial supporting force at the top end of the drill-string. This load is to hold the drill-string and often almost equal to the weight of the drill-string. A drill-string is also subjected to various dynamic forces, including: fluid pressure fluctuations, internal and external damping forces, centrifugal

forces, and interactions with the wall. The three types of vibration are caused by these loads or their combinations. An important cause of lateral vibrations is out-of-balance forces in the drill-collars, resulting in a whirling motion, just as in an unbalanced centrifuge. Another cause of lateral vibration is the friction between the rotating drill-string and the borehole wall, which can produce a backward rolling motion of the drill-string along the wall. The torsional vibration is caused by a nonlinear relationship between the torque and the rotary speed at the bit. The axial vibration is caused by the variations of axial loads. The drilling fluid flows down through the hollow drill pipe and exits from the end of drill-string. That has some effects on the vibrational behavior and the stability of drill-string.

Drill-string vibration is an important cause of premature failure of bits, equipment and other drill-string components. When a crack in the drill-string is detected during the drilling process, the drill-string has to be removed from the hole to exchange the failed component. If the crack is not detected it may result in parting of the drill-string. After removing the top part of the drill-string the remaining part has to be fished out of the hole with special equipment. In the worst case the bottom part of the drill-string is not recovered, expensive equipment is lost, and a part of the hole has to be abandoned. At best, costly drilling time is wasted. Drill-string vibration can also cause problems with the directional control of the drill-string during the deviated drilling, can reduce the rate of penetration, and can cause damage to the borehole wall resulting in a collapsed or vastly oversized borehole. Because of the complex loading conditions, the bit may bounce on the cutting surface resulting in bit damage; severe bending moments may develop in the

BHA leading to fatigue failures; forward whirling may cause wear against the bore hole, and backward whirl due to the friction of the wall may result in fatigue failure. These phenomena are all hazardous to drilling operations.

The study of the stability of a drilling system arose from a desire to improve the drilling efficiency and protect expensive down-hole components. How to avoid or decrease the vibrations of the drill-string has been studied for decades. Traditionally, research into the avoidance of drill-string failures has concentrated on the material strength of the drill-string components rather than on the dynamic loadings. Research into the dynamic loadings appears to have started around 1960. Many theoretical analyses and field measurements have been performed since then and provided a large amount of information on dynamic drill-string behaviors. Control of vibration and dynamics in the oil and gas drilling process is very important for the industry to decrease the failures of expensive drill-strings and improve the drilling efficiency. But this is very difficult because of the system's inherent non-linearity and other uncertainties involved in the problem. The three main steering parameters of the drilling process are related to the rock cutting process at the bit: the hook load at the top end of the drill-string, the rotary speed at the surface and the flow rate. However, the driller has only partial control over these parameters, and instead controls three steering parameters at the surface that to a limited extent correspond to their downhole counterparts. Variations in the hook load caused by lowering or raising the hook give a crude measure of the WOB. The WOB has a typically desired value between 0 and 250 kN. The rotary speed at the surface is the angular velocity of the top end of the drill-string. This parameter can be accurately controlled, but

it may differ drastically from the instantaneous rotary speed at the bit because of the torsional flexibility of the drill-string. The average values of the rotary speed at the surface and downhole are, of course, equal. Typically desired rotary speeds are between 50 and 200 revolutions per minute (rpm) for the conventional rotary drilling. The flow rate is the volume of the drilling fluid pumped down through the drill-string. Under normal circumstances the flow rate through the pumps at the surface is equal to the flow rate through the nozzles at the bit, and can be accurately controlled because it is produced by a positive-displacement pump. Typical flow rates are between 10 and 50 L/s [1].

The motivation for this dissertation is the need to understand the complex vibration states that such a drill-string can exhibit in order to better control its constructive and destructive potential. A mathematical model will be proposed to describe the steady-state stability of a long, vertical, rectilinear drill-string. An accurate drill-string dynamic model can only be described by a set of non-linear differential equations. The model will account for a complex combination of static and dynamic loads that affect the behavior of a drill-string. Analysis of behaviors of the drill-string is based on the evaluation of steady-state stability. We will use a Rayleigh-Ritz method [2] to find the critical load combinations of the drill-string for different loading conditions. The mode shape corresponding to each loading condition is also computed. The effects of the different loads on the stability of the drill-string are also analyzed. With these results, we can understand more deeply the dynamics of the drilling process and predict the instability of the drilling system. The goal of this dissertation is to identify and describe the most important vibration mechanisms in the drill-string, to develop analytical and numerical

models of these phenomena and to verify them through the use of a finite element analysis.

1.3 Outline of the Dissertation

This dissertation concentrates on the understanding of steady-state stability of the drill-string. Vibrations caused by different loads such as the hook load, the self-weight of the drill-string, the whirling of the drill-string, and the end torque are included. These studies will help us gain insights into the behaviors of the drill-string and provide information about how to improve control and reduce costs of the drilling process.

In the second chapter, researches into the avoidance of drill-string failures are mentioned at first. Several different aspects of the vibration phenomenon of the drill-string are studied by different researchers. The problem we are interested in is stated in the next. A rotating coordinate system is used to describe vibrations of the drill-string. The equation of the motion of the drill-string is provided and the innovations about our study also are included.

In the third chapter, the analytical method is used to solve several cases with simple loading conditions applied on the drill-string. These loading conditions include constant axial load only, constant whirling only, constant end torque only, constant axial load and whirling applied together, constant axial load and end torque applied together. The first critical load parameters and the corresponding mode shapes are obtained for these cases.

In the fourth chapter, the Rayleigh-Ritz method is introduced at the beginning and then used to solve the several cases with different loading conditions applied. All cases solved

in Chapter 3 are solved again with the Rayleigh-Ritz method. The case with constant whirling and end torque, and the case with constant axial load, whirling and end torque are also solved. The self-weight of the drill-string is included for several cases and we find it changes the performance of stability significantly.

In the fifth chapter, COMSOL and ABAQUS are used as validation methods to confirm the results for several different cases. COMSOL is abandoned because we think ABAQUS is better to solve our problem. The analytical solution for a case with fixed-free boundary conditions is used to verify the ABAQUS result and two other cases with different loading conditions are analyzed.

In the sixth chapter, comparisons between the results from the analytical method and the Rayleigh-Ritz method are made. All results have close agreement and show that the Rayleigh-Ritz method is a good method to analyze our problem with more complex loading conditions.

In the seventh chapter, the results obtained so far are concluded. Several suggestions are made for future research.

CHAPTER 2

PROBLEM STATEMENT

This chapter briefly introduces the new technologies in the drilling system and reviews the historical notes in this field. It also mentions the innovations of our study.

2.1 Introduction

As the technology improving over the years, there are two kinds of drilling wells: the vertical drilling well and the directional drilling well. A vertical well is one that is characterized by a generally vertical wellbore track and is the most widely used well type worldwide. Because the risk of vertical well construction is relatively low, the techniques for drilling such a well are relatively simple and the maintenance of the subsequent oil extraction operation is relatively easy. Directional drilling is the real marvel of engineering and scientific innovation. The concept of directional drilling is drilling wells at multiple angles, not just vertically, to better reach and produce oil and gas reserves. It enables operators to maximize returns from each well and also produces positive results for the environment. One type of the directional drilling, the horizontal drilling, is used to drastically increase production. A horizontal well is drilled across an oil and gas formation, increasing production by as much as 20 times more than that of its vertical counterpart. Horizontal drilling is the term used for any wellbore that is inclined more than 80 degrees from the vertical, and it can even include more than a 90-degree angle. There are also many other technical improvements in the drilling system such as using polycrystalline diamond compact (PDC) bit to crush the rock, using a downhole motor to

generate rotation of the bit, and using downhole measurement-while-drilling (MWD) tools to obtain survey data of the drilling process. To study the stability of the drill-string, we simplify the system and view the drill-string as a long shaft (1–8 km). It is intuitive that such a long rotating system is subjected to severe vibrations during the drilling process. This chapter aims at clarifying the problem we are interested in and reviewing the innovations in this field.

2.2 Historical Notes

Research into the avoidance of drill-string failures has been the subject of much research and many articles in the past. Traditionally, study has been concentrated on the material strength of the drill-string components rather than on the dynamic loading. Research into the dynamic loading appears to have started around 1960, when the first surface measurements were made that indicated the occurrence of torsional and axial vibrations [3]. In 1968 a series of downhole measurement were performed which provided a large amount of information on dynamic drill-string behavior [4, 5].

Buckling of the drill-string and drill-string vibrations are common and damaging phenomena that have been extensively described. A drill-string can be viewed as a long column constrained at both ends, and many researchers have studied the buckling problem of columns under different load conditions with different boundary conditions. A.G. Greenhill [6] established a formula to describe the buckling phenomenon of shafts, which is made to transmit at once a thrust and a twisting moment. He worked out a mathematical investigation to get the critical buckling the thrust and the twisting moment. Capelushnikov [7] appears to have been one of the first investigators who attempted to

explain the possible causes of borehole deviation in terms of analytical investigations into beam mechanics and elastic bending theory. Clark [8] presented a qualitative categorization of the four main modes of a string of drill pipe and described three states of instability which can exist: buckling of the drill column due to the WOB, the spiral deformation of the string due to twisting of the pipe, the instability may occur as a result of the speed of rotation.

Work initiated in the 1950s by Lubinski and Woods [9-12] and Rollins and Bachman [13] gave the oil and gas industry its first practical methods of analyzing the bending drill-string. Lubinski [14] applied the theory of elastic stability to analyze a drill string of uniform cross section in a vertical hole. He determined the critical conditions which cause buckling as a function of the WOB for straight sections of pipe. He found out that carrying weights on the bit which are slightly less than the critical value of the third order is better than using any smaller value of weight at which the string is already buckled. In 1956, Rollins [15] converted the Woods and Lubinski data into more useable numerical tables which included representative conditions for popular borehole and collar sizes of the times for various inclination angles, formation dips, and crookedness classifications.

Ziegler [16] analyzed a problem of a shaft buckled by end torque only with fixed-fixed boundary conditions. He showed that buckling is not caused only by compression and a shaft may also become unstable under the action of a torque. The smallest buckling moment was obtained by the same method Greenhill used. Timoshenko [17] dealt with a vertical beam under its own weight with fixed-free boundary conditions. The critical length of the beam was calculated with a method involving Bessel's functions. Mclachlan

[18] did a similar research also using Bessel functions a little later and had the same results. Tan and Digby [19] determined a number of different equilibrium helical buckling configurations for a tubing or drill string confined within a cylindrical casing and buckled under static compressive forces. The solutions relating the buckling load and the post-buckling configuration were given explicitly for the string of weight and at any inclined positions. Tan and Forsman [20] also conducted experiments on laboratory buckling tests of strings and the results were compared with theoretical formulas. A proposed approximate formula for estimating the friction force provided more accurate results. Chen and Li [21] studied the deformation of a thin elastic rod constrained inside a cylindrical tube and under the action of an end twisting moment. They presented a complete analysis on the deformation when the dimensionless twisting moment was increased from zero. The numerical results were found to agree very well with those predicted analytically. Coomer [22] discussed the motion of idealized inextensible strings and analyzed the equations of motion for closed-loop configurations, free of body forces and open hanging strings whirling under gravity. The results provided a useful theoretical background for an analysis of a laboratory exploration of whirling chains. Virgin [23] found the natural frequencies of a vibrating beam under an axial load, which has similarities with a rotary drill-string under axial loads. He analyzed the beam with fixed-pinned boundary conditions and gave the relation between the axial load and the natural frequency.

Dareing and Livesay [24] discussed longitudinal and angular drill-string vibrations and supporting field measurements taken with a special downhole recording instrument.

Computer programs were used to calculate vibrations and field measurements were used to check computer calculations. Johancsik [25] developed a computer model to predict drill-string torque and drag. Sliding friction is concluded to be the major source of torque and drag in directional wells. Gulyaev [26-30] analyzed the quasi-static stability of a rotating drill-string rotating with constant speed under the longitudinal non-uniform preloading, action of torque, inertia forces of rotation and internal flows of the drilling fluid. He showed that the buckling mode of the drill-string is helical within a section subjected to compressive forces. Techniques for determining the critical rotary speeds of drill-strings make it possible to develop measures to prevent accidents during deep drilling operations. Tucker [31-34] discussed the vibrational states experienced by the active components of a drilling assembly such as that found in the oil or gas industry in the context of an integrated mathematical model. The model was used to discuss the stability of vertical axis-symmetric drill-string configurations under both coupled torsional, axial and lateral perturbations as well as general non-perturbative coupled vibrational states under extreme conditions of lateral whirl. Yigit [35-37] presented a dynamic model for coupled torsional and bending vibrations of drill-strings. The dynamics of actively controlled drill-strings was also studied. Transverse vibrations of drill-strings caused by axial loading and impact with the wellbore wall were studied. The simulation results agreed well with laboratory and field observations when the stick-slip vibrations occur. Zare [38] presented a finite element model using ANSYS software to investigate the drill-string lateral vibrations in slightly deviated wells. The model was developed in the presence of mud, friction and nonlinear contact between drill-string and

wellbore wall. The model was compared with experimental results obtained from several BHA configurations giving excellent results. Khulief [39] formulated a dynamic model of the drill-string including both drill-pipe and drill-collars. The equation of motion was derived using Lagrangian approach together with the finite element method. The developed model was integrated into a computational scheme to calculate the modal characteristics and to perform time-response analysis of the drill-string system. Chen [40] investigated the relationship between the axial critical force under sinusoid bending and the maximum speed of drill-string, and then obtained a mathematics model for the speed-axis critical force. They found that the axis critical force will be obviously less than that under the static state. Meng [41] studied the influence of the different well inclination angle and stiffness on the buckling load. Their results showed that the buckling load increases nonlinearly with the well inclination angle; the larger the stiffness of drill pipes, the higher the buckling load.

Hiddabi [42] presented a non-linear dynamic inversion control design method to suppress the lateral and the torsion vibrations of a drill-string. It was found that the designed controller is effective in suppressing the torsion vibrations and reducing the lateral vibrations significantly. The study of Dunayevsky and Abbasslan [43] centered on calculations of stable rotary speed ranges for a given set of drill-string parameters and were presented in vibration “severity” vs. rotary speed plots. The critical rotary speeds, which correspond to the rapidly growing lateral vibrations, were pinpointed by spikes on the severity plots[43]. In Hakimi and Moradi’s study [44], the differential quadrature method (DQM) was applied to analyze the drill-string vibrations in a nearly vertical hole.

The numerical results obtained from a series of case studies confirmed the efficiency and accuracy of the method in dealing with drill-string vibration problems. Liao [45] developed reduced-order models of a drill-string system and studied the predictions of these models, and made qualitative comparisons with experimental studies. Palmov [46] analyzed the stability of an drill-string rotation in his study. The drill pipe was represented by a one-dimensional continuum in torsion, while the bottom-hole-assembly was considered to be a rigid body. Shyu [47] found and discussed mathematical models for explaining and predicting the bending vibrations of rotating drill-strings. Experiments carried out in the laboratory confirmed the existence of the linear and parametric coupling between axial forces and bending vibration.

Alamo and Weber [48] developed a Cosserat model to provide an accurate way of modeling long slender beams. Their results showed the linear and nonlinear time responses of the system and the high accuracy of the dynamic responses was achieved by dividing the system into a few elements which is much less than the traditional FE methods and simulation times are greatly reduced through this approach. Heisig [49] presented an analytical solution for natural frequencies and the threshold rotary speed of a drill-string lying on the low side of hole in a horizontal borehole. Animated time domain simulations with this model provided deeper insight into the dynamic behavior of the drill-string and showed that a drill-string in a horizontal borehole can vibrate in a snaking or in a whirling mode. Voronov [50] analyzed the nonlinear dynamics of a tool commonly employed in deep hole drilling. The obtained results allowed the prediction of conditions for stable continuous cutting and unstable regions. The time domain

simulation allowed determination of the chip shape most suitable for certain work-piece material and tool geometry.

In Huang's study [51], critical buckling loads and natural frequencies of lateral vibration modes were determined for a long vertical pipe, suspended in a fluid, simply supported at the top and vertically guided at the bottom. Their findings showed that the magnitude of the critical buckling force becomes independent of drill pipe length as drilling depth increases. Qian [52] developed a theoretical model for the vibration and stability of a vertical pipe subjected concurrently to two axial flows. It was shown that the vibrations were closely related to the degree of confinement of the outer annular channel. Schmalhorst [53] developed a new drill-string dynamics model taking into account the interaction between the drill-string and the instationary mud flow circulation. The application helped to avoid critical operating conditions and to select the corresponding system parameters.

Though there is an abundance of literature and research identifying drill-string vibrations and some analysis has been carried out through approximated methods, there is limited research available on the stability analysis of the drill-string. Most such research targets BHA stability or other aspects, not the whole drill-string. Further, no work is found to provide a framework for formally analyzing the stability of the drill-string in steady-state with axial loads, end torque and whirling together.

2.3 Problem Statement

Depending on drilling conditions, rotating drill-strings are subject to many different loads: the axial loads along the axis of the drill-string, the lateral bending moment at any cross section of the drill-string, the input torque applied at the top and the resisting torques applied to the bit at the bottom, the friction due to the flow of the drilling fluid, the forces due to contact with borehole, and so on. All these loads are coupled and applied to the system at the same time to cause buckling and complex vibrations. Excessive vibrations have been observed to cause damage to the drilling system [54]. As a consequence, the drilling process becomes inefficient and costly. Some of these adverse phenomena can be avoided through theoretical simulation of the buckling and vibration of drill-strings and identification of their critical configurations. Thus, vibrations of the drill-strings must be studied and their effects should be controlled for the drilling process to be optimal and economical.

For our problem, we consider a drill-string of length L. To describe the buckling and vibrations of the drill-string, we choose an inertial coordinate system (fixed frame) $O-XYZ$ with the origin at the point of suspension (the top end) of the drill-string and a coordinate system (rotating frame) $O-xyz$ rotating together with the drill-string about the OZ-axis with a constant angular velocity ω. The axes OZ and Oz coincide with the initial axial line of the drill-string when it is straight. The deflections of the drill-string in the direction of the axes Ox and Oy are denoted by $u(z,t)$ and $v(z,t)$; the torsional twisting deflection of the drill-string about the axis OZ and the axial displacement along

the axis Oz are not considered in our study. The coordinate system we use is shown in Figure 2.1.

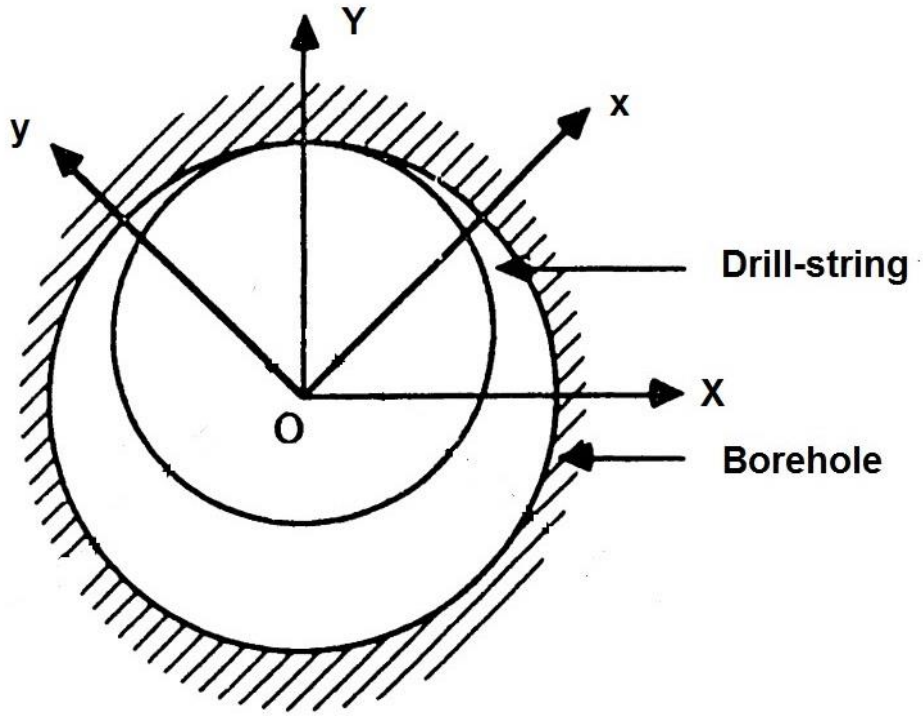

Figure 2.1 Definition of the Coordinate Systems

We use the coordinate system Oxyz to describe the deflections of the drill-string. When we considered the axial load, the end torque, the whirling and the drag force by the drilling fluid, we have the equations of motion of the drill-string [28] in the planes Oxz and Oyz of the rotating coordinate system Oxyz as followed

$$EI\,\frac{\partial^4 u}{\partial z^4}-\frac{\partial}{\partial z}\left(P(z)\frac{\partial u}{\partial z}\right)-\frac{\partial^2}{\partial z^2}\left(M\frac{\partial v}{\partial z}\right)-m\omega^2 u+m_f V^2\frac{\partial^2 u}{\partial z^2}-2m\omega\frac{\partial v}{\partial t}$$

$$+C_f\frac{\partial u}{\partial z}\sqrt{\left(\frac{\partial u}{\partial t}\right)^2+\left(\frac{\partial v}{\partial t}\right)^2}+m\frac{\partial^2 u}{\partial t^2}=0$$

$$EI\ \frac{\partial^4 v}{\partial z^4} - \frac{\partial}{\partial z}\left(P(z)\frac{\partial v}{\partial z}\right) + \frac{\partial^2}{\partial z^2}\left(M\frac{\partial u}{\partial z}\right) - m\omega^2 v + m_f V^2 \frac{\partial^2 v}{\partial z^2} + 2m\omega\frac{\partial u}{\partial t}$$

$$+ C_f \frac{\partial v}{\partial z}\sqrt{\left(\frac{\partial u}{\partial t}\right)^2 + \left(\frac{\partial v}{\partial t}\right)^2} + m\frac{\partial^2 v}{\partial t^2} = 0.$$

in which EI is the flexural stiffness of the drill-string, m is mass per unit length of the drill-string, m_f is the fluid's mass per unit length of the drill-string's cross section, C_f is the drag coefficient of the drilling fluid, V is the velocity of the fluid outside the drill-string, $P(z)$ is the axial force at an arbitrary cross section of the drill-string, M is the constant end torque applied to the drill-string at the origin, and t is time.

The system of equations makes it possible to examine the stability of a drill-string. The axial force $P(z)$ is constant for some loading conditions and variable when the self-weight of the drill-string is considered. The end torque M is assumed to be constant along the drill-string. When the drill-string is in the steady state and the drilling fluid is not considered, the system of equations become

$$EI\ \frac{\partial^4 u}{\partial z^4} - \frac{\partial}{\partial z}\left(P(z)\frac{\partial u}{\partial z}\right) - \frac{\partial^2}{\partial z^2}\left(M\frac{\partial v}{\partial z}\right) - m\omega^2 u = 0$$

$$EI\ \frac{\partial^4 v}{\partial z^4} - \frac{\partial}{\partial z}\left(P(z)\frac{\partial v}{\partial z}\right) + \frac{\partial^2}{\partial z^2}\left(M\frac{\partial u}{\partial z}\right) - m\omega^2 v = 0.$$

We have the boundary conditions for the drill-string: clamped at both ends but the top end can slide in the axis OZ. So we have the equations:

$$u(0) = v(0) = 0, \quad \left.\frac{du}{dz}\right|_{z=0} = \left.\frac{dv}{dz}\right|_{z=0} = 0$$

$$u(L) = v(L) = 0, \quad \left.\frac{d^4u}{dz^4}\right|_{z=L} = \left.\frac{d^4v}{dz^4}\right|_{z=L} = 0.$$

With the constant rotary speed of the drill-string ω, we will seek to determine the critical loads at which the drill-string buckles. Because of the highly complex governing equations, analytic methods fail to solve the system of equations and numerical approaches should be used. Here we will use the Rayleigh-Ritz method to solve this problem. We will build a mathematical model for the whole drill-string and analyze the steady state. We can get the critical load combinations of the steady state for different loading conditions of the system to tell if the system is stable or give an advance warning to the operator if the system is going to become unstable. Because we do not simulate the time-history vibration of the system, the model does not involve severe computational difficulties.

2.4 Innovations

Because of many factors affecting the vibrations of the drill-string and the complex real-time situations during the drilling process, the drill-string system has very complex vibration behaviors. Simulating the "time history" of a complex dynamic drill-string is time-consuming and expensive. For a finite element model in the time domain, it may take hours even for a powerful computer to simulate the real drill-string vibrations only for a few seconds. Furthermore, we cannot know the specific initial conditions that the drill-string system will have in the field. The number of possible combinations of initial conditions is infinite. So, any assumed set of different initial conditions used to generate some number of simulated time histories for a specified drill-string and drill path may not

capture the specific conditions found in the field. As a consequence of this, simulated time histories may fail to predict severe vibration and damage. Because of the long time required for computation, it is not practical to use time-domain analysis of the complex vibration behaviors of the drill-string system for on-site, real-time monitoring of the system’s stability. But simulating a drill-string's time history is not the only way to analyze its dynamics and to predict severe vibrations.

In "steady-state motion", all dynamic quantities are either constant or periodic. For a dynamic system operating near a "stable" steady-state motion, small disturbances do not cause severe vibration. But for a system operating near an "unstable" steady-state motion, vibration can quickly become severe. The actual motion of a drill-string is almost always near some steady-state motion. When the drill-string operates without severe vibration, the nearby steady-state motion must be stable. As drilling proceeds, it would be useful to be able to predict unstable steady-state motions that would occur if drilling proceeded without adjusting drilling parameters (torque and WOB).

Analyzing the stability of a structure's steady-state motion is far less computationally intensive than generating its time history and does not require guessing initial conditions. By analyzing the stability of the steady-state motion near which a drill-string is operating, and by assuming no adjustment in drilling parameters, it should be possible to predict whether the string will encounter unstable conditions in the next portion of the planned drill path.

As shown in the literature review, no researcher has published an analysis of the stability of the drill-string in the steady state that considers all aspects needed for a realistic model.

Previously published analyses of the stability of steady-state motion of a drill-string only have treated extremely simple cases. We are developing a computational tool for analyzing the stability of more realistic cases. We would treat a straight, vertical, whirling drill-string with variable axial load and applied torque at the ends while whirling at the same time. This is the originality of this dissertation and is potentially a significant step for the study of vibrations of drill-string systems.

CHAPTER 3

ANALYTICAL SOLUTIONS FOR SIMPLE CASES

This chapter introduces the analytical solutions for some simple cases with different loading conditions. The first critical values of different parameters are obtained and the corresponding mode shapes are also illustrated.

3.1 Introduction

We analyze the stability of a drill-string under different loading conditions with the same boundary conditions. We assume that the drill-string has a clamped constraint at the bottom end and a clamped constraint (but slide-free in axial direction) at the top end. So, for both ends, there is zero deflection and zero slope. For some simple cases, we can get analytical solutions. But for other complex cases, it is not possible to solve the analytically. Table 1 lists loading cases with analytical solutions.

Table 3.1 Loading Cases with Analytical Solutions

	Axial Load	Whirl	Torsion	Distributed Axial Load
1	Yes	No	No	No
2	No	Yes	No	No
3	No	No	Yes	No
4	Yes	Yes	No	No
5	Yes	No	Yes	No

To illustrate the analytical method solving this problem, we present some simple cases with different loading conditions here. We have the solutions and results below to illustrate the analytical methods we use here.

3.2 Solving Simple Cases with Different Loading Conditions

3.2.1 Constant Axial Load Only

With the constant axial load applied only, we have a planar buckling problem. At the critical value of the axial load, the system becomes unstable and the drill-string buckles. The differential equation of the system for the steady state is simplified and shown as below [55]

$$EI\ \frac{d^4}{dz^4}u(z) + P\frac{d^2}{dz^2}u(z) = 0.$$

Define the axial load parameter $\alpha = \frac{PL^2}{EI}$, the dimensionless coordiante $\zeta = \frac{z}{L}$, and we have the dimensionless differential equation

$$\frac{d^4}{dz^4}u(\zeta) + \alpha\frac{\partial^2}{\partial z^2}u(\zeta) = 0$$

for which the general solutions are

$$u(\zeta) = A\ cos\left(\sqrt{\alpha}\zeta\right) + B\ sin\left(\sqrt{\alpha}\zeta\right) + C\zeta + D$$

with the boundary conditions:

$$u(0) = u(1) = u'(0) = u'(1) = 0.$$

Appling the boundary conditions to the dimensionless equation, we get

$$\begin{gathered} A + D = 0 \\ A\cos(\sqrt{\alpha}) + B\sin(\sqrt{\alpha}) + C + D = 0 \\ B\sqrt{\alpha} + D = 0 \\ -A\sqrt{\alpha}\sin(\sqrt{\alpha}) + B\sqrt{\alpha}\cos(\sqrt{\alpha}) + C = 0 \end{gathered}.$$

For non-trivial solution, the characteristic equation is

$$\begin{vmatrix} 1 & 0 & 0 & 1 \\ \cos(\sqrt{\alpha}) & \sin(\sqrt{\alpha}) & 1 & 1 \\ 0 & \sqrt{\alpha} & 0 & 1 \\ -\sqrt{\alpha}\sin(\sqrt{\alpha}) & \sqrt{\alpha}\cos(\sqrt{\alpha}) & 1 & 0 \end{vmatrix} = 0.$$

This gives the analytical solution of the first critical axial load parameter $\alpha = 4\pi^2$ at which the drill-string buckles. From the definition of the axial load parameter, we have the first critical axial load $P_{cr} = \frac{4\pi^2 EI}{L^2}$. Substituting the first critical axial load parameter into the general solution, we can get the function of mode shape for the first critical load:

$$f_{MS} = 1 - \cos(2\pi\zeta).$$

The mode shape given by the equation above is shown in Figure 3.1.

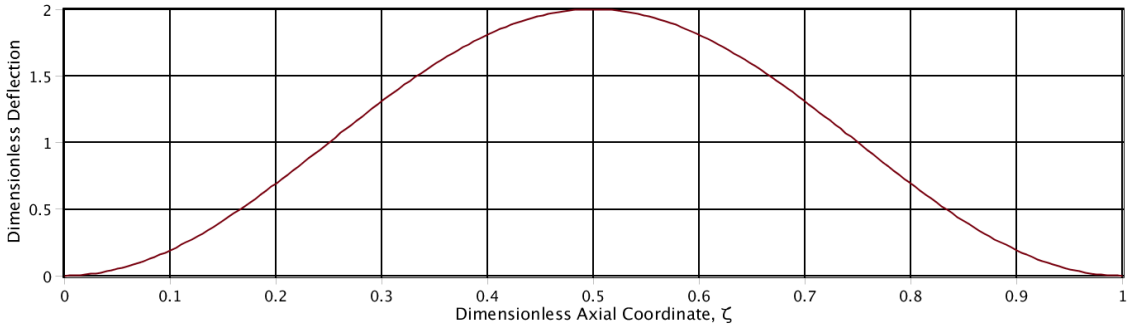

Figure 3.1 Mode Shape for the Case with Constant Axial Load Only

Because we can choose an arbitrary coefficient in front of the function of the mode shape to have the deflection function of the drill-string, the maximum deflection is arbitrary. We find that the maximum deflection is located at $\zeta = 0.5$ and we normalize it to 1. The function of the deflection is

$$u(\zeta) = 0.5 - 0.5cos(2\pi\zeta).$$

The plot of the deflection is shown in Figure 3.2.

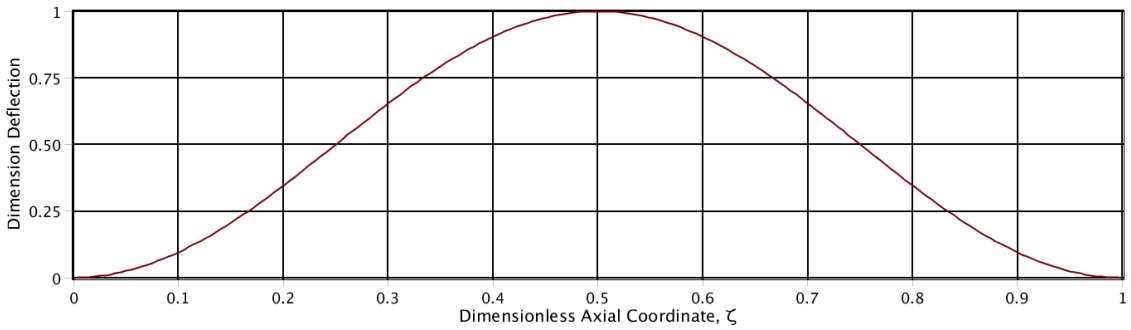

Figure 3.2 Deflection for the Case with Constant Axial Load Only

3.2.2 Constant Whirling Only

When there is not any external load applied and the drill-string is whirling at a constant speed only, we still have a planar buckling problem. At the critical value of the whirling speed, the system becomes unstable and the drill-string buckles. The differential equation of the system for the steady state is simplified and shown as below

$$EI\ \frac{d^4}{dz^4}u(z) - m\Omega^2 u(z) = 0.$$

Define the whirling speed parameter $\beta = \frac{m\Omega^2 L^4}{EI}$, the dimensionless coordiante $\zeta = \frac{z}{L}$, and we have the dimensionless differential equation

$$\frac{d^4}{dz^4}u(\zeta) - \beta\, u(\zeta) = 0$$

for which the general solutions are

$$u(\zeta) = A\, cosh\left(\sqrt[4]{\beta}\zeta\right) + B\, sinh\left(\sqrt[4]{\beta}\zeta\right) + C\, cos\left(\sqrt[4]{\beta}\zeta\right) + D\, sin\left(\sqrt[4]{\beta}\zeta\right)$$

with the boundary conditions

$$u(0) = u(1) = u'(0) = u'(1) = 0.$$

Appling the boundary conditions to the dimensionless differential equation, we get

$$\begin{gathered} A + C = 0 \\ A\, cosh\left(\sqrt[4]{\beta}\right) + B\, sinh\left(\sqrt[4]{\beta}\right) + C\, cos\left(\sqrt[4]{\beta}\right) + D\, sin\left(\sqrt[4]{\beta}\right) = 0 \\ B + D = 0 \\ A\, sinh\left(\sqrt[4]{\beta}\right) + B\, cosh\left(\sqrt[4]{\beta}\right) - C\, sin\left(\sqrt[4]{\beta}\right) + D\, cos\left(\sqrt[4]{\beta}\right) = 0 \end{gathered}.$$

For non-trivial solution, the characteristic equation is

$$\begin{vmatrix} 1 & 0 & 1 & 0 \\ cosh\left(\sqrt[4]{\beta}\right) & sinh\left(\sqrt[4]{\beta}\right) & cos\left(\sqrt[4]{\beta}\right)1 & sin\left(\sqrt[4]{\beta}\right)1 \\ 0 & \sqrt{\alpha} & 0 & 1 \\ sinh\left(\sqrt[4]{\beta}\right) & cosh\left(\sqrt[4]{\beta}\right) & -sin\left(\sqrt[4]{\beta}\right) & cos\left(\sqrt[4]{\beta}\right) \end{vmatrix} = 0.$$

This gives the analytical solution of the first critical whirling speed parameter $\beta = 500.564$ at which the drill-string buckles. From the definition of the whirling speed parameter, we have the first critical whirling speed $\Omega_{cr} = \sqrt{\frac{500.564\ EI}{mL^4}}$. Substituting the first critical whirling speed parameter into the general solution, we can get the mode shape for the first critical load as

$$f_{MS} = 1.018\, cosh(4.73\,\zeta) - sinh(4.73\,\zeta) - 1.018\, cos(4.73\,\zeta) + sin(4.73\,\zeta).$$

The mode shape given by the equation above is shown in Figure 3.3.

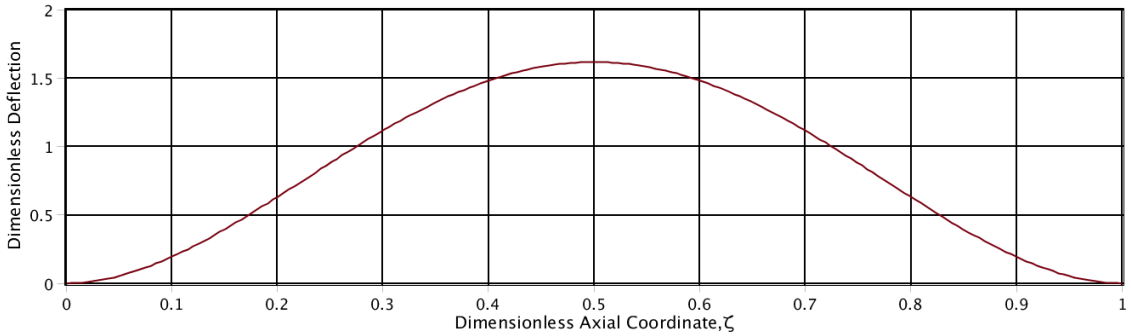

Figure 3.3 Mode Shape for the Case with Constant Whirling Only

Because we can choose an arbitrary coefficient in front of the function of the mode shape to have the deflection function of the drill-string, the maximum deflection is arbitrary. We find that the maximum deflection is located at $\zeta = 0.5$ and we normalize it to 1. The function of the deflection is

$$u(\zeta) = 0.630\, cosh(4.73\, \zeta) - 0.619\, sinh(4.73\, \zeta) - 0.630\, cos(4.73\, \zeta) + 0.629\, sin(4.73\, \zeta).$$

The plot of the deflection is shown in Figure 3.4.

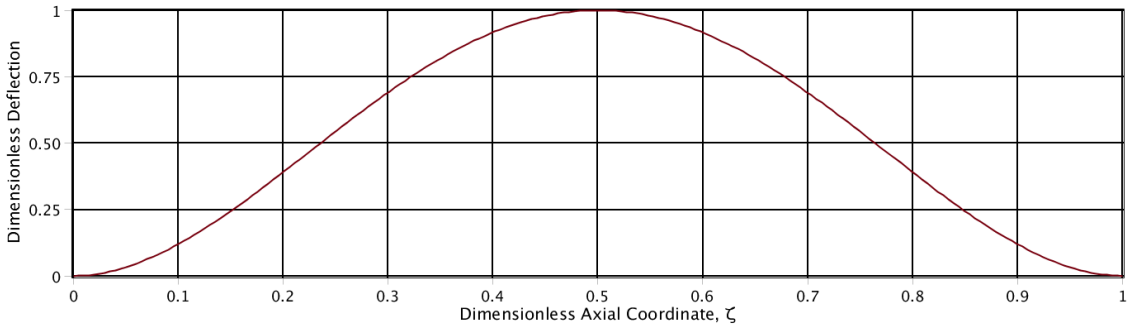

Figure 3.4 Deflection for the Case with Constant Whirling Only

3.2.3 Constant End Torque Only

With the constant end torque applied only, we have a non-planar buckling problem. Ziegler [16] had studied a similar problem but with different boundary conditions. At the critical value of the end torque, the system becomes unstable and the drill-string buckles. The differential equation of the system for the steady state is simplified and shown as below

$$EI\ \frac{\partial^4}{\partial z^4}u(z) + M\frac{\partial^3}{\partial z^3}v(z) = 0$$
$$EI\ \frac{\partial^4}{\partial z^4}v(z) - M\frac{\partial^3}{\partial z^3}u(z) = 0$$

.

Define the end torque parameter $\lambda = \frac{ML}{EI}$, the dimensionless coordiante $\zeta = \frac{z}{L}$, and introduce a complex deflection $r(\zeta) = u(\zeta) + i\ v(\zeta)$, we have the dimensionless differential equation

$$\frac{d^4}{dz^4}r(\zeta) - i\ \lambda\ \frac{d^3}{dz^3}r(\zeta) = 0.$$

The general solutions of the above equation are

$$r(\zeta) = A_1\cos(\lambda\,\zeta) + i\ A_1\sin(\lambda\,\zeta) + i\ A_2\cos(\lambda\,\zeta) - A_2\sin(\lambda\,\zeta) + A_3\,\zeta^2 + i\ A_4\,\zeta^2 + A_5\,\zeta + i\ A_6\zeta + A_7 + i\ A_8$$

with the boundary conditions

$$r(0) = r(1) = r'(0) = r'(1) = 0.$$

Appling the boundary conditions to the dimensionless differential equation, we get

$$A_1 + A_7 = 0$$
$$-\lambda\, A_2 + A_5 = 0$$
$$A_2 + A_8 = 0$$
$$\lambda\, A_1 + A_6 = 0$$
$$A_1\, cos(\lambda) - A_2\, sin(\lambda) + A_3 + A_5 + A_7 = 0$$
$$-A_1 \lambda\, sin(\lambda) - A_2\, \lambda\, cos(\lambda) + 2\, A_3 + A_5 = 0$$
$$A_1\, sin(\lambda) + A_2\, cos(\lambda) + A_4 + A_6 + A_8 = 0$$
$$A_1\, \lambda\, cos(\lambda) - A_2\, \lambda\, sin(\lambda) + 2\, A_4 + A_6 = 0$$

.

For non-trivial solution, the characteristic equation is

$$\begin{vmatrix} 1 & 0 & 0 & 0 & 0 & 0 & 1 & 0 \\ 0 & -\lambda & 0 & 0 & 1 & 0 & 0 & 0 \\ 0 & 1 & 0 & 0 & 0 & 0 & 0 & 1 \\ \lambda & 0 & 0 & 0 & 0 & 1 & 0 & 0 \\ cos(\lambda) & -sin(\lambda) & 1 & 0 & 1 & 0 & 1 & 0 \\ -\lambda\, sin(\lambda) & -\lambda\, cos(\lambda) & 2 & 0 & 1 & 0 & 0 & 0 \\ sin(\lambda) & cos(\lambda) & 0 & 1 & 0 & 1 & 0 & 1 \\ \lambda\, cos(\lambda) & -\lambda\, sin(\lambda) & 0 & 2 & 0 & 1 & 0 & 0 \end{vmatrix} = 0.$$

This gives the analytical solution of the first critical end torque parameter $\lambda = 8.987$ at which the drill-string buckles. From the definition of the end torque parameter, we have the first critical end torque $M_{cr} = \frac{8.987\, EI}{L}$. To describe the deflection functions of the drill-string, we choose two coefficients A_7 and A_8. Substituting the first critical end torque parameter into the general solution, we can get the mode shape for the first critical load. This mode shape has two different functions as

$$f1_{MS} = -0.563\, cos(8.987\, \zeta) - 1.072\, \zeta^2 + 0.563$$
$$f1_{MS} = 0.298\, sin(8.987\, \zeta) + 2.550\, \zeta^2 - 2.676\, \zeta^{\cdot}$$

The mode shape given by the equations above is shown in Figure 3.5.

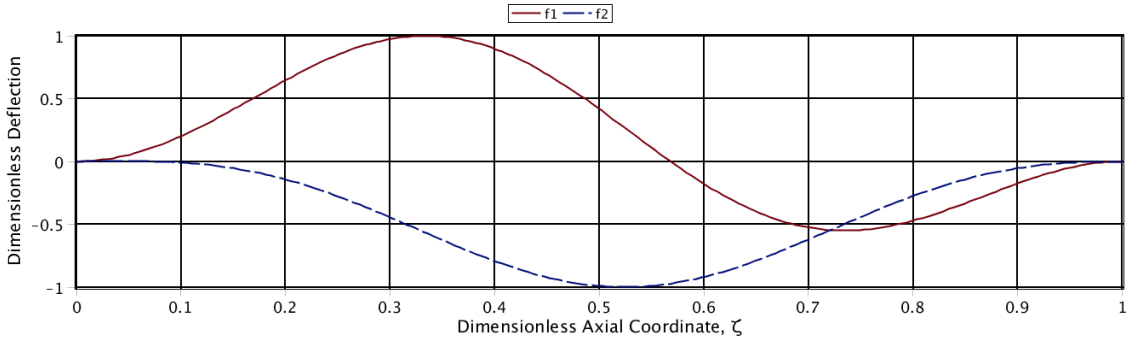

Figure 3.5 Mode Shape for the Case with Constant End Torque Only

A_7 and A_8 are chosen to describe the deflection functions as below

$$u(\zeta) = A_7\, f1_{MS} + A_8\, f2_{MS}$$
$$v(\zeta) = A_8\, f1_{MS} - A_7\, f2_{MS}.$$

A_7 and A_8 can be any arbitrary values and the maximum deflection of the drill-string is arbitrary. We found the maximum deflection is located at $\zeta = 0.334$ for the first function of the mode shape and $\zeta = 0.524$ for the second function of the mode shape. We set $A_7 = A_8 = 1$, which makes the ratio of the two coefficients equal to 1, to check the deflections of the drill-string. The maximum deflections have been normalized to ±1 and the deflection functions are below as

$$u(\zeta) = -0.292\, cos(8.987\, \zeta) + 0.292\, sin(8.987\, \zeta) + 1.945\, \zeta^2 - 2.625\, \zeta + 0.292$$
$$v(\zeta) = -0.230\, sin(8.987\, \zeta) - 0.230\, cos(8.987\, \zeta) - 2.411\, \zeta^2 - 2.070\, \zeta + 0.230.$$

We found the maximum deflection is located at $\zeta = 0.436$ for the deflection in the direction of the axis Ox and $\zeta = 0.618$ for the deflection in the direction of the axis Oy. The plot of the deflection is shown in Figure 3.6.

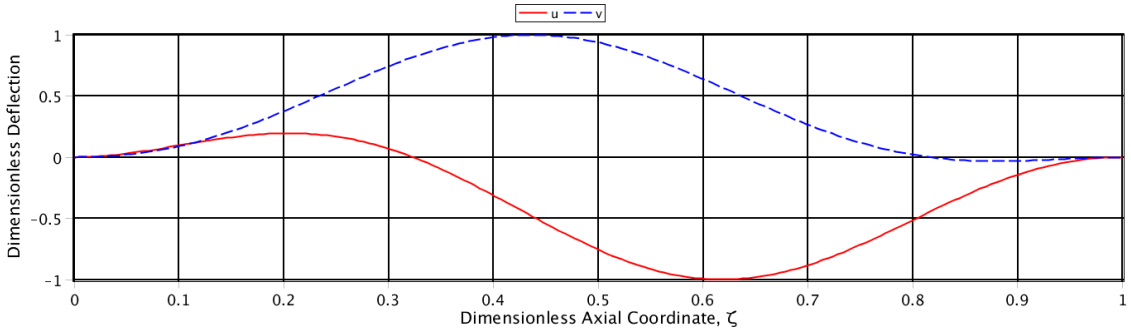

Figure 3.6 Deflections for the Case with Constant End Torque Only

It is obvious that changing the ratio of A_7 and A_8 changes the deflection functions. But we find out that changing this ratio is equivalent to a rigid-body rotation of the mode shape relative to the coordinate system O-XYZ. We choose 5 different ratios of A_7 and A_8 to check the deflections of the drill-string. Figure 3.7 is the radial deflection (the maximum deflection in radial direction at every cross section) plot with 5 different ratios of A_7 and A_8. We can see that all curves are same, which mean that the drill-string has same radial deflections at any cross section.

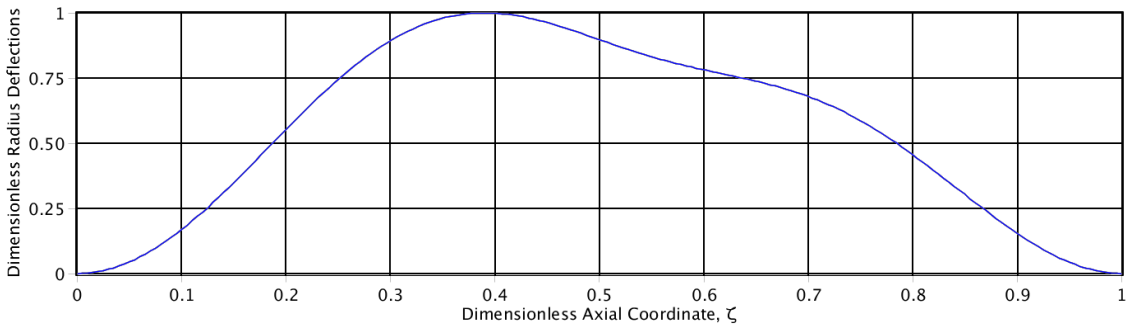

Figure 3.7 Radial Deflections with Different Ratios of A_7 and A_8

Figure 3.8 is the 3-D plot of the radial deflections with different ratios of A_7 and A_8. Figure 3.9 is the same deflections looking downward from the top end of the drill-string.

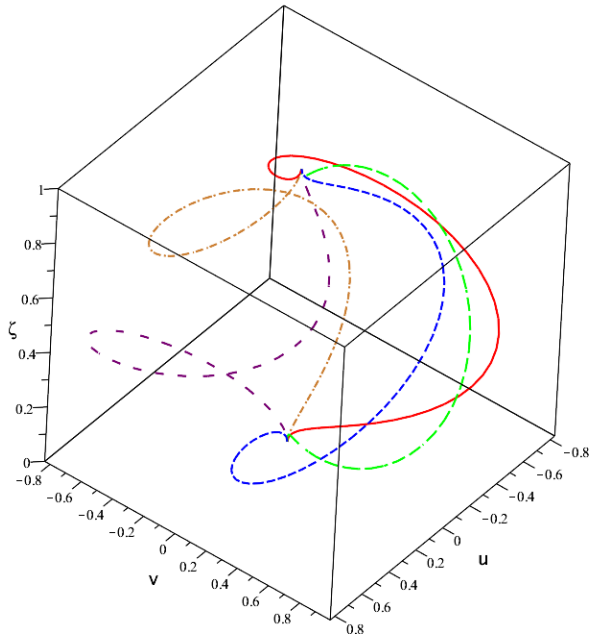

Figure 3.8 Radial Deflections with Different Ratio of A_7 and A_8

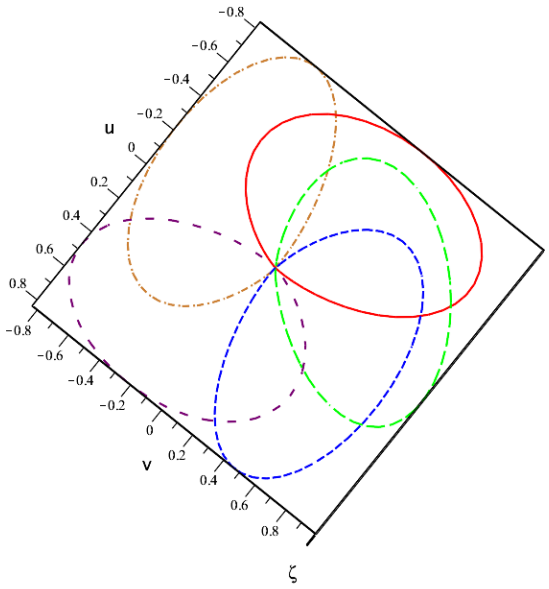

Figure 3.9 Vertical View of Radial Deflections with Different Ratio of A_7 and A_8

3.2.4 Constant Axial Load and Whirling

With the constant axial load is applied to the drill-string while whirling, we still have a planar buckling problem. At a critical combination of the axial load and the whirling speed, the system becomes unstable and the drill-string buckles. The differential equation of the system for the steady state is simplified and shown as below [23]

$$EI\ \frac{d^4}{dz^4}u(z) + P\frac{\partial^2}{\partial z^2}u(z) - m\Omega^2 u(z) = 0.$$

Define the axial load parameter $\alpha = \frac{PL^2}{EI}$, the whirling speed parameter $\beta = \frac{m\Omega^2 L^4}{EI}$, and the dimensionless coordinate $\zeta = \frac{z}{L}$, we have the dimensionless differential equation

$$\frac{d^4}{dz^4}u(\zeta) + \alpha\frac{\partial^2}{\partial z^2}u(\zeta) - \beta\, u(\zeta) = 0.$$

Define $R = \sqrt{-\frac{\alpha}{2} + \sqrt{\frac{\alpha^2}{4} + \beta}}, S = \sqrt{\frac{\alpha}{2} + \sqrt{\frac{\alpha^2}{4} + \beta}}$, and the general solutions are

$$u(\zeta) = A\ sinh(R\ \zeta) + B\ cosh(R\ \zeta) + C\ sin(S\ \zeta) + D\ cos(S\ \zeta)$$

with the boundary conditions

$$u(0) = u(1) = u'(0) = u'(1) = 0.$$

Theses equations lead to

$$\begin{gathered} B + D = 0 \\ A\ sinh(R) + B\ cosh(R) + C\ sin(S) + D\ cos(S) = 0 \\ A\ R + C\ S = 0 \\ A\ R\ cosh(R) + B\ R\ sinh(R) + C\ S\ cos(S) - D\ S\ sin(S) = 0 \end{gathered}$$

For non-trivial solution, the characteristic equation is

$$\begin{vmatrix} 0 & 1 & 0 & 1 \\ sinh(R) & cosh(R) & sin(S) & cos(S) \\ R & 0 & S & 0 \\ R\,cosh(R) & R\,sinh(R) & S\,cos(S) & -S\,sin(S) \end{vmatrix} = 0.$$

When the axial load parameter $\alpha = 0$, which is the case with whirling only, we get the first critical whirling speed parameter $\beta_{max} = 500.564$. When the whirling speed parameter $\beta = 0$, which is the case with the constant axial load only, the first critical axial load parameter $\alpha_{max} = 4\,\pi^2$. For each different axial load parameter smaller than α_{max}, there is a corresponding whirling speed parameter smaller than β_{max} to make the drill-string buckle. As the axial load parameter α increased from 0 to α_{max}, the whirling speed parameter β is decreased from β_{max} to 0. The two values comprise of a critical combination of the axial load parameter and the whirling speed parameter. The interaction of critical combinations of the axial load parameter and the whirling speed parameter is shown in Figure 3.10.

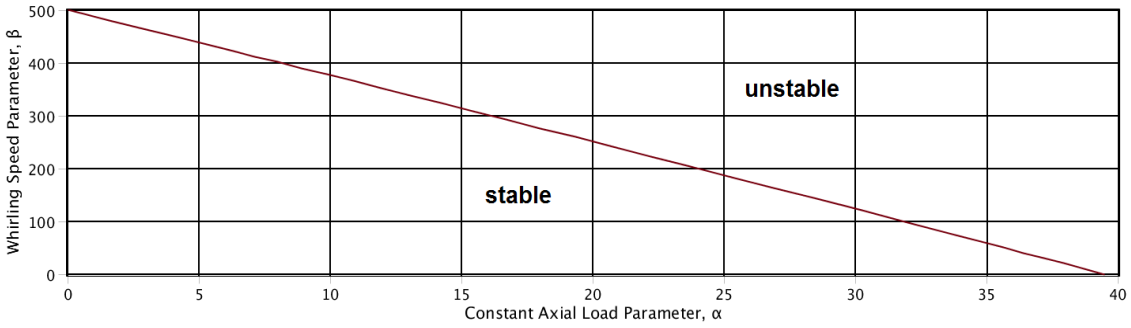

Figure 3.10 Interaction of α and β

Since the mode shape is different for each critical combination, we choose the specific case with $\alpha = \pi^2, \beta = 378.768$ to check the mode shape of the deflection function.

Substituting them into R and S, we have $R = 3.890$ and $S = 5.000$ for this specified case. The mode shape is

$$f_{MS} = cosh(3.890\,\zeta) - 0.960\,sinh(3.890\,\zeta) - cos(5.000\,\zeta) + 0.747\,sin(5.000\,\zeta)$$

The mode shape given by the equation above is shown in Figure 3.11.

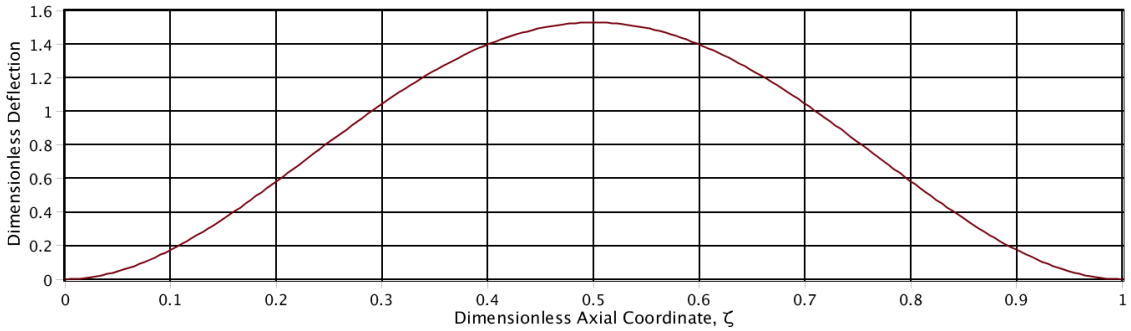

Figure 3.11 Mode Shape for the Case with $\alpha = \pi^2, \beta = 378.768$

The maximum deflection of the solution is arbitrary and we normalize it to 1. We found the maximum deflection is located at $\zeta = 0.5$. We have the function of the deflection as below.

$$u(\zeta) = 0.654\,cosh(3.890\,\zeta) - 0.628\,sinh(3.890\,\zeta) - 0.654\,cos(5.000\,\zeta) + 0.489\,sin(5.000\,\zeta)$$

The plot of the deflection is shown in Figure 3.12.

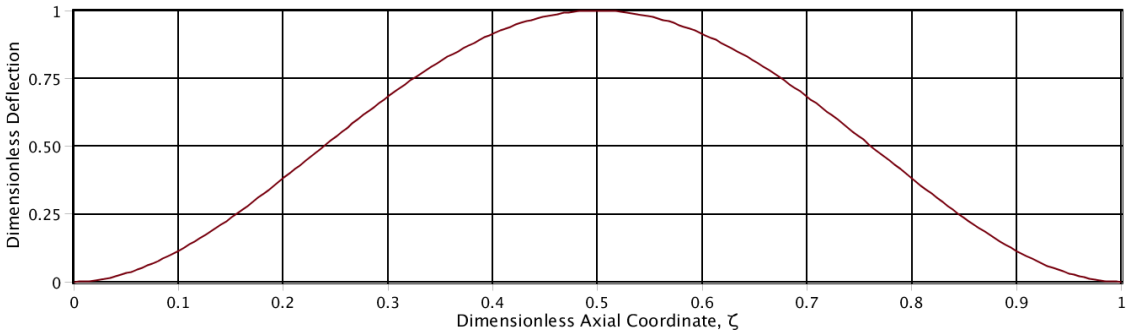

Figure 3.12 Deflection for the Case with $\alpha = \pi^2, \beta = 378.768$

3.2.5 Constant Axial Load and End Torque

With the constant axial load and the end torque applied to the drill-string together, we now have a non-planar buckling problem. At a critical combination of the axial load and the end torque, the system becomes unstable and the drill-string buckles. The differential equation of the system for the steady state is simplified and shown as below

$$EI\ \frac{\partial^4}{\partial z^4}u(z) + M\frac{\partial^3}{\partial z^3}v(z) + P\frac{\partial^2}{\partial z^2}u(z) = 0$$
$$EI\ \frac{\partial^4}{\partial z^4}v(z) - M\frac{\partial^3}{\partial z^3}u(z) + P\frac{\partial^2}{\partial z^2}v(z) = 0$$

.

Define the axial load parameter $\alpha = \frac{PL^2}{EI}$, the end torque parameter $\lambda = \frac{ML}{EI}$, and the dimensionless coordiante $\zeta = \frac{z}{L}$, and introduce a complex deflection $r(\zeta) = u(\zeta) + i\ v(\zeta)$, we have the dimensionless differential equation for this case

$$\frac{d^4}{dz^4}r(\zeta) - i\ \lambda\ \frac{d^3}{dz^3}r(\zeta) + \alpha\ \frac{d^2}{dz^2}r(\zeta) = 0.$$

Define $R = \frac{1}{2}(\lambda + \sqrt{\lambda^2 + 4\ \alpha})$, $S = \frac{1}{2}(\lambda - \sqrt{\lambda^2 + 4\ \alpha})$, and the general solutions are

$$r(\zeta) = (A_1 + i\,A_2)(\cos(R\,\zeta) + i\,A_2\sin(R\,\zeta)) + (A_3 + i\,A_4)(\cos(S\,\zeta) + i\,A_4\sin(S\,\zeta))$$
$$+ (A_5 + i\,A_6)\zeta + A_7 \; + i\,A_8$$

with the boundary conditions

$$r(0) = r(1) = r'(0) = r'(1) = 0.$$

Appling the boundary conditions to the dimensionless differential equation, we get

$$\begin{gathered} A_1 + A_3 + A_7 = 0 \\ -R\,A_2 - S\,A_4 + A_5 = 0 \\ A_2 + A_4 + A_8 = 0 \\ R\,A_1 + S\,A_3 + A_6 = 0 \\ A_1\,cos(R) - A_2\,sin(R) + A_3\,cos(S) - A_4\,sin(S) + A_5 \; + A_7 = 0 \\ -A_1 R\,sin(R) - A_2\,R\,cos(R) - \; A_3 S\,sin(S) - A_4\,S\,cos(S) + A_5 \; = 0 \\ A_1\,sin(R) + A_2\,cos(R) + A_3\,sin(S) + A_4\,cos(S) + A_6 + \; A_8 = 0 \\ A_1\,R\,cos(R) - \; A_2\,R\,sin(R) + A_3\,S\,cos(S) - \; A_4\,S\,sin(S) + \; A_6 = 0 \end{gathered} .$$

For non-trivial solution, the characteristic equation is

$$\begin{vmatrix} 1 & 0 & 1 & 0 & 0 & 0 & 1 & 0 \\ 0 & -R & 0 & -S & 1 & 0 & 0 & 0 \\ 0 & 1 & 0 & 1 & 0 & 0 & 0 & 1 \\ R & 0 & S & 0 & 0 & 1 & 0 & 0 \\ cos(R) & -sin(R) & cos(S) & -sin(S) & 1 & 0 & 1 & 0 \\ -R\,sin(R) & -R\,cos(R) & -R\,sin(S) & -R\,cos(S) & 1 & 0 & 0 & 0 \\ sin(R) & cos(R) & sin(S) & cos(S) & 0 & 1 & 0 & 1 \\ R\,cos(R) & -R\,sin(R) & S\,cos(S) & -S\,sin(S) & 0 & 1 & 0 & 0 \end{vmatrix} = 0.$$

When the axial load parameter $\alpha = 0$, which is the case with the end torque only, we get the first critical end torque parameter $\lambda_{max} = 8.987$. When the constant end torque parameter $\lambda = 0$, which is the case with the constant axial load only, the first critical axial load parameter $\alpha_{max} = 39.478$. For each different axial load parameter smaller than α_{max}, there is a corresponding constant end torque parameter smaller than λ_{max} to

make the drill-string buckle. As the axial load parameter α increased from 0 to α_{max}, the constant end torque parameter λ is decreased from λ_{max} to 0. The two values comprise of a critical combination of the axial load parameter and the constant end torque parameter. The interaction of critical combinations of the constant axial load parameter and the constant end torque parameter is shown in Figure 3.13.

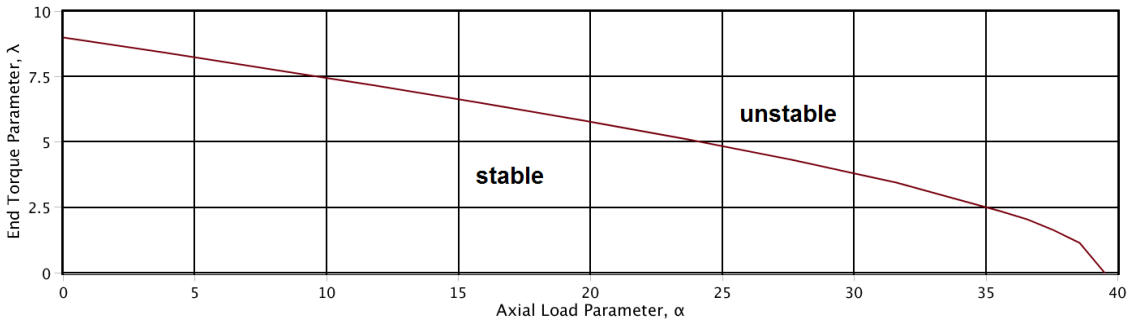

Figure 3.13 Interaction of α and λ

Since the mode shape is different for each critical combination, we choose the specific case with $\alpha = \pi^2, \lambda = 7.472$ to check the mode shape of the deflection function. Substituting them into R and S, we have $R = 8.875$ and $S = -0.338$ for this specified case. This mode shape has two different functions as

$$f1_{MS} = 0.0293\ cos(8.875\ \zeta) + 0.295\ sin(8.875\ \zeta) - 44.488\ cos(0.338\ \zeta)$$
$$+ 0.295\ sin(0.338\ \zeta) - 2.715\ \zeta + 44.459$$

$$f2_{MS} = 0.600\ cos(8.875\ \zeta) - 0.060\ sin(8.875\ \zeta) - 0.600\ cos(0.338\ \zeta)$$
$$- 90.599\ sin(0.338\ \zeta)31.153\ \zeta$$

The mode shape given by the equation above is shown in Figure 3.14.

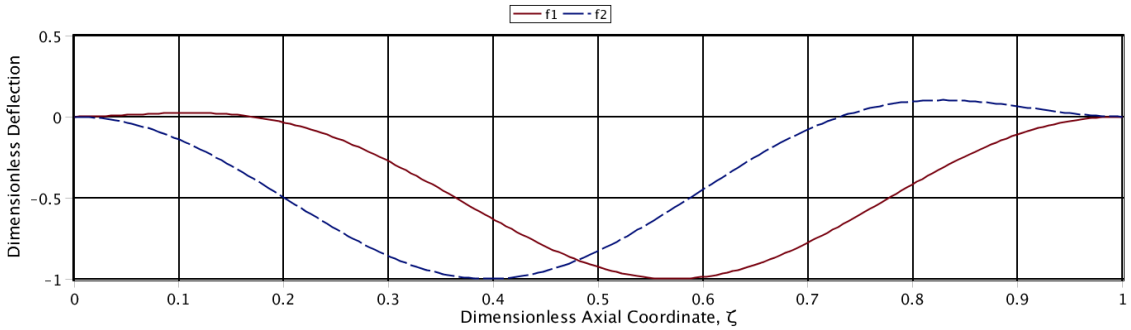

Figure 3.14 Mode Shape for the Case with $\alpha = \pi^2, \lambda = 7.472$

A_7 and A_8 are chosen to describe the deflection functions as below

$$u(\zeta) = A_7\, f1_{MS} + A_8\, f2_{MS}$$
$$v(\zeta) = A_8\, f1_{MS} - A_7\, f2_{MS}.$$

A_7 and A_8 can be any arbitrary values and the maximum deflection of the drill-string is arbitrary. We found the maximum deflection is located at $\zeta = 0.571$ for the first function of the mode shape and $\zeta = 0.395$ for the second function of the mode shape. We set $A_7 = A_8 = 1$, which makes the ratio of the two coefficients equal to 1, to check the deflections of the drill-string. The maximum deflections have been normalized to ±1 and the deflection functions are below as

$$u(\zeta) = 0.151\, cos(8.617\, \zeta) + 0.252\, sin(8.617\, \zeta) - 2.843\, cos(1.145\, \zeta)$$
$$- 2.440\, sin(1.145\, \zeta) + 0.627\, \zeta + 2.692$$

$$v(\zeta) = -0.574\, cos(8.617\, \zeta) + 0.0.345\, sin(8.617\, \zeta) - 5.568\, cos(1.145\, \zeta)$$
$$+ 6.486\, sin(1.145\, \zeta) - 10.398\, \zeta + 6.142$$

We found the maximum deflection is located at $\zeta = 0.485$ for the deflection in the direction of the axis Ox and $\zeta = 0.679$ in the direction of the axis Oy.

The deflection plots are shown in Figure 3.15.

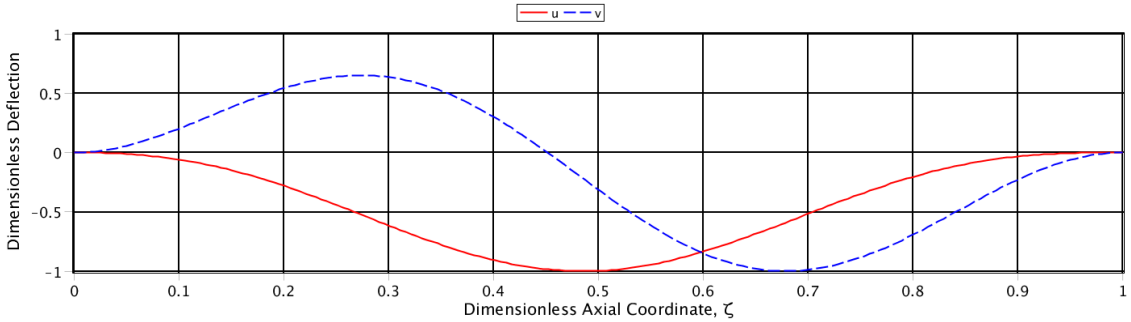

Figure 3.15 Deflections for the Case with $\alpha = \pi^2, \lambda = 7.472$

We know that changing the ratio of A_7 and A_8 is equivalent to a rigid-body rotation of the mode shape relative to the coordinate system O-XYZ. We choose 5 different ratios of A_7 and A_8 to check the deflections of the drill-string. Figure 3.16 is the radial deflection (the maximum deflection in radial direction at every cross section) plot with 5 different ratios of A_7 and A_8. We can see that all curves are same, which mean that the drill-string has same radial deflections at any cross section.

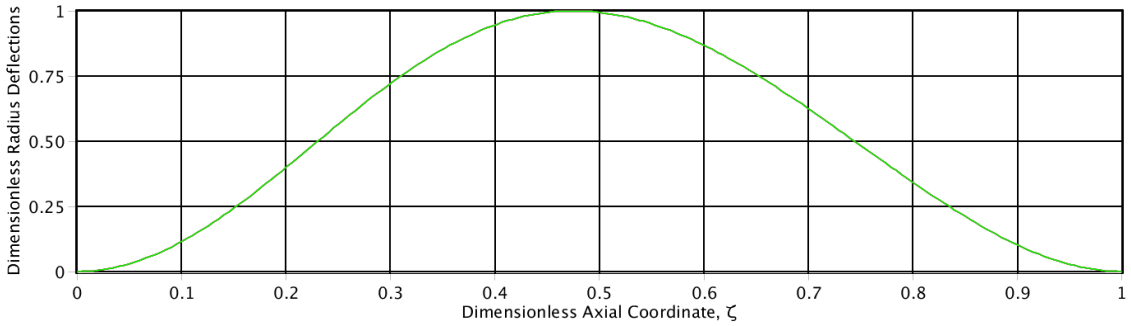

Figure 3.16 Radial Deflections with Different Ratios of A_7 and A_8

Figure 3.17 is the 3-D plot of the radial deflections with different ratios of A_7 and A_8. Figure 3.18 is the same deflections looking downward from the top end of the drill-string.

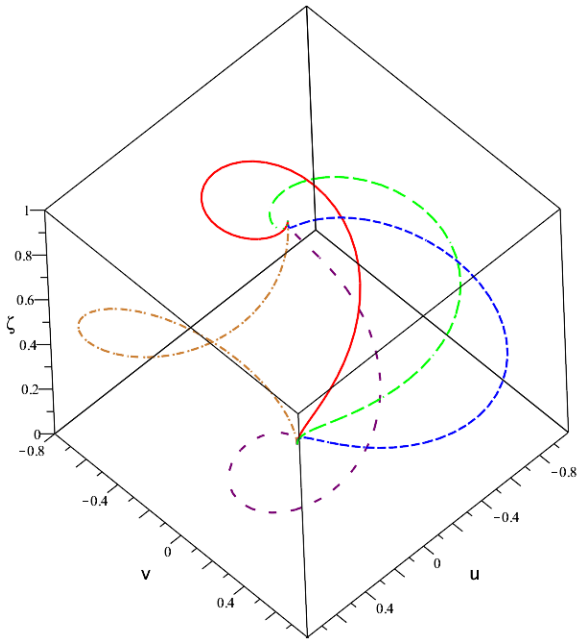

Figure 3.17 Radial Deflections with Different Ratio of A_7 and A_8

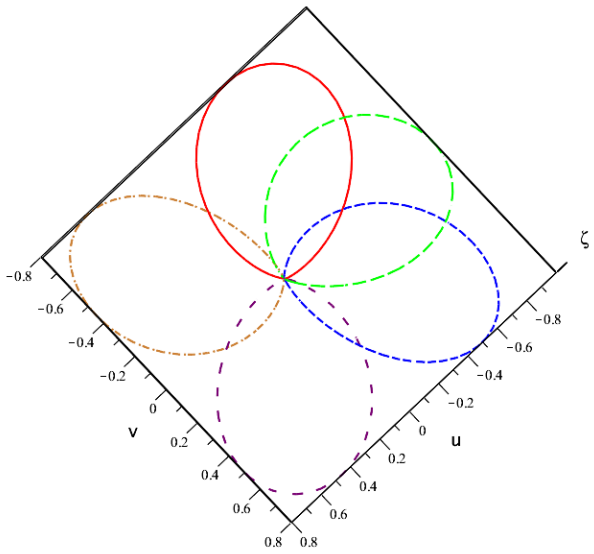

Figure 3.18 Vertical View of Radial Deflections with Different Ratio of A_7 and A_8

CHAPTER 4

THE RAYLEIGH-RITZ SOLUTIONS FOR COMPLEX CASES

This chapter introduces the Rayleigh-Ritz solutions for some complex cases with different loading conditions. The simple cases solved in Chapter 3 are also solved with the Rayleigh-Ritz method. The first critical values of different parameters are obtained and the corresponding mode shapes are illustrated.

4.1 Introduction

When the loading conditions get more complex, it is difficult, for some cases impossible, to analyze the stability of a drill-string system with analytical methods. Table 4.1 lists loading cases without analytical solutions.

Table 4.1 Loading Cases without Analytical Solutions

	Axial Load	Whirl	Torsion	Distributed Axial Load
1	No	Yes	Yes	No
2	Yes	Yes	Yes	No
3	Yes	No	No	Yes
4	No	No	Yes	Yes
5	Yes	No	Yes	Yes
6	Yes	Yes	Yes	Yes

We use the Rayleigh-Ritz energy method to solve these loading cases. We assume that the drill-string has the same boundary conditions as before, which a clamped constraint at the bottom end and a clamped constraint (but slide-free in axial direction) at the top end. So, for both ends, there is zero deflection and zero slope.

4.2 The Rayleigh-Ritz Method

As discussed above, analytical solutions exist for several simple cases. But for more realistic cases, we must use a numerical method. In what follows, we apply the Rayleigh-Ritz method to analyze our problem. To illustrate the Rayleigh-Ritz method solving this problem, we first use it to get numerical solutions for the simple cases with analytical solution. Then we apply the method to more complicated cases.

When the drill-string whirls at a constant angular velocity ω, its kinetic energy is

$$T = \frac{1}{2}\int_0^L m\,\omega^2\,[u(z)^2 + v(z)^2]^2\,dz.$$

As a result of its bending, the drill-string's elastic strain energy is

$$U = \frac{1}{2}\int_0^L EI\,[(u''(z))^2 + (v''(z))^2]\,dz.$$

The work done by the constant axial load is [56]

$$W_P = \frac{1}{2}\int_0^L P\,[(u'(z))^2 + (v'(z))^2]\,dz.$$

The work done by the applied end torque is [21]

$$W_M = \frac{1}{2}\int_0^L M\,[u'(z)\,v''(z)\; - u''(z)\,v'(z)]\,dz.$$

By Hamilton's principle, the displacements satisfy all boundary conditions at $z = 0$ and $z = L$, and also minimize the Hamiltonian, which is

$$H = T - U + W_P + W_M.$$

In the Rayleigh-Ritz method, we approximate the deflections of the drill-string with a linear combination of some chosen functions. For n-term approximation,

$$u(z) = L\sum_1^n a_n\,f_n(\zeta) = L\,\{f(\zeta)\}^T\,\{a\}$$
$$v(z) = L\sum_1^n b_n\,f_n(\zeta) = L\,\{f(\zeta)\}^T\,\{b\}$$

where $\zeta = \frac{z}{L}$ with yet-to-be-determined displacement functions

$$\{f(\zeta)\} = \begin{Bmatrix} f_1(\zeta) \\ f_2(\zeta) \\ f_3(\zeta) \\ \cdot \\ \cdot \\ f_n(\zeta) \end{Bmatrix}$$

and constants

$$\{a\} = \begin{Bmatrix} a_1 \\ a_2 \\ a_3 \\ \cdot \\ \cdot \\ a_n \end{Bmatrix} \; and \; \{b\} = \begin{Bmatrix} b_1 \\ b_2 \\ b_3 \\ \cdot \\ \cdot \\ b_n \end{Bmatrix}.$$

The N-term approximation requires polynomials of order n+3 in ζ. The complexity of the problem requires a relatively high-order Rayleigh-Ritz method for accurate solutions. Seven terms are used to generate all of the results discussed below. Functions used for the seven-term approximation are

$$\begin{aligned} f_1(\zeta) &= \zeta^2 - 2\,\zeta^3 + \zeta^4 \\ f_2(\zeta) &= \zeta^3 - 2\,\zeta^4 + \zeta^5 \\ f_3(\zeta) &= \zeta^4 - 2\,\zeta^5 + \zeta^6 \\ f_4(\zeta) &= \zeta^5 - 2\,\zeta^6 + \zeta^7 \\ f_5(\zeta) &= \zeta^6 - 2\,\zeta^7 + \zeta^8 \\ f_6(\zeta) &= \zeta^7 - 2\,\zeta^8 + \zeta^9 \\ f_7(\zeta) &= \zeta^8 - 2\,\zeta^9 + \zeta^{10} \end{aligned} .$$

All of these functions satisfy all of the boundary conditions of the problem. The minimization of the Hamiltonian implies that

$$\begin{aligned} \frac{\partial H}{\partial a_i} &= 0, i = 1,2,\dots,7 \\ \frac{\partial H}{\partial b_i} &= 0, i = 1,2,\dots,7 \end{aligned} .$$

Let the dimensionless Hamiltonian be

$$H^* = \frac{LH}{EI}.$$

It follows that

$$H^* = \frac{1}{2}\{c\}^T\,[G]\,\{c\}$$

where

$$\{c\} = \begin{Bmatrix} a_1 \\ \cdot \\ \cdot \\ a_7 \\ b_1 \\ \cdot \\ \cdot \\ b_7 \end{Bmatrix}$$

$$[G] = \beta\,[M] - [K] + \alpha\,[J] + \lambda\,[Q]$$

$$M_{ij} = \int_0^1 f_i(\zeta)\, f_j(\zeta)\, d\zeta$$

$$K_{ij} = \int_0^1 f_i''(\zeta)\, f_j''(\zeta)\, d\zeta$$

$$J_{ij} = \int_0^1 f_i'(\zeta)\, f_j'(\zeta)\, d\zeta$$

$$Q_{ij} = \int_0^1 [f_i'(\zeta)\, f_j''(\zeta) - [f_i''(\zeta)\, f_j'(\zeta)]\, d\zeta$$

From left to right, the four terms in the matrix $[G]$ correspond to the drill-string's kinetic energy, its elastic strain energy, the work done by the axial load and the work done by the torque applied at $z = 0$.

Hamilton's principle then requires that $[G]\{c\} = 0$. Critical combinations of the these different parameters occur when

$$|G| = 0.$$

And the form of $[G]$ is different for different loading conditions.

When there is a variable axial load (the self-weight of the drill-string) in the system, it is again much harder to find the analytical solution for the system. The matrix $[J]$ will not be constant because of the self-weight of the drill-string. Let the WOB be P_L and the tensile load at the top (the hook load) be P_H. The hook load P_H is

$$P_H = \int_0^L mgdz - P_L$$

and the axial load $P(z)$ at an arbitrary cross section is

$$P(z) = P_L - \int_0^z mgdz$$

The hook load P_H and the axial load $P(z)$ are related by

$$P_H = mgL - P_L$$
$$P(z) = P_H + mg(z - L) = mgz - P_H.$$

The work done by the axial load $P(z)$ is

$$W_P = \frac{1}{2}\int_0^L (mgz - P_H)\,[(u'(z))^2 + (v'(z))^2]\,dz.$$

Define the self-weight parameter $\varphi = \frac{mgL^3}{EI}$, the hook load parameter $\gamma = \frac{P_H L^2}{EI}$. Then the matrix $[G]$ becomes

$$[G] = \beta\,[M] - [K] + \varphi\,[J_V] - \gamma\,[J_H]$$

in which

$$J_{V\,ij} = \int_0^1 \zeta\, f_i'(\zeta)\, f_j'(\zeta)\, d\zeta$$

$$J_{H\,ij} = \int_0^1 f_i'(\zeta)\, f_j'(\zeta)\, d\zeta$$

Obviously, the hook load cannot be larger than the drill-string weight, and this gives $\varphi - \gamma > 0$. The Rayleigh-Ritz method can then be applied as before.

4.3 Solving Cases with Different Loading Conditions

4.3.1 Constant Axial Load Only

With the constant axial load applied only and no other loads applied, the matrix $[G]$ is simplified to

$$[G] = -[K] + \alpha\,[J]$$

Substituting the predefined polynomial function into this equation and then solving the equation $|G| = 0$ by the Hamilton's principle gives the first critical axial load parameter $\alpha = 39.487$ and the first critical axial load $P_{cr} = \frac{\alpha\, EI}{L^2}$. We can get the mode shape for the first critical load as

$$f_{MS} = 0.972\,\zeta^2 + 0.004\,\zeta^3 - 3.253\,\zeta^4 + 0.359\,\zeta^5 + 2.780\,\zeta^6 + 3.514\,\zeta^7 - 8.379\,\zeta^8 + 5.000\,\zeta^9 - \zeta^{10}.$$

The mode shape given by the equation above is shown in Figure 4.1. Because we can choose an arbitrary coefficient in front of the function of the mode shape to have the

deflection function of the drill-string, the maximum deflection of the solution is arbitrary. We found the maximum deflection is located at $\zeta = 0.5$ and we normalize it to 1.

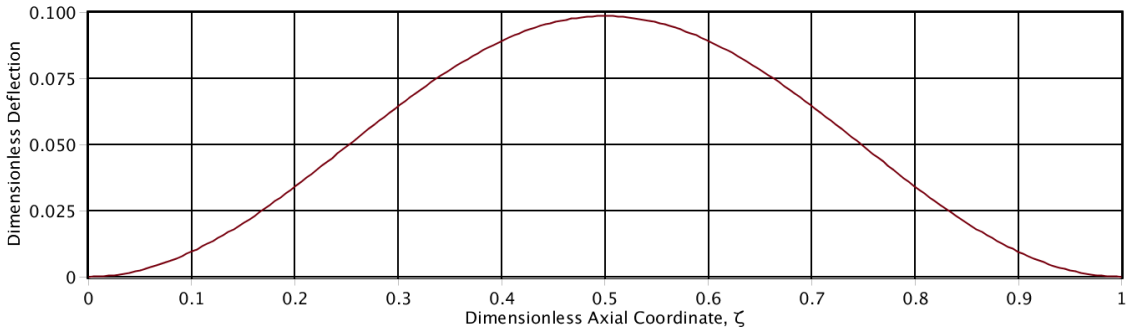

Figure 4.1 Mode Shape for the Case with Constant Axial Load Only

The function of the deflection is

$$u(\zeta) = 9.869\,\zeta^2 + 0.040\,\zeta^3 - 33.004\,\zeta^4 + 3.648\,\zeta^5 + 28.222\,\zeta^6 + 35.668\,\zeta^7 - 85.042\,\zeta^8 + 50.750\,\zeta^9 - 10.150\,\zeta^{10}.$$

The plot of the deflection is shown in Figure 4.2.

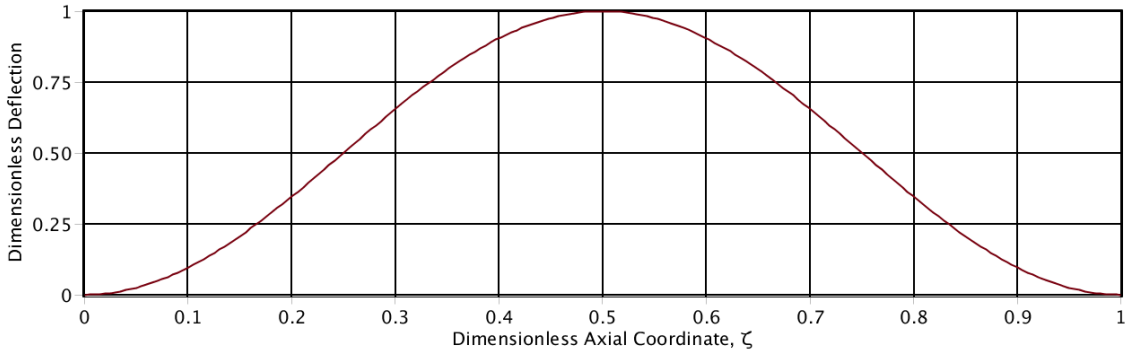

Figure 4.2 Deflection for the Case with Constant Axial Load Only

4.3.2 Constant Whirling Only

When the drill-string is whirling only and no other loads applied, the matrix $[G]$ is simplified to

$$[G] = -[K] + \beta\,[M]$$

Substituting the predefined polynomial function into this equation and then solving the equation $|G| = 0$ by the Hamilton's principle gives the first critical whirling speed parameter $\beta = 500.564$ and the first critical whirling speed $\Omega_{cr} = \sqrt{\frac{\beta\, EI}{mL^4}}$. We can get the mode shape for the first critical load as

$$f_{MS} = 14.510\,\zeta^2 + 22.475\,\zeta^3 - 0.047\,\zeta^4 + 0.311\,\zeta^5 + 2.780\,\zeta^6 + 18.946\,\zeta^7 - 10.328\,\zeta^8 - 4.918\,\zeta^9 - \zeta^{10}.$$

The mode shape given by the equation above is shown in Figure 4.3.

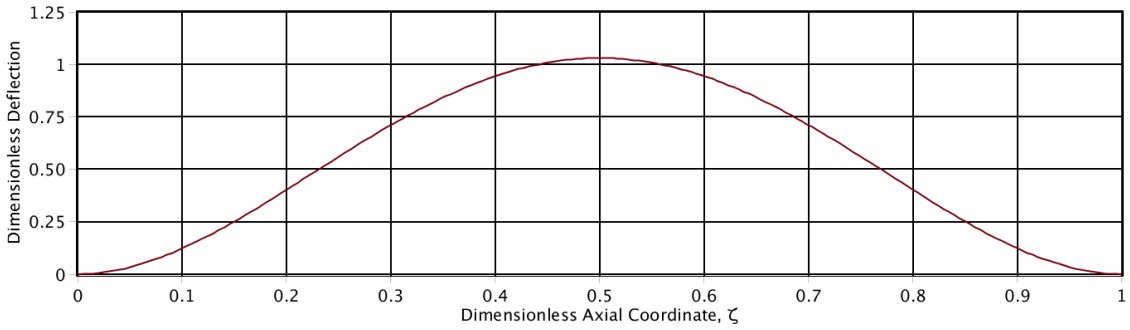

Figure 4.3 Mode Shape for the Case with Constant Whirling Only

The maximum deflection of the solution is arbitrary because the coefficient in front of the function of the mode shape is arbitrary. We found the maximum deflection is located at $\zeta = 0.5$ for this case and we normalize it to 1. The function of the deflection is

$u(\zeta) = 14.088\,\zeta^2 - 21.820\,\zeta^3 - 0.045\,\zeta^4 + 0.302\,\zeta^5 + 18.393\,\zeta^6 - 10.027\,\zeta^7 - 4.775\,\zeta^8 + 4.854\,\zeta^9 - 0.971\,\zeta^{10}$.

The plot of the deflection is shown in Figure 4.4.

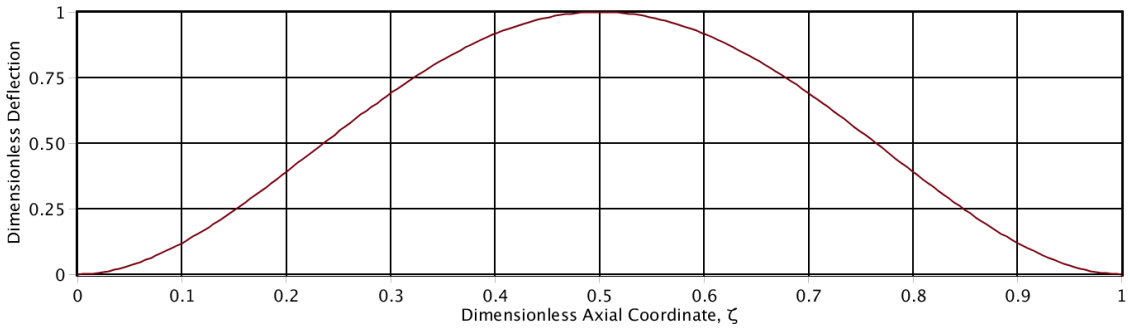

Figure 4.4 Deflection for the Case with Constant Whirling Only

4.3.3 Constant End Torque Only

With only the constant end torque applied and no other loads applied, the matrix $[G]$ is simplified to

$$[G] = -[K] + \lambda\,[Q]$$

Substituting the predefined polynomial function into this equation and then solving the equation $|G| = 0$ by the Hamilton's principle gives the first critical end torque parameter $\lambda = 8.987$ and the first critical end torque $M_{cr} = \frac{8.987\,EI}{L}$. We can get the function of mode shape for the first critical load. This mode shape has two different functions as

$$f1_{MS} = 29.218\,\zeta^2 - 29.589\,\zeta^3 - 82.966\,\zeta^4 - 517.100\,\zeta^5 + 2292.280\,\zeta^6 - 3143.530\,\zeta^7 + 1866.463\,\zeta^8 - 414.775\,\zeta^9$$

$$f2_{MS} = -0.000607\,\zeta^2 - 35.046\,\zeta^3 + 26.645\,\zeta^4 + 59.581\,\zeta^5 + 310.403\,\zeta^6$$
$$- 1178.719\,\zeta^7 + 1414.238\,\zeta^8 - 746.379\,\zeta^9 + 149.277\,\zeta^{10}.$$

The mode shape given by the equation above is shown in Figure 4.5.

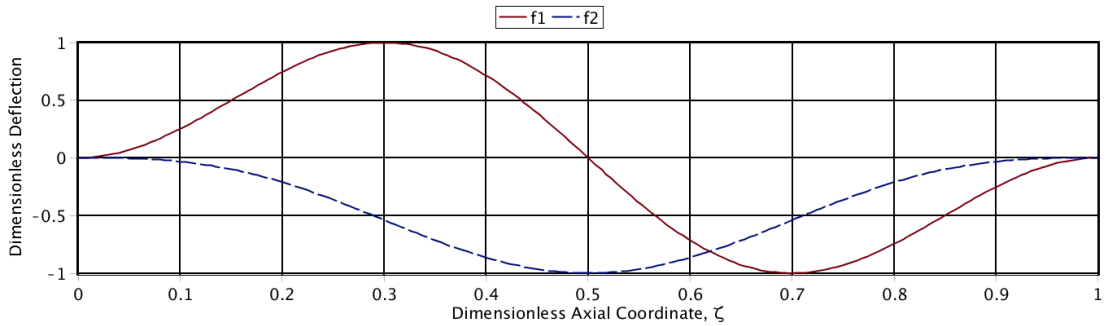

Figure 4.5 Mode Shape for the Case with Constant End Torque Only

A_7 and A_8 are chosen to describe the deflection functions as below

$$u(\zeta) = A_7\,f1_{MS} + A_8\,f2_{MS}$$
$$v(\zeta) = A_8\,f1_{MS} - A_7\,f2_{MS}.$$

A_7 and A_8 are any arbitrary values and the maximum deflections of the solution are arbitrary. We found the maximum deflection is located at $\zeta = 0.301$ for the first function of the mode shape and $\zeta = 0.500$ for the second function of the mode shape. We set $A_7 = A_8 = 1$, which makes the ratio of the two coefficients equal to 1, to check the deflections of the drill-string. The maximum deflections have been normalized to -1 and the deflection functions are below as

$$u(\zeta) = 10.154\,\zeta^2 - 40.706\,\zeta^3 - 5.705\,\zeta^4 - 128.001\,\zeta^5 + 1066.148\,\zeta^6$$
$$- 2115.767\,\zeta^7 + 1876.363\,\zeta^8 - 792.069\,\zeta^9 + 129.584\,\zeta^{10}$$

$$v(\zeta) = -10.156\,\zeta^2 - 20.140\,\zeta^3 + 51.969\,\zeta^4 + 231.458\,\zeta^5 - 527.281\,\zeta^6 + 69.343\,\zeta^7 + 579.004\,\zeta^8 - 503.790\,\zeta^9 + 129.593\,\zeta^{10}.$$

We found the maximum deflection is located at $\zeta = 0.591$ for the deflection in the direction of the axis Ox and $\zeta = 0.409$ for the deflection in the direction of the axis Oy. The deflection plots are shown in Figure 4.6.

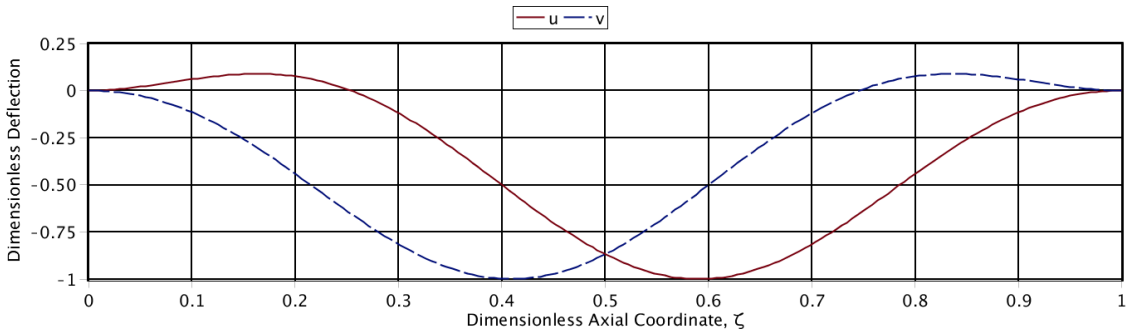

Figure 4.6 Deflection for the Case with Constant End Torque Only

We know that changing the ratio of A_7 and A_8 is equivalent to a rigid-body rotation of the mode shape relative to the coordinate system O-XYZ. We choose 5 different ratios of A_7 and A_8 to check the deflections of the drill-string. Figure 4.7 is the Radial deflection (the maximum deflection in Radial at every cross section) plot with 5 different ratios of A_7 and A_8. We can see that all curves are same, which mean that the drill-string has same radial deflections at any cross section.

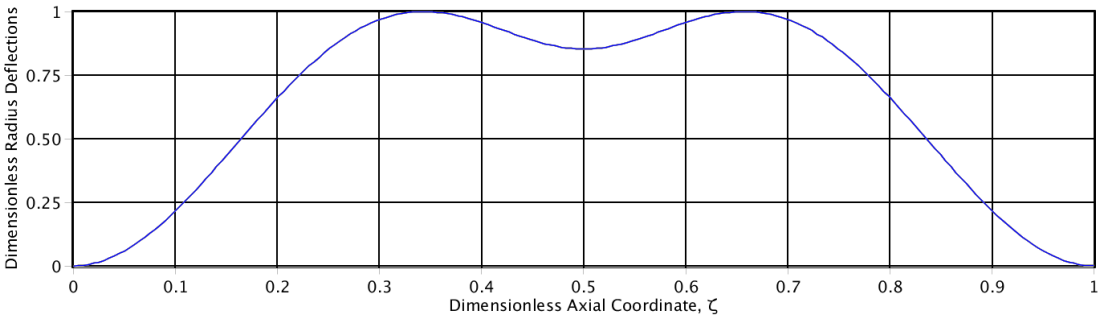

Figure 4.7 Radial Deflections with Different Ratios of A_7 and A_8

Figure 4.8 is the 3-D plot of the radial deflections with different ratios of A_7 and A_8. Figure 4.9 is the same plot when looking downward from the top end of the drill-string.

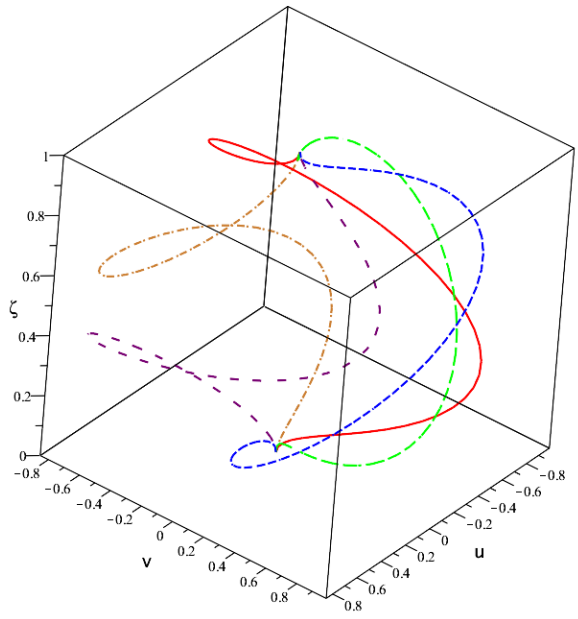

Figure 4.8 Radial Deflections with Different Ratios of A_7 and A_8

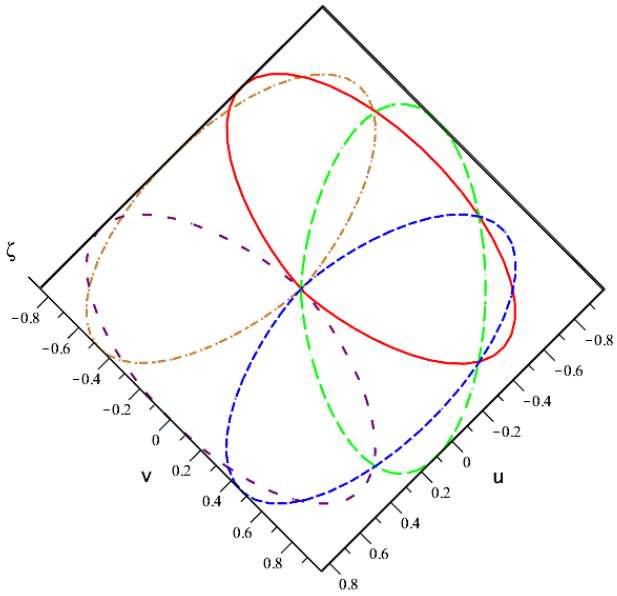

Figure 4.9 Vertical View of Radial Deflections with Different Ratios of A_7 and A_8

4.3.4 Constant Axial Load and Whirling

With the constant axial load is applied while whirling, the matrix $[G]$ is simplified to

$$[G] = -[K] + \beta\,[M] + \alpha\,[J]$$

Substituting the predefined polynomial function into this equation and then solving the equation $|G| = 0$ by the Hamilton's principle gives the critical loads. When the axial load parameter $\alpha = 0$, which is the case with whirling only, we get the first critical whirling speed parameter $\beta_{max} = 500.564$. When the whirling speed parameter $\beta = 0$, which is the case with the constant axial load only, the first critical axial load parameter $\alpha_{max} = 39.478$. For each different axial load parameter smaller than α_{max}, there is a corresponding whirling speed parameter smaller than β_{max} to make the drill-string

buckle. As the axial load parameter α increased from 0 to α_{max}, the whirling speed parameter β is decreased from β_{max} to 0. The two values comprise of a critical combination of the axial load parameter and the whirling speed parameter. The interaction of critical combinations of the axial load parameter and the whirling speed parameter is shown in Figure 4.10.

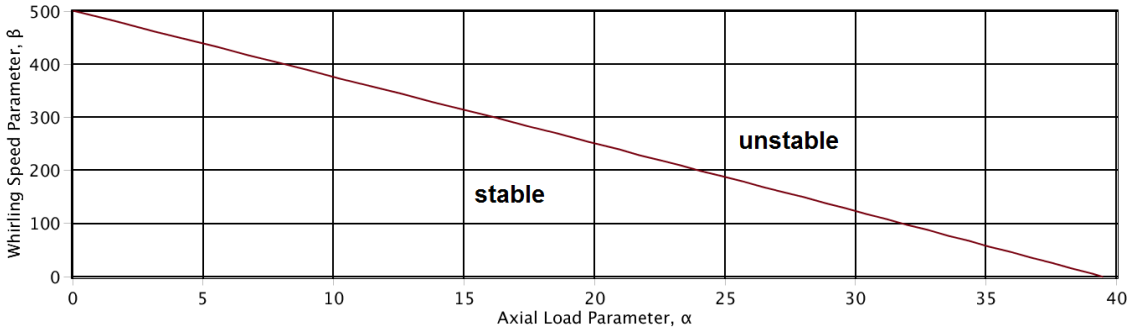

Figure 4.10 Interaction of α and β

Since the mode shape is different for each critical combination, we choose for convenience the specific case with $\alpha = \pi^2, \beta = 378.768$ to illustrate the mode shape for this case. For this specified case, we have the mode shape for the first critical load as below

$$f_{MS} = 7.285\,\zeta^2 - 9.066\,\zeta^3 - 6.020\,\zeta^4 + 4.687\,\zeta^5 + 8.731\,\zeta^6 - 2.823\,\zeta^7 - 6.794\,\zeta^8 + 5.000\,\zeta^9 - \zeta^{10}.$$

The mode shape given by the solution is shown in Figure 4.11.

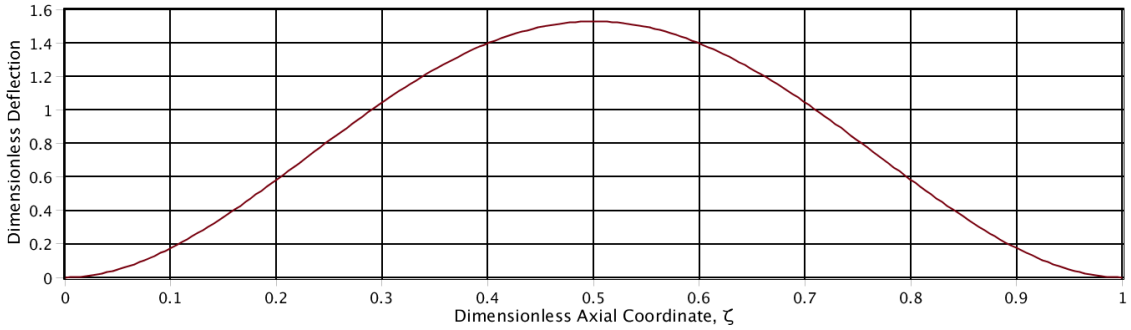

Figure 4.11 Mode Shape for the Case with $\alpha = \pi^2, \beta = 378.768$

As before, the deflection has been normalized relative to its maximum deflection which is located at $\zeta = 0.5$. We have the function of the deflection as below

$$u(\zeta) = 13.131\,\zeta^2 - 16.341\,\zeta^3 - 10.851\,\zeta^4 + 8.449\,\zeta^5 + 15.738\,\zeta^6 - 5.089\,\zeta^7 - 12.247\,\zeta^8 + 9.013\,\zeta^9 - 1.803\,\zeta^{10}.$$

The plot of the deflection is shown in Figure 4.12.

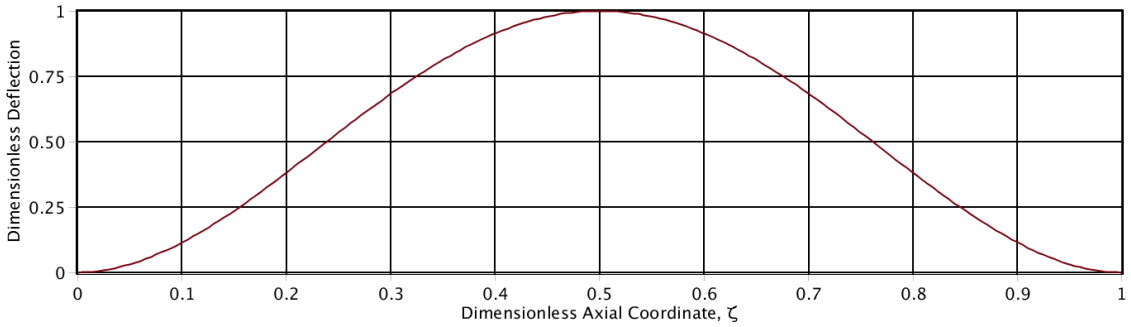

Figure 4.12 Deflection for the Case with $\alpha = \pi^2, \beta = 378.768$

4.3.5 Constant Axial Load and End Torque

With the constant axial load and end torque applied to the drill-string together, the matrix $[G]$ is simplified to

$$[G] = -[K] + \lambda\,[Q] + \alpha\,[J]$$

Substituting the predefined polynomial function into this equation and then solving the equation $|G| = 0$ by the Hamilton's principle gives the critical loads. When the axial load parameter $\alpha = 0$, which is the case with the end torque only, we get the first critical end torque parameter $\lambda_{max} = 8.987$. When the constant end torque parameter $\lambda = 0$, which is the case with the constant axial load only, the first critical axial load parameter $\alpha_{max} = 39.478$. For each different axial load parameter smaller than α_{max}, there is a corresponding constant end torque parameter smaller than λ_{max} to make the drill-string buckle. As the axial load parameter α increased from 0 to α_{max}, the constant end torque parameter λ is decreased from λ_{max} to 0. The two values comprise of a critical combination of the axial load parameter and the constant end torque parameter. The interaction of critical combinations of the constant axial load parameter and the constant end torque parameter is shown in Figure 4.13.

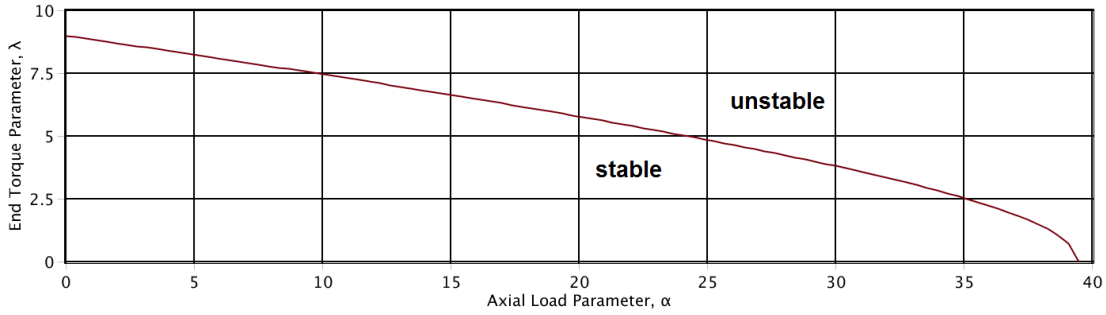

Figure 4.13 Interaction of α and λ

Since the mode shape is different for each critical combination, we choose the specific case with $\alpha = \pi^2, \lambda = 7.472$ to illustrate the mode shape for this case. For this specified

case, this mode shape has two different functions. We have the mode shape for the first critical load as below

$$f1_{MS} = 0.075\,\zeta^2 - 0.108\,\zeta^3 - 0.177\,\zeta^4 - 0.857\,\zeta^5 + 4.328\,\zeta^6 - 6.094\,\zeta^7 + 3.643\,\zeta^8 - 0.810\,\zeta^9$$

$$f2_{MS} = -0.0134\,\zeta^2 - 0.2126\,\zeta^3 + 0.443\,\zeta^4 - 0.673\,\zeta^5 + 3.674\,\zeta^6 - 8.956\,\zeta^7 + 9.739\,\zeta^8 - 5.000\,\zeta^9 + \zeta^{10}.$$

The mode shape given by the equation above is shown in Figure 4.14. A_7 and A_8 are chosen to describe the deflection functions as below

$$u(\zeta) = A_7\,f1_{MS} + A_8\,f2_{MS}$$
$$v(\zeta) = A_8\,f1_{MS} - A_7\,f2_{MS}.$$

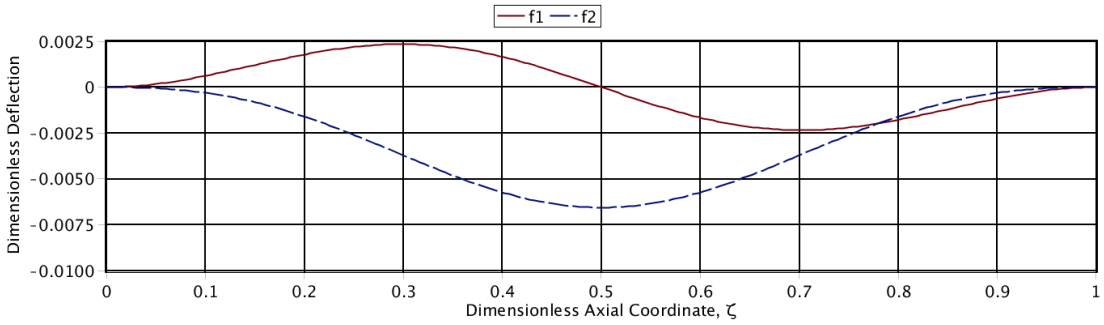

Figure 4.14 Mode Shape for the Case with $\alpha = \pi^2, \lambda = 7.472$

A_7 and A_8 can be any arbitrary values and the maximum deflection of the drill-string is arbitrary. We found the maximum deflection is located at $\zeta = 0.298$ for the first function of the mode shape and $\zeta = 0.500$ for the second function of the mode shape. We set $A_7 = A_8 = 1$, which makes the ratio of the two coefficients equal to 1, to check the deflections of the drill-string. The maximum deflections have been normalized to ±1 and

the deflection functions are shown as below

$$u(\zeta) = 8.292\,\zeta^2 - 43.214\,\zeta^3 + 35.797\,\zeta^4 - 206.420\,\zeta^5 + 1079.319\,\zeta^6 - 2030.118\,\zeta^7 + 1805.109\,\zeta^8 - 783.657\,\zeta^9 + 134.892\,\zeta^{10}$$

$$v(\zeta) = -11.907\,\zeta^2 - 14.018\,\zeta^3 + 83.603\,\zeta^4 + 24.770\,\zeta^5 - 88.260\,\zeta^6 - 386.162\,\zeta^7 + 822.369\,\zeta^8 - 565.298\,\zeta^9 + 134.903\,\zeta^{10}.$$

We found the maximum deflection is located at $\zeta = 0.485$ for the deflection in the direction of the axis Ox and $\zeta = 0.679$ for the deflection in the direction of the axis Oy. The plot of the deflection is shown in Figure 4.15.

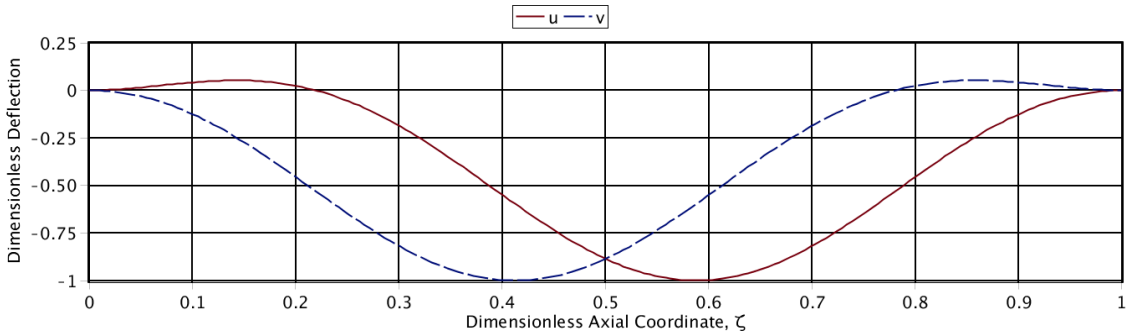

Figure 4.15 Deflections for the Case with $\alpha = \pi^2, \lambda = 7.472$

We know that changing the ratio of A_7 and A_8 is equivalent to a rigid-body rotation of the mode shape relative to the coordinate system O-XYZ. We choose 5 different ratios of A_7 and A_8 to check the deflections of the drill-string. Figure 4.16 is the Radial deflection (the maximum deflection in Radial at every cross section) plot with 5 different ratios of A_7 and A_8. We can see that all curves are same, which mean that the drill-string has same radial deflections at any cross section.

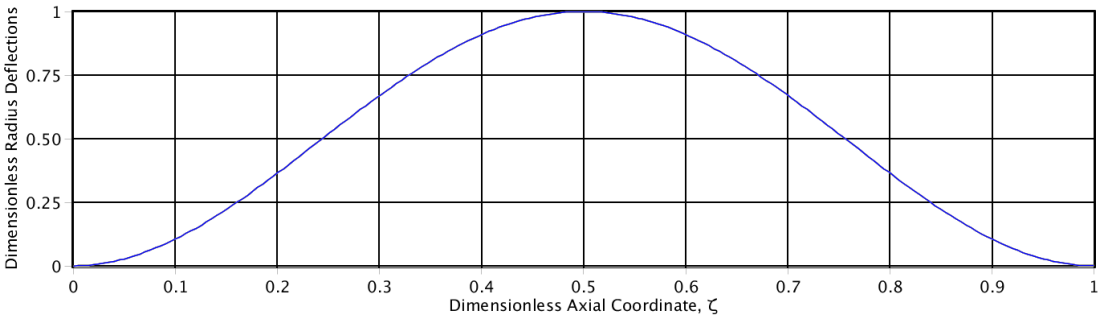

Figure 4.16 Radial Deflections with Different Ratios of A_7 and A_8

Figure 4.17 is the 3-D plot of the radial deflections with different ratios of A_7 and A_8. Figure 4.18 is the same deflections when looking downward from the top end of the drill-string.

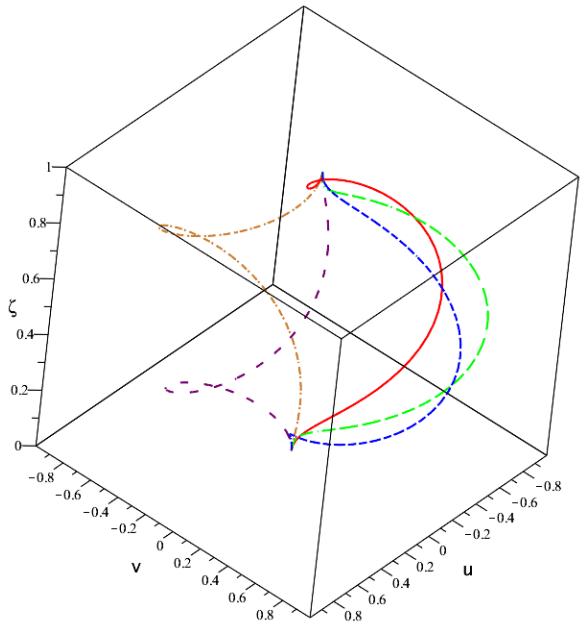

Figure 4.17 Radial Deflections with Different Ratios of A_7 and A_8

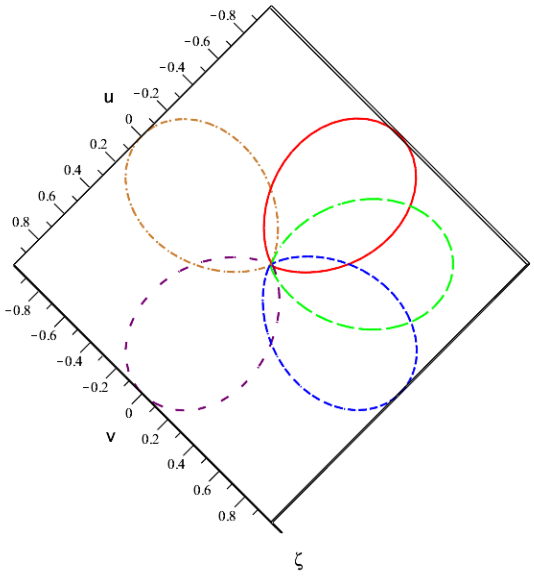

Figure 4.18 Vertical View of Radial Deflections with Different Ratios of A_7 and A_8

4.3.6 Constant Whirling and End Torque

With the constant end torque applied while whirling, the matrix $[G]$ is simplified to

$$[G] = -[K] + \lambda\,[Q] + \beta\,[M]$$

Substituting the predefined polynomial function into this equation and then solving the equation $|G| = 0$ by the Hamilton's principle gives the critical loads. When the whirling speed parameter $\beta = 0$, which is the case with the end torque only, we get the first critical end torque parameter $\lambda_{max} = 8.987$. When the constant end torque parameter $\lambda = 0$, which is the case with the constant whirling only, the first critical whirling speed parameter $\beta_{max} = 500.564$. For each different whirling speed parameter smaller than β_{max}, there is a corresponding constant end torque parameter smaller than λ_{max} to make the drill-string buckle. As the whirling speed parameter β increased

from 0 to β_{max}, the constant end torque parameter λ is decreased from λ_{max} to 0. The two values comprise of a critical combination of the whirling speed parameter and the constant end torque parameter. The interaction of critical combinations of the constant whirling speed parameter and the constant end torque parameter is shown in Figure 4.19.

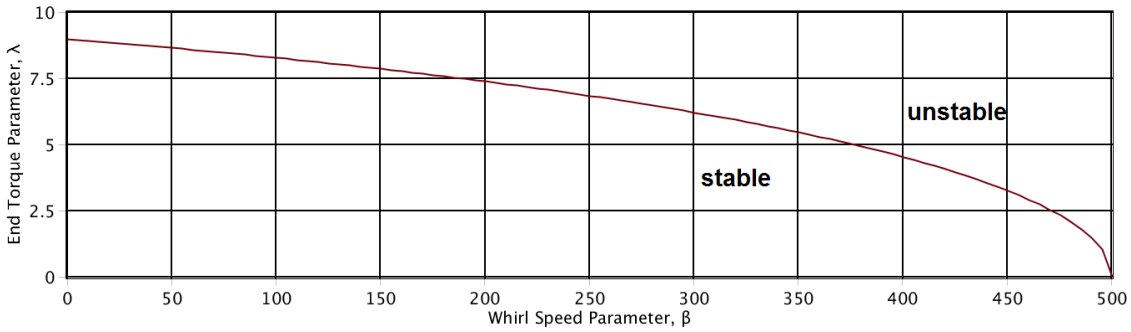

Figure 4.19 Interaction of Interaction of β and λ

Since the mode shape is different for each critical combination, we choose the specific case with $\beta = 110.124, \lambda = 8.190$ to illustrate the mode shape for this case. For this specified case, this mode shape has two different functions. We have the mode shape for the first critical load as below

$$f1_{MS} = 0.136\,\zeta^2 - 0.214\,\zeta^3 - 0.378\,\zeta^4 - 1.192\,\zeta^5 + 6.023\,\zeta^6 - 8.870\,\zeta^7 + 5.362\,\zeta^8 - 1.192\,\zeta^9$$

$$f2_{MS} = -0.0326\,\zeta^2 - 0.323\,\zeta^3 + 0.441\,\zeta^4 + 0.603\,\zeta^5 + 1.235\,\zeta^6 - 7.230\,\zeta^7 + 9.307\,\zeta^8 - 5.000\,\zeta^9 + \zeta^{10}.$$

The mode shape given by the equation above is shown in Figure 4.20.

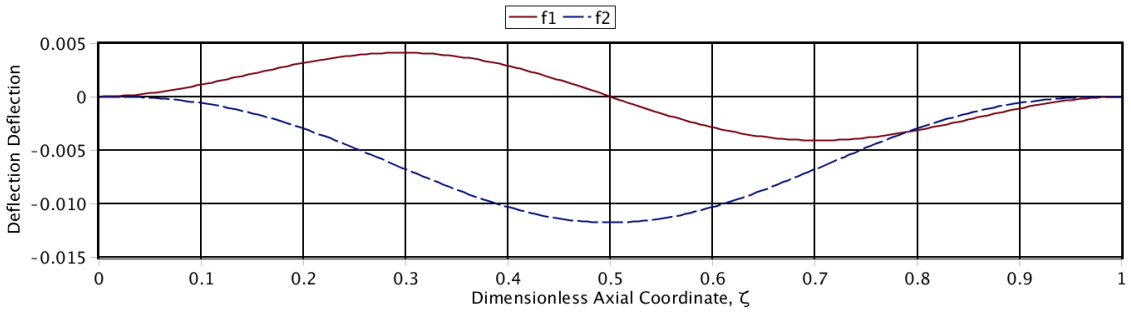

Figure 4.20 Mode Shape for the Case with $\boldsymbol{\beta = 110.124,\ \lambda = 8.190}$

A_7 and A_8 are chosen to describe the deflection functions as below

$$u(\zeta) = A_7\, f1_{MS} + A_8\, f2_{MS}$$
$$v(\zeta) = A_8\, f1_{MS} - A_7\, f2_{MS}.$$

A_7 and A_8 can be any arbitrary values and the maximum deflection of the drill-string is arbitrary. We found the maximum deflection is located at $\zeta = 0.297$ for the first function of the mode shape and $\zeta = 0.500$ for the second function of the mode shape. We set $A_7 = A_8 = 1$, which makes the ratio of the two coefficients equal to 1, to check the deflections of the drill-string. The maximum deflections have been normalized to ±1 and the deflection functions are shown as below

$$u(\zeta) = 7.829\,\zeta^2 - 40.574\,\zeta^3 + 4.752\,\zeta^4 - 19.960\,\zeta^5 + 547.819\,\zeta^6 - 1215.237\,\zeta^7 + 1107.216\,\zeta^8 - 467.324\,\zeta^9 + 75.479\,\zeta^{10}$$

$$v(\zeta) = -12.746\,\zeta^2 - 8.246\zeta^3 + 61.817\,\zeta^4 + 110.014\,\zeta^5 - 361.457\,\zeta^6 + 123.814\,\zeta^7 + 297.788\,\zeta^8 - 287.472\,\zeta^9 + 75.488\,\zeta^{10}.$$

We found the maximum deflection is located at $\zeta = 0.588$ for the deflection in the direction of the axis Ox and $\zeta = 0.412$ for the deflection in the direction of the axis Oy.

The plot of the deflection is shown in Figure 4.21.

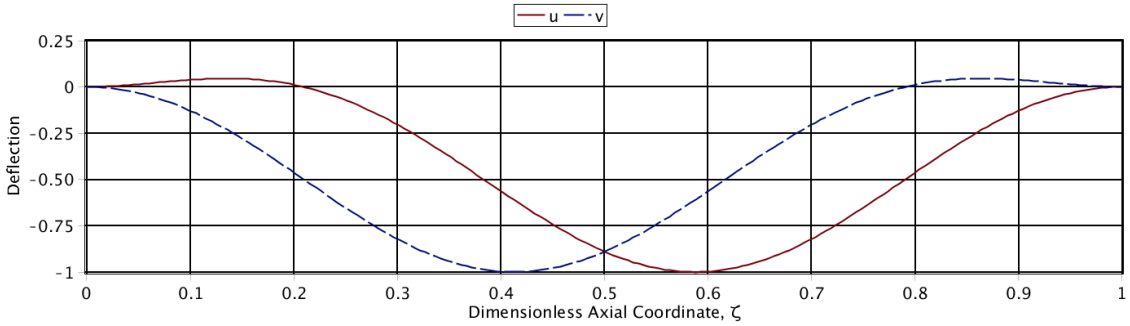

Figure 4.21 Deflection for the Case with $\boldsymbol{\beta = 110.124, \lambda = 8.190}$

We know that changing the ratio of A_7 and A_8 is equivalent to a rigid-body rotation of the mode shape relative to the coordinate system O-XYZ. We choose 5 different ratios of A_7 and A_8 to check the deflections of the drill-string. Figure 4.22 is the Radial deflection (the maximum deflection in Radial at every cross section) plot with 5 different ratios of A_7 and A_8. We can see that all curves are same, which mean that the drill-string has same radial deflections at any cross section.

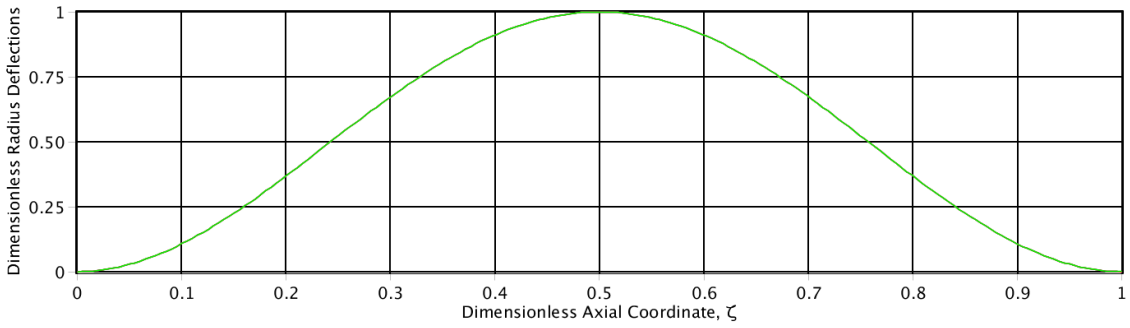

Figure 4.22 Radial Deflections with Different Ratios of A_7 and A_8

Figure 4.23 is the 3-D plot of the radial deflections with different ratios of A_7 and A_8. Figure 4.24 is the same deflections when looking downward from the top end of the drill-string.

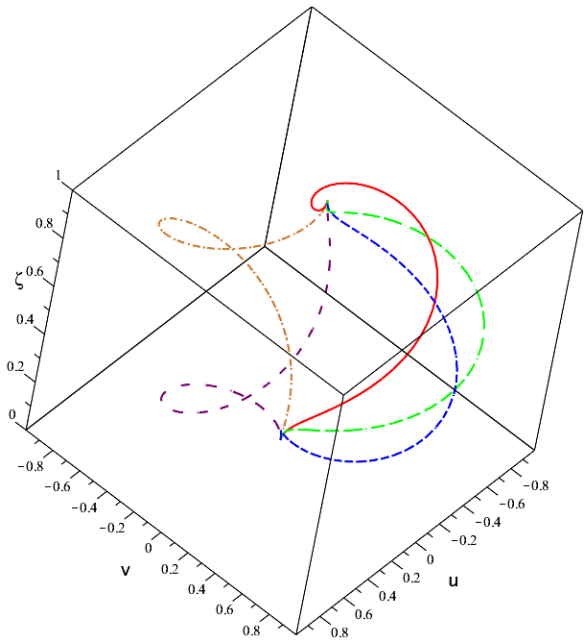

Figure 4.23 Radial Deflections with Different Ratios of A_7 and A_8

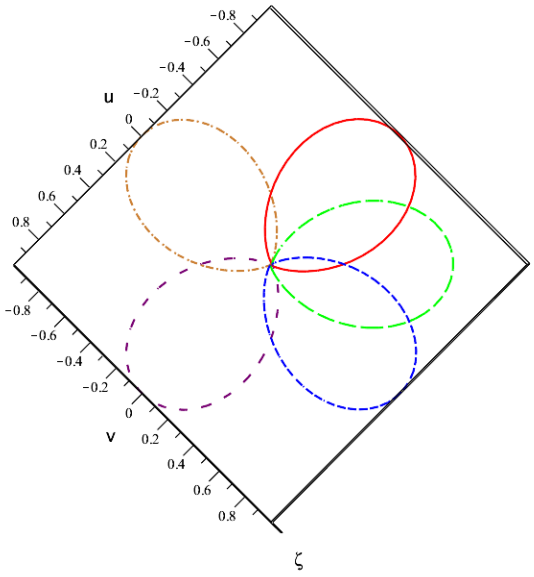

Figure 4.24 Vertical View of Radial Deflections with Different Ratios of A_7 and A_8

4.3.7 Constant Axial Load and End Torque and Whirling

With the constant axial load and the constant end torque applied to the drill-string while whirling at a constant speed, the matrix $[G]$ is simplified to

$$[G] = -[K] + \alpha\,[J] + \beta\,[M] + \lambda\,[Q].$$

Substituting the predefined polynomial function into this equation and then solving the equation $|G| = 0$ by the Hamilton's principle gives the critical loads. The three parameters are shown in the system at the same time. When the axial load parameter $\alpha = 0$ and the whirling speed parameter $\beta = 0$, which is the case with the end torque only, we get the first critical end torque parameter $\lambda_{max} = 8.987$. When the whirling speed parameter $\beta = 0$ and the constant end torque parameter $\lambda = 0$, which is the case with the constant axial load only, the first critical axial load parameter $\alpha_{max} = 39.478$. When he

axial load parameter $\alpha = 0$ and the constant end torque parameter $\lambda = 0$, which is the case with the constant whirling speed only, the first critical axial load parameter $\beta_{max} = 500.564$. For each different axial load parameter smaller than α_{max}, there is a corresponding combination of the end torque parameter smaller than λ_{max} and the whirling parameter smaller than β_{max} to make the drill-string buckle. We choose 4 different axial load parameters to run the calculation and get four different curves for the end torque parameter and the whirling parameter. The three values comprise of a critical combination of the axial load parameter, the constant end torque parameter and the whirling parameter. The interaction of critical combinations of these three parameters is shown in Figure 4.25. For each axial load parameter, the drill-string is stable when the combination of the end torque parameter and the whirling parameter is in the area under the curve.

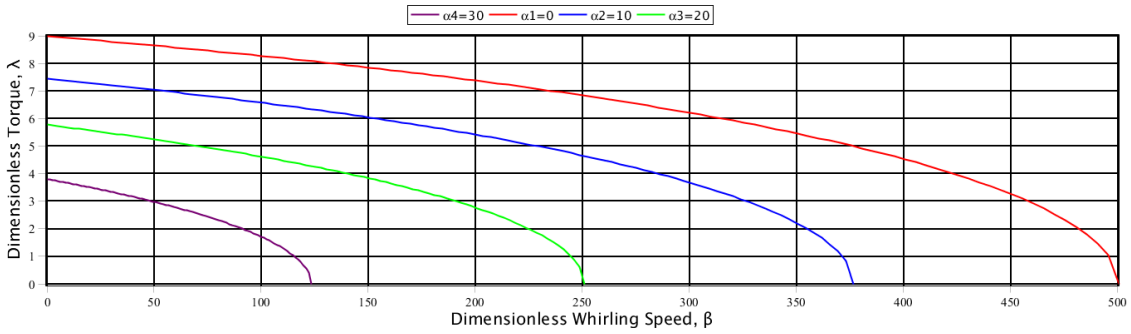

Figure 4.25 Interaction of α, β and λ

Since the mode shape is different for each critical combination, we choose the specific case with $\alpha = 10, \beta = 154.459,\ \lambda = 5.991$ to check the mode shape of the deflection function. For this specified case, this mode shape has two different functions. We have the functions of the mode shape for the first critical load as below

$$f1_{MS} = 37.689\,\zeta^2 - 80.757\,\zeta^3 - 65.566\,\zeta^4 - 21.784\,\zeta^5 + 855.627\,\zeta^6 - 1398.323\,\zeta^7 + 865.455\,\zeta^8 - 192.340\,\zeta^9$$

$$f2_{MS} = -6.361\,\zeta^2 - 15.718\,\zeta^3 + 53.525\,\zeta^4 - 43.786\,\zeta^5 + 176.947\,\zeta^6 - 500.625\,\zeta^7 + 577.021\,\zeta^8 - 301.258\,\zeta^9 + 60.256\,\zeta^{10}.$$

The mode shape given by the equation above is shown in Figure 4.26.

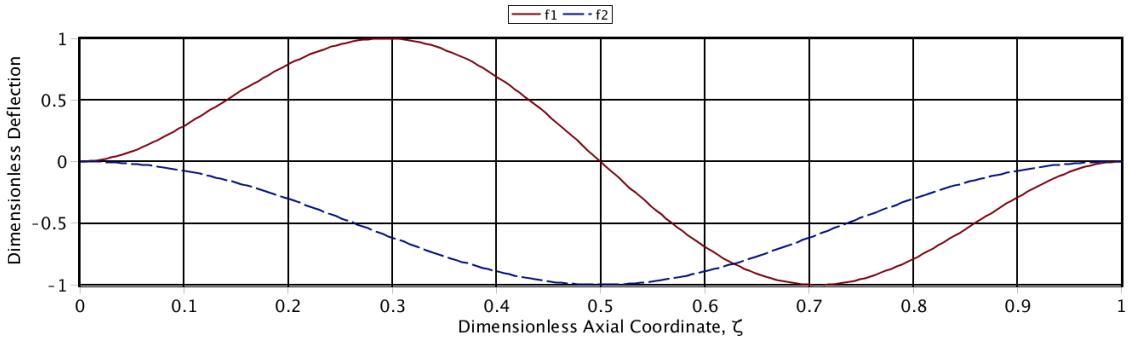

Figure 4.26 Mode Shape for the Case with $\alpha = 10, \beta = 154.459,\ \lambda = 5.991$

A_7 and A_8 are chosen to describe the deflection functions as below

$$u(\zeta) = A_7\, f1_{MS} + A_8\, f2_{MS}$$
$$v(\zeta) = A_8\, f1_{MS} - A_7\, f2_{MS}.$$

A_7 and A_8 are any arbitrary values and the maximum deflections of the solution are arbitrary. We found the maximum deflection is located at $\zeta = 0.292$ for the first function of the mode shape and $\zeta = 0.500$ for the second function of the mode shape. We set $A_7 = A_8 = 1$, which makes the ratio of the two coefficients equal to 1, to check the deflections of the drill-string. The maximum deflections have been normalized to -1 and the deflection functions are shown as below

$$u(\zeta) = 3.413\,\zeta^2 - 34.434\,\zeta^3 + 33.299\,\zeta^4 - 45.833\,\zeta^5 + 374.449\,\zeta^6 - 807.347\,\zeta^7 + 746.581\,\zeta^8 - 325.810\,\zeta^9 + 55.682\,\zeta^{10}$$

$$v(\zeta) = -15.163\,\zeta^2 + 5.381\,\zeta^3 + 65.597\,\zeta^4 - 35.076\,\zeta^5 - 47.396\,\zeta^6 - 117.853\,\zeta^7 + 319.728\,\zeta^8 - 230.875\,\zeta^9 + 55.658\,\zeta^{10}.$$

We found the maximum deflection is located at $\zeta = 0.578$ for the deflection in the direction of the axis Ox and $\zeta = 0.422$ for the deflection in the direction of the axis Oy. The plot of the deflection is shown in Figure 4.27

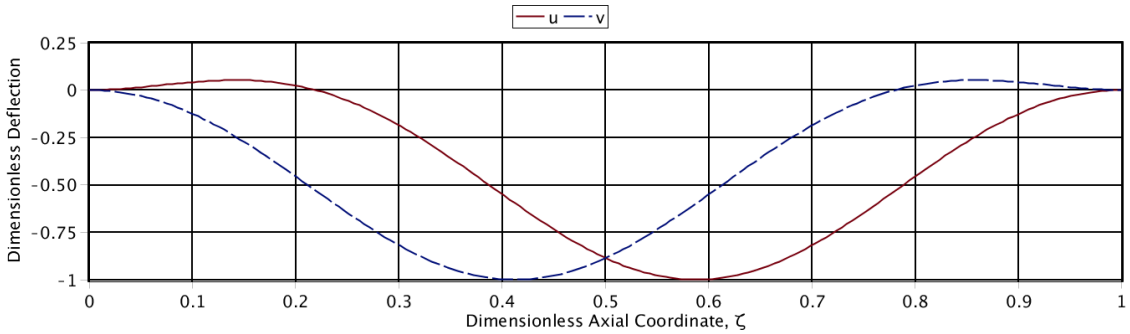

Figure 4.27 Deflection for the Case with $\alpha = 10, \beta = 154.459,\ \lambda = 5.991$

We know that changing the ratio of A_7 and A_8 is equivalent to a rigid-body rotation of the mode shape relative to the coordinate system O-XYZ. We choose 5 different ratios of A_7 and A_8 to check the deflections of the drill-string. Figure 4.28 is the Radial deflection (the maximum deflection in Radial at every cross section) plot with 5 different ratios of A_7 and A_8. We can see that all curves are same, which mean that the drill-string has same radial deflections at any cross section.

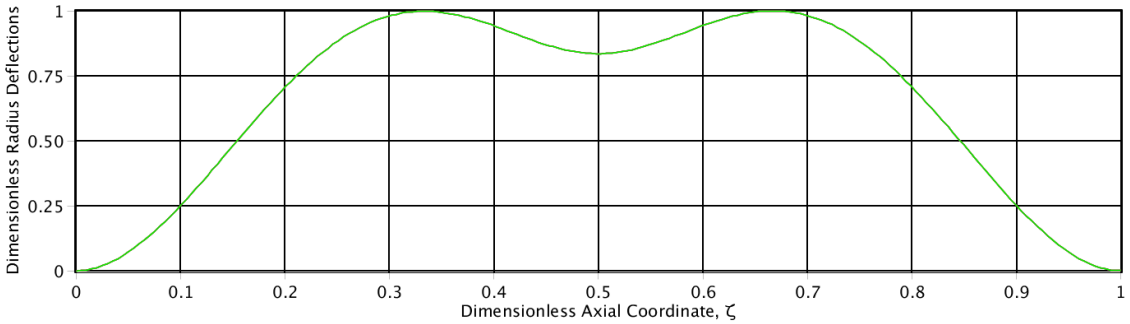

Figure 4.28 Radial Deflections with Different Ratios of A_7 and A_8

Figure 4.29 is the 3-D plot of the radial deflections with different ratios of A_7 and A_8.

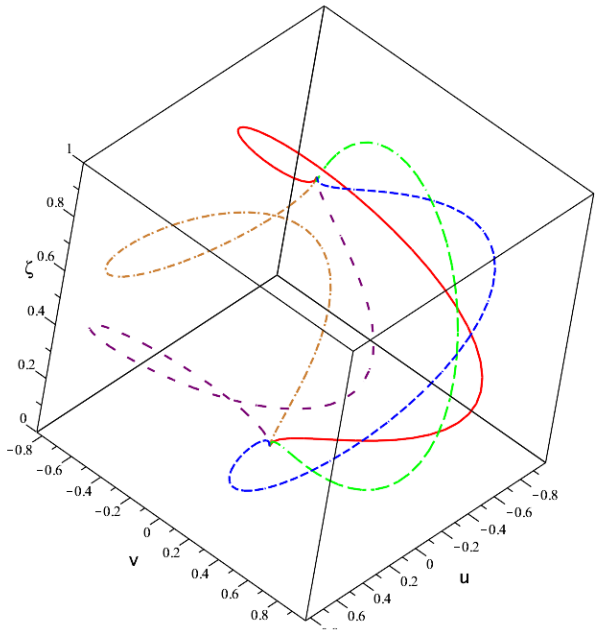

Figure 4.29 Radial Deflections with Different Ratios of A_7 and A_8

Figure 4.30 is the same plot when looking downward from the top end of the drill-string.

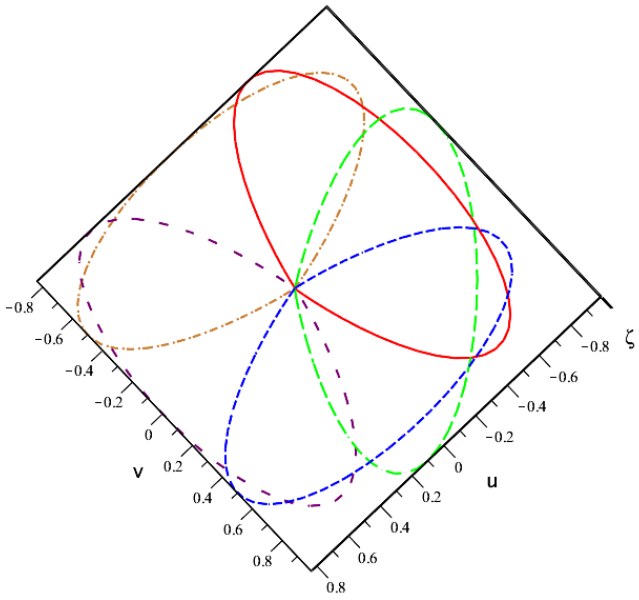

Figure 4.30 Vertical View of Radial Deflections with Different Ratios of A_7 and A_8

4.3.8 Constant and Variable Axial Loads

When there is a variable axial load (the self-weight of the drill-string) in the system, no analytical solution exists. Instead, we use the Rayleigh-Ritz method to solve the problem. The matrix $[J]$ will not be constant because of the self-weight. When the constant axial load is applied to a drill-string with the self-weight included, the matrix $[G]$ becomes

$$[G] = -[K] + \varphi\,[J_V] - \gamma\,[J_H]$$

The hook load cannot be larger than the drill-string weight, and this gives $\alpha - \gamma > 0$. The Rayleigh-Ritz method can then be applied as before. Substituting the predefined polynomial function into this equation and then solving the equation $|G| = 0$ by the Hamilton's principle gives the critical loads. When the hook load parameter $\gamma = 0$, which

is the case with the self-weight only and no hook load presented, this gives the first critical buckling self-weight parameter $\varphi_{min} = 74.629$. With the hook load parameter γ increased, the self-weight parameter φ will become larger. Because when the hook load become larger, we need a larger self-weight to make the drill-string buckle. We do not treat the condition that $\gamma < 0$ which means that hook load becomes compression. A combination of critical loads makes the drill-string buckle. The interaction of critical combinations of the hook load parameter and the self-weight parameter is shown in Figure 4.31. The drill-string is stable when the combination of the hook load parameter and the self-weight parameter is in the area under the curve.

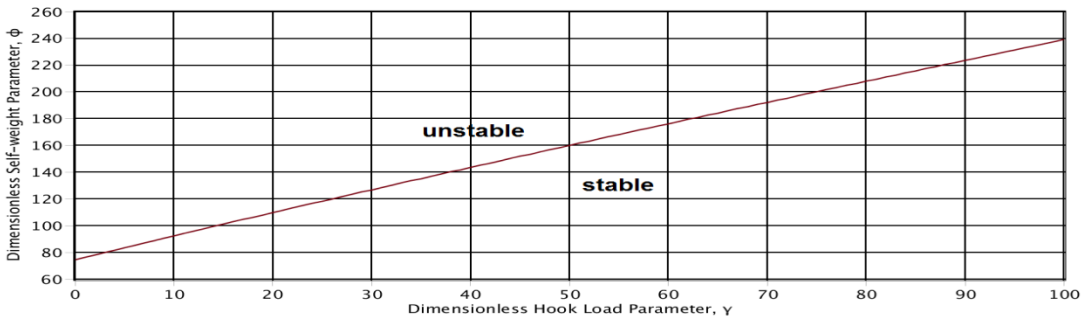

Figure 4.31 Interaction of γ and φ

Since the mode shape is different for each critical combination, we choose the specific case with $\gamma = 80, \varphi = 208.048$ to illustrate the mode shape. For this specified case, it is a planar problem and this mode shape has one function. We have the mode shape for the first critical load as below and the mode shape given by the equation is shown in Figure 4.32.

$$f_{MS} = 3.079\,\zeta^2 - 9.301\,\zeta^3 + 52.795\,\zeta^4 - 217.724\,\zeta^5 + 588.550\,\zeta^6 - 1004.035\,\zeta^7 + 983.583\,\zeta^8 - 496.951\,\zeta^9 + 100\,\zeta^{10}.$$

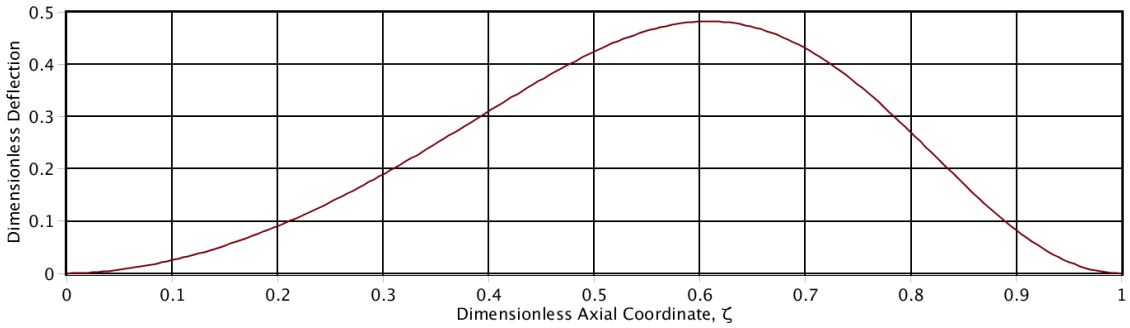

Figure 4.32 Mode Shape for the Case with $\gamma = 80, \varphi = 208.048$

Because we can choose an arbitrary coefficient in front of the function of the mode shape to have the deflection function of the drill-string, the maximum deflection of the solution is arbitrary. We found the maximum deflection is located at $\zeta = 0.608$ and we normalize it to 1. The function of the deflection is as below and the plot of the deflection is shown in Figure 4.33.

$$u(\zeta) = 6.390\,\zeta^2 - 19.304\,\zeta^3 + 109.576\,\zeta^4 - 451.882\,\zeta^5 + 1221.530\,\zeta^6 - 2083.854\,\zeta^7 + 2041.406\,\zeta^8 - 1031.410\,\zeta^9 + 207.548\,\zeta^{10}.$$

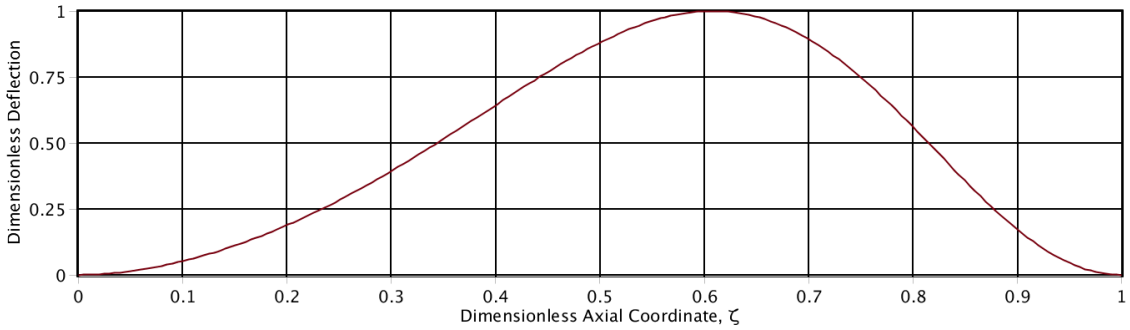

Figure 4.33 Deflection for the Case with $\gamma = 80, \varphi = 208.048$

4.3.9 Self-weight and Constant End Torque

When the constant end torque is applied to the drill-string with the self-weight included, the matrix $[G]$ becomes

$$[G] = -[K] + \varphi\,[J_V] + \lambda\,[Q].$$

Substituting the predefined polynomial function into this equation and then solving the equation $|G| = 0$ by the Hamilton's principle gives the critical loads. When the self-weight parameter $\varphi = 0$, which is the case with the end torque only, this gives the first critical buckling end torque parameter $\lambda_{max} = 8.987$. When the end torque parameter $\lambda = 0$, which is the case with the self-weight only, this gives the first critical buckling self-weight parameter $\varphi_{max} = 74.629$. A combination of critical loads makes the drill-string buckle. The interaction of critical combinations of the hook load parameter and the self-weight parameter is shown in Figure 4.34.

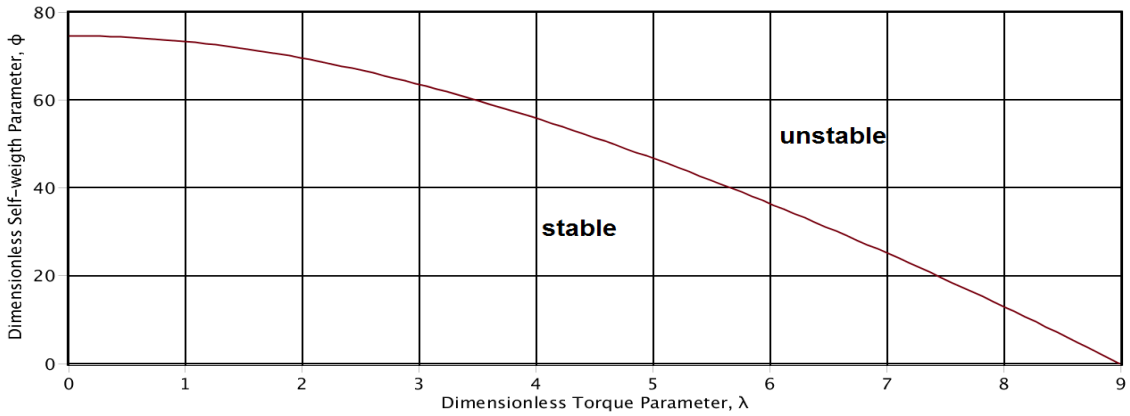

Figure 4.34 Interaction of λ and φ

For each different end torque parameter λ smaller than λ_{max}, there is a corresponding self-weight parameter φ smaller than φ_{max} to make the drill-string buckle. The drill-

string is stable when the combination of the end torque parameter and the self-weight parameter is in the area under the curve.

Since the mode shape is different for each critical combination, we choose the specific case with $\varphi = 51.458, \lambda = 4.493$ to illustrate the mode shape. For this specified case, this mode shape has two different functions. We have the functions of mode shape for the first critical load as below

$$f1_{MS} = -5.236\,\zeta^2 - 10.127\,\zeta^3 + 36.165\,\zeta^4 - 85.135\,\zeta^5 + 293.192\,\zeta^6 - 476.525\,\zeta^7 + 330.603\,\zeta^8 - 82.937\,\zeta^9$$

$$f2_{MS} = -31.754\,\zeta^2 + 54.497\,\zeta^3 + 94.738\,\zeta^4 - 346.737\,\zeta^5 + 1045.239\,\zeta^6 - 2467.376\,\zeta^7 + 2964.763\,\zeta^8 - 1670.546\,\zeta^9 + 357.176\,\zeta^{10}.$$

The mode shape given by the equation above is shown in Figure 4.35.

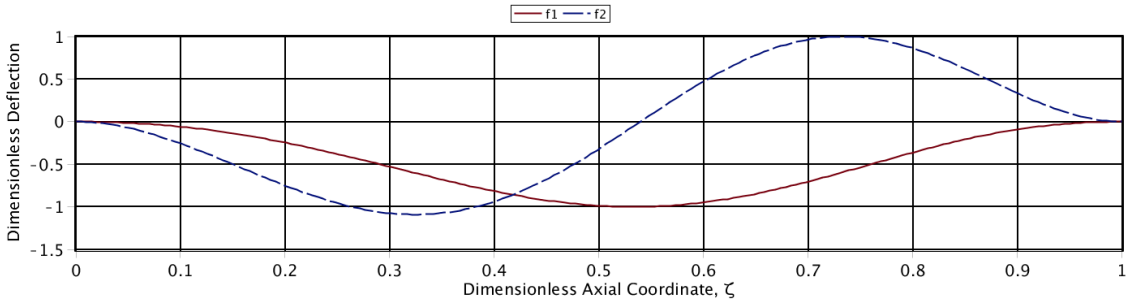

Figure 4.35 Mode Shape for the Case with $\varphi = 51.458, \lambda = 4.493$

A_7 and A_8 are chosen to describe the deflection functions as below

$$u(\zeta) = A_7\, f1_{MS} + A_8\, f2_{MS}$$
$$v(\zeta) = A_8\, f1_{MS} - A_7\, f2_{MS}.$$

A_7 and A_8 are any arbitrary values and the maximum deflections of the solution are

arbitrary. We found the maximum deflection is located at $\zeta = 0.533$ for the first function of the mode shape and $\zeta = 0.324$ for the second function of the mode shape. We set $A_7 = A_8 = 1$, which makes the ratio of two coefficients equal to 1, to illustrate the mode shape. The arbitrary maximum/minimum deflections have been normalized to 1 and the deflection functions are shown as below

$$u(\zeta) = 20.867\,\zeta^2 - 25.031\,\zeta^3 - 73.847\,\zeta^4 + 243.636\,\zeta^5 - 755.060\,\zeta^6 + 1660.765\,\zeta^7 - 1859.040\,\zeta^8 + 989.206\,\zeta^9 - 201.496\,\zeta^{10}$$

$$v(\zeta) = -15.820\,\zeta^2 + 38.554\,\zeta^3 + 34.944\,\zeta^4 - 156.067\,\zeta^5 + 448.658\,\zeta^6 - 1187.707\,\zeta^7 + 1571.494\,\zeta^8 - 947.140\,\zeta^9 + 213.085\,\zeta^{10}.$$

We found the maximum deflection is located at $\zeta = 0.375$ for the deflection in the direction of the axis Ox and $\zeta = 0.685$ for the deflection in the direction of the axis Oy. The plot of the deflection is shown in Figure 4.36

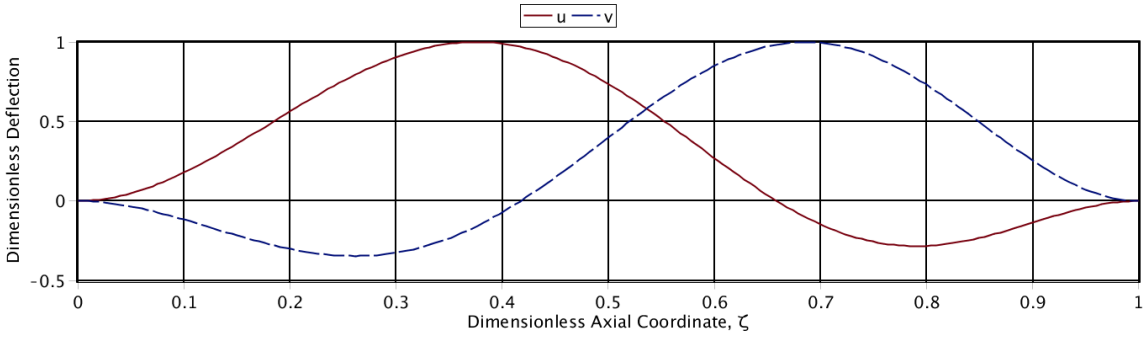

Figure 4.36 Deflection for the Case with $\varphi = 51.458, \lambda = 4.493$

We know that changing the ratio of A_7 and A_8 is equivalent to a rigid-body rotation of the mode shape relative to the coordinate system O-XYZ. We choose 5 different ratios of A_7 and A_8 to check the deflections of the drill-string. Figure 4.37 is the radial

deflection (the maximum deflection in radial direction at every cross section) plot with 5 different ratios of A_7 and A_8. We can see that all curves are same, which mean that the drill-string has same Radial deflections at any cross section.

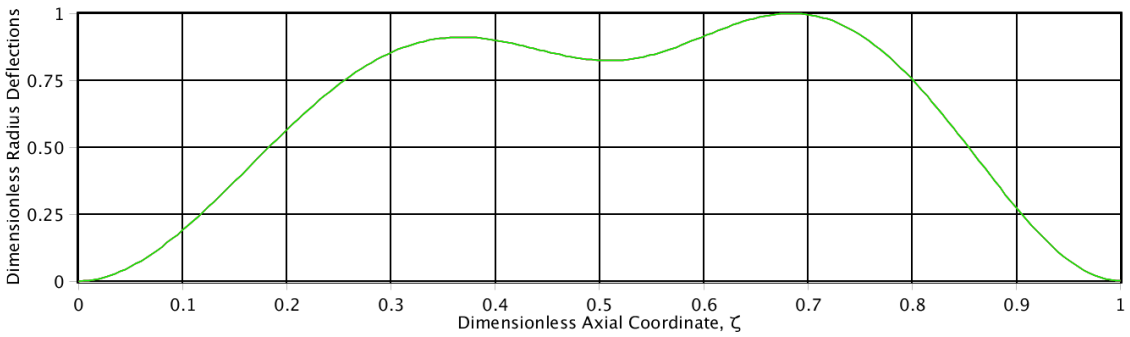

Figure 4.37 Radial Deflections with Different Ratios of A_7 and A_8

Figure 4.38 is the 3-D plot of the Radial deflections with different ratios of A_7 and A_8.

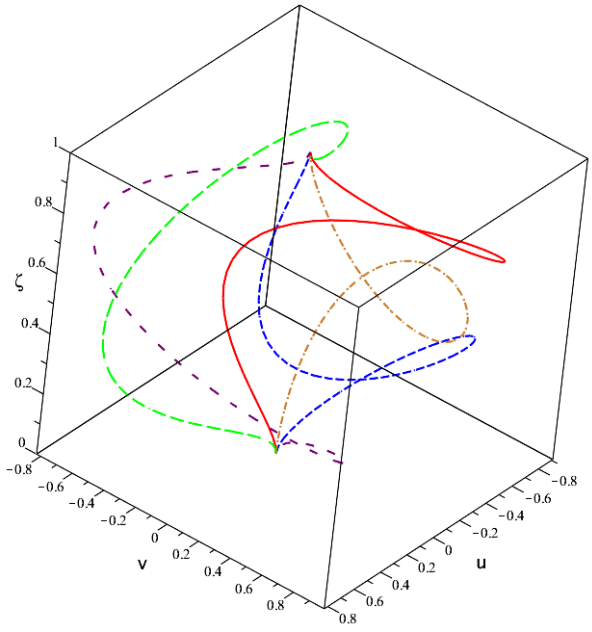

Figure 4.38 Radial Deflections with Different Ratios of A_7 and A_8

Figure 4.39 is the same plot when looking downward from the top end of the drill-string.

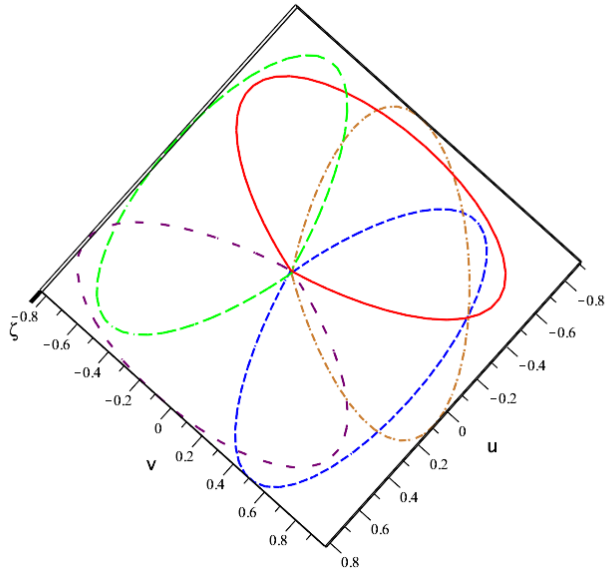

Figure 4. 39 Vertical View of Radial Deflections with Different Ratios of A_7 and A_8

4.3.10 Variable Axial Load and Hook Load and Constant End Torque

When the hook load and the constant end torque are applied to the drill-string with the self-weight included, the matrix $[G]$ becomes

$$[G] = -[K] + \varphi\,[J_V] - \gamma\,[J_H] + \lambda\,[Q].$$

Substituting the predefined polynomial function into this equation and then solving the equation $|G| = 0$ by the Hamilton's principle gives the critical loads. The three parameters are shown in the system at the same time. When the self-weight parameter $\varphi = 0$ and the hook load parameter $\gamma = 0$, which is the case with the end torque only, we get the first critical end torque parameter. When the hook load

parameter $\gamma = 0$ and the constant end torque parameter $\lambda = 0$, which is the case with the self-weight only, the first critical self-weight parameter $\varphi_{max} = 74.629$. When the self-weight parameter $\varphi = 0$ and the constant end torque parameter $\lambda = 0$, which is the case with the hook load only, the hook load has to be a compression to make the drill-string buckle. We do not consider this case here. For each different self-weight parameter smaller than φ_{max}, there is a corresponding combination of the end torque parameter and the hook load parameter to make the drill-string buckle. We choose 4 different axial load parameters to run the calculation and get four different curves for the end torque parameter and the whirling parameter. The three values comprise of a critical combination of the axial load parameter, the constant end torque parameter and the whirling parameter. The interaction of critical combinations of these three parameters is shown in Figure 4.40.

Figure 4.40 Interaction of φ, γ and λ

With the self-weight parameter γ increased, the hook load parameter φ will become larger. For self-weight parameter, the drill-string is stable when the combination of the end torque parameter and the hook load parameter is in the area under the curve.

Since the mode shape is different for each critical combination, we choose the specific case with $\varphi = 74.629,\ \gamma = 56.718, \lambda = 11.379$ to illustrate the mode shape. For this specified case, this mode shape has two different functions. We have the functions of mode shape for the first critical load as below

$$f1_{MS} = 0.881\,\zeta^2 - 39.086\,\zeta^3 + 176.744\,\zeta^4 - 767.125\,\zeta^5 + 2053.361\,\zeta^6 - 2751.135\,\zeta^7 + 1755.318\,\zeta^8 - 428.958\,\zeta^9$$

$$f2_{MS} = -13.632\,\zeta^2 - 3.642\,\zeta^3 + 228.062\,\zeta^4 - 1128.380\,\zeta^5 + 3941.870\,\zeta^6 - 7911.501\,\zeta^7 + 8429.967\,\zeta^8 - 4484.833\,\zeta^9 + 942.089\,\zeta^{10}.$$

The mode shape given by the equation above is shown in Figure 4.41.

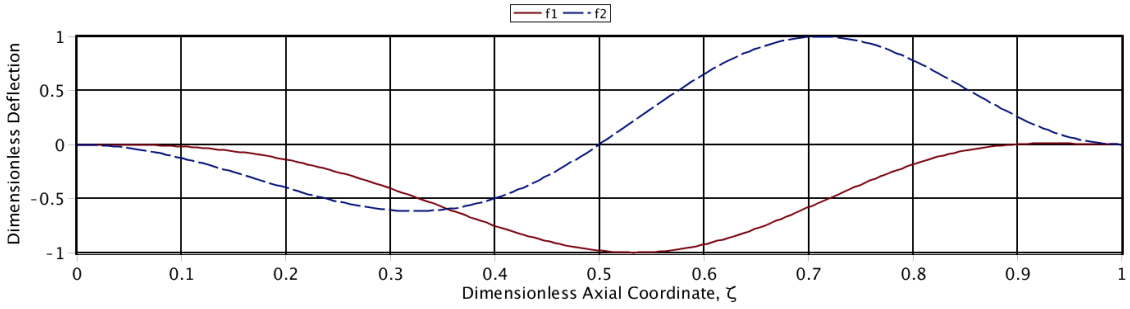

Figure 4.41 Mode Shape for the Case with $\varphi = 74.629,\ \gamma = 56.718, \lambda = 11.379$

A_7 and A_8 are chosen to describe the deflection functions as below

$$u(\zeta) = A_7\, f1_{MS} + A_8\, f2_{MS}$$
$$v(\zeta) = A_8\, f1_{MS} - A_7\, f2_{MS}.$$

A_7 and A_8 are any arbitrary values and the maximum deflections of the solution are arbitrary. We found the maximum deflection is located at $\zeta = 0.533$ for the first function of the mode shape and $\zeta = 0.711$ for the second function of the mode shape. We

set $A_7 = A_8 = 1$, which makes the ratio of two coefficients equal to 1, to illustrate the mode shape. We found the maximum deflections are located at $\zeta = 0.402$ in the x-axis and $\zeta = 0.651$ in the y-axis. The arbitrary maximum/minimum deflections have been set to ±1 and the deflection functions are shown as below

$$u(\zeta) = 10.206\,\zeta^2 + 34.200\,\zeta^3 - 324.010\,\zeta^4 + 1517.176\,\zeta^5 - 4789.627\,\zeta^6 + 8534.452\,\zeta^7 - 8152.378\,\zeta^8 + 3933.035\,\zeta^9 - 754.055\,\zeta^{10}$$

$$v(\zeta) = -8.714\,\zeta^2 + 23.282\,\zeta^3 + 30.814\,\zeta^4 - 216.914\,\zeta^5 + 1133.949\,\zeta^6 - 3098.524\,\zeta^7 + 4007.770\,\zeta^8 - 2435.336\,\zeta^9 + 565.674\,\zeta^{10}.$$

We found the maximum deflection is located at $\zeta = 0.401$ for the deflection in the direction of the axis Ox and $\zeta = 0.651$ for the deflection in the direction of the axis Oy. The plot of the deflection is shown in Figure 4.42.

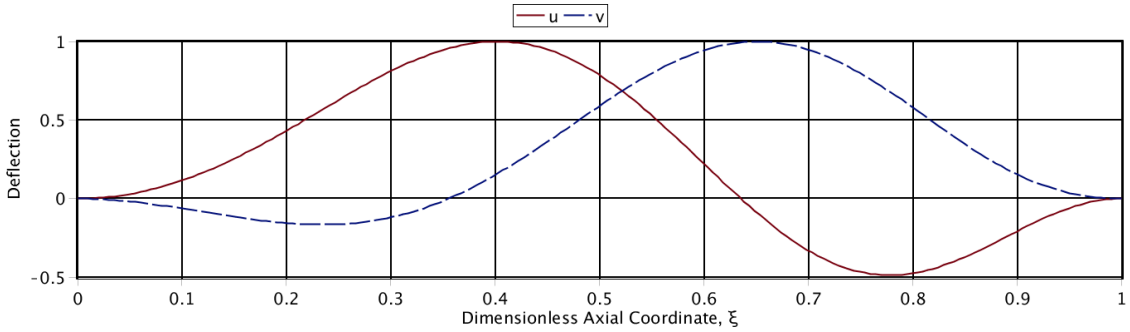

Figure 4.42 Deflection for the Case with $\varphi = 74.629$, $\gamma = 56.718, \lambda = 11.379$

We know that changing the ratio of A_7 and A_8 is equivalent to a rigid-body rotation of the mode shape relative to the coordinate system O-XYZ. We choose 5 different ratios of A_7 and A_8 to check the deflections of the drill-string. Figure 4.43 is the radial deflection plot with 5 different ratios of A_7 and A_8.

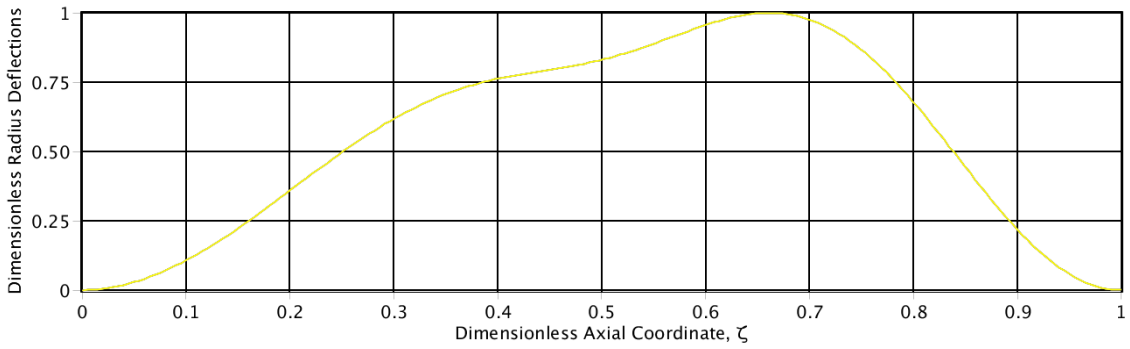

Figure 4.43 Radial Deflections with Different Ratios of A_7 and A_8

We can see that all curves are same, which mean that the drill-string has same radial deflections at any cross section. Figure 4.44 is the 3-D plot of the radial deflections with different ratios of A_7 and A_8.

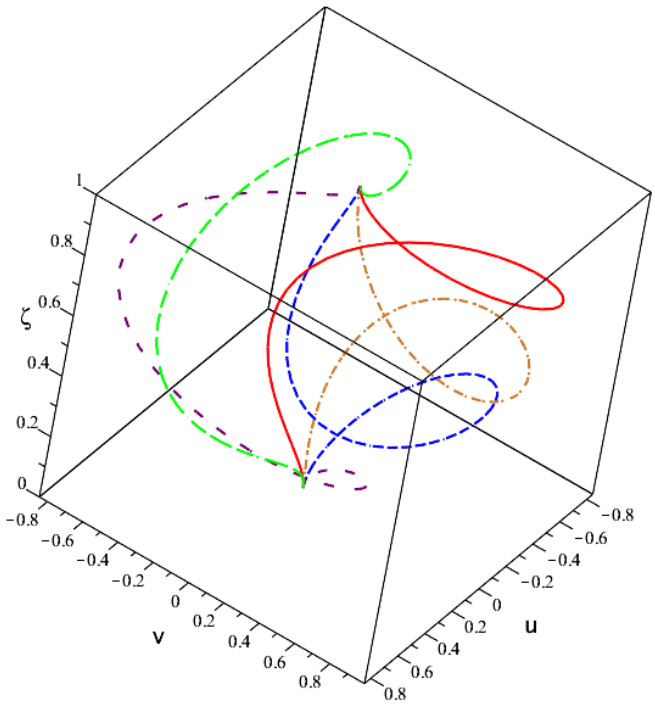

Figure 4.44 Radial Deflections with Different Ratios of A_7 and A_8

Figure 4.45 is the same plot when looking downward from the top end of the drill-string.

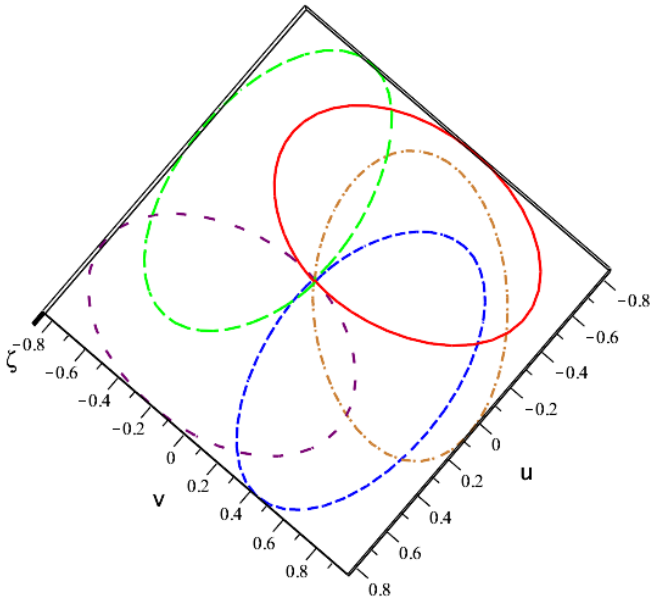

Figure 4.45 Vertical View of Radial Deflections with Different Ratios of A_7 and A_8

4.3.11 Self-weight and Hook Load and Constant End Torque and Whirling

When all these four loads are considered in the system, all matrices can be obtained as before and we have the following matrix equation

$$[G] = -[K] + \beta\,[M] + \varphi\,[J_V] - \gamma\,[J_H] + \lambda\,[Q].$$

Substituting the predefined polynomial function into this equation and then solving the equation $|G| = 0$ by the Hamilton's principle gives the critical loads. The four parameters are shown in the system at the same time. We have same critical values as before when each load applied separately. We chose the case with the self-weight parameter $\varphi = 74.629$ and four different hook load parameters to illustrate the mode shape. A

combination of four critical loads makes the drill-string buckle. The interaction of critical combinations of these three parameters is shown in Figure 4.46

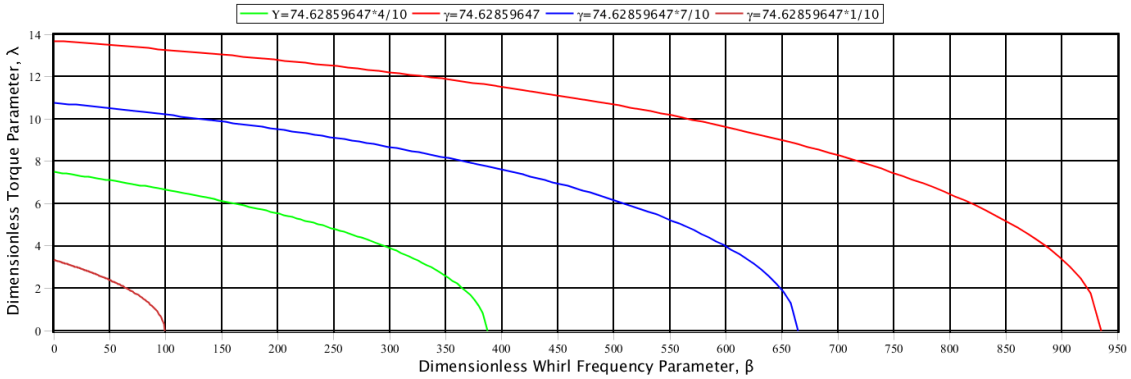

Figure 4.46 Interaction of φ, γ, λ and β

For each hook load parameter, the drill-string is stable when the combination of the end torque parameter and the whirling parameter is in the area under the curve.

Since the mode shape is different for each critical combination, we choose the specific case with $\varphi = \frac{74.629}{2}$, $\gamma = \frac{74.629}{20}$, $\beta = 198.063$, $\lambda = 4.176$ to check the mode shape of the deflection function. For this specified case, this mode shape has two different functions. We have the functions of the mode shape for the first critical load as below

$$f1_{MS} = -7.906\,\zeta^2 - 1.159\,\zeta^3 + 23.463\,\zeta^4 - 28.916\,\zeta^5 + 102.625\,\zeta^6 - 196.297\,\zeta^7 + 145.347\,\zeta^8 - 37.160\,\zeta^9$$

$$f2_{MS} = -31.874\,\zeta^2 + 73.780\,\zeta^3 + 10.978\,\zeta^4 - 118.526\,\zeta^5 + 287.108\,\zeta^6 - 802.804\,\zeta^7 + 1082.231\,\zeta^8 - 639.193\,\zeta^9 + 138.300\,\zeta^{10}.$$

The mode shape given by the equation above is shown in Figure 4.47.

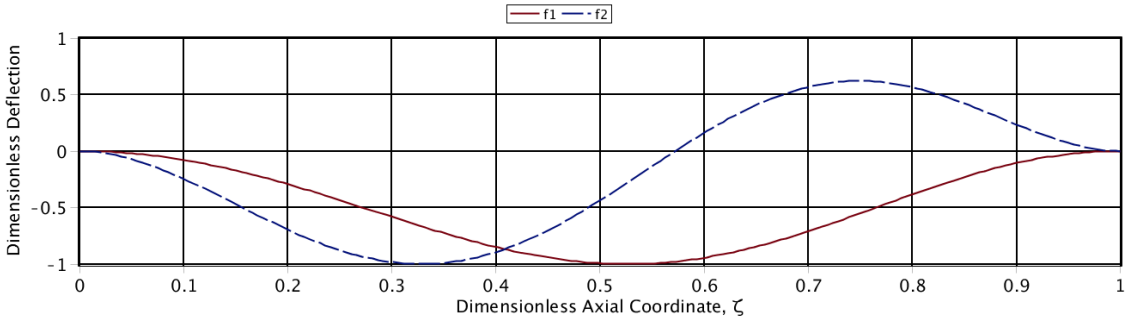

Figure 4.47 Mode Shape for the Case with

$$\boldsymbol{\varphi = \frac{74.629}{2}}, \qquad \boldsymbol{\gamma = \frac{74.629}{20}}, \boldsymbol{\beta = 198.063}, \qquad \boldsymbol{\lambda = 4.176}$$

A_7 and A_8 are chosen to describe the deflection functions as below

$$u(\zeta) = A_7\, f1_{MS} + A_8\, f2_{MS}$$
$$v(\zeta) = A_8\, f1_{MS} - A_7\, f2_{MS}.$$

A_7 and A_8 are any arbitrary values and the maximum deflections of the solution are arbitrary. We found the maximum deflection is located at $\zeta = 0.526$ for the first function of the mode shape and $\zeta = 0.329$ for the second function of the mode shape. We set $A_7 = A_8 = 1$, which makes the ratio of two coefficients equal to 1, to check the deflections of the drill-string. We found the maximum deflections are located at $\zeta = 0.386$ in the x-axis and $\zeta = 0.684$ in the y-axis. The arbitrary maximum/minimum deflections have been normalized to 1 and the deflections functions are shown as below

$$u(\zeta) = 22.743\,\zeta^2 - 41.520\,\zeta^3 - 19.691\,\zeta^4 + 84.294\,\zeta^5 - 222.815\,\zeta^6 + 571.199\,\zeta^7 - 701.822\,\zeta^8 + 386.680\,\zeta^9 - 79.068\,\zeta^{10}$$

$$v(\zeta) = -18.652\,\zeta^2 + 58.316\,\zeta^3 - 9.716\,\zeta^4 - 69.733\,\zeta^5 + 143.563\,\zeta^6 - 471.979\,\zeta^7 + 729.076\,\zeta^8 - 468.498\,\zeta^9 + 107.624\,\zeta^{10}.$$

We found the maximum deflection is located at $\zeta = 0.386$ for the deflection in the direction of the axis Ox and $\zeta = 0.684$ for the deflection in the direction of the axis Oy. The plot of the deflection is shown in Figure 4.48

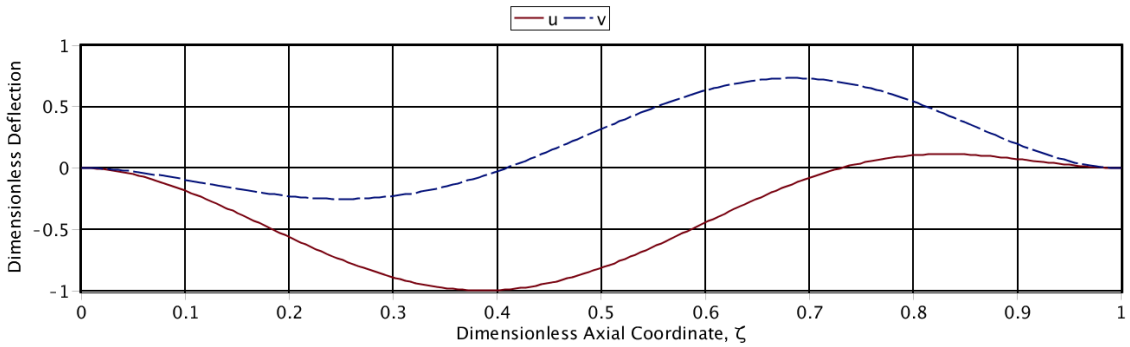

Figure 4.48 Deflections for the Case with

$$\boldsymbol{\varphi = \frac{74.629}{2}}, \qquad \boldsymbol{\gamma = \frac{74.629}{20}}, \boldsymbol{\beta = 198.063}, \qquad \boldsymbol{\lambda = 4.176}$$

We know that changing the ratio of A_7 and A_8 is equivalent to a rigid-body rotation of the mode shape relative to the coordinate system O-XYZ. We choose 5 different ratios of A_7 and A_8 to check the deflections of the drill-string. Figure 4.49 is the radial deflection (the maximum deflection in radial direction at every cross section) plot with 5 different ratios of A_7 and A_8. We can see that all curves are same, which mean that the drill-string has same radial deflections at any cross section.

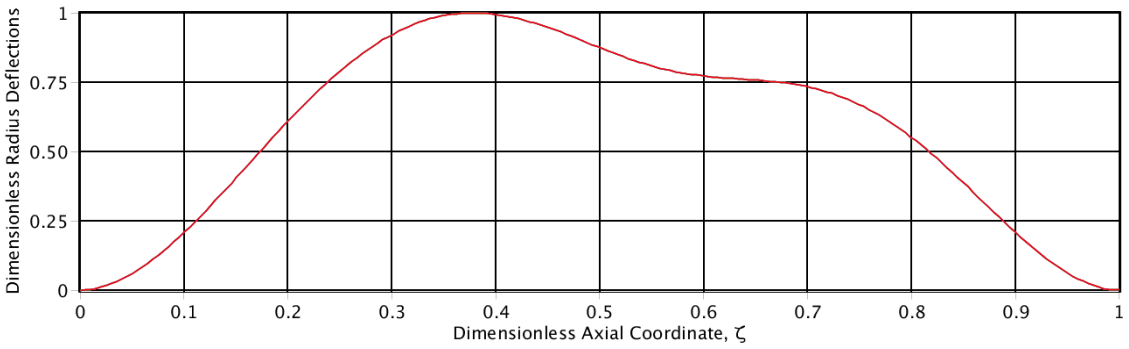

Figure 4.49 Radial Deflections with Different Ratios of A_7 and A_8

Figure 4.50 is the 3-D plot of the Radial deflections with different ratios of A_7 and A_8.

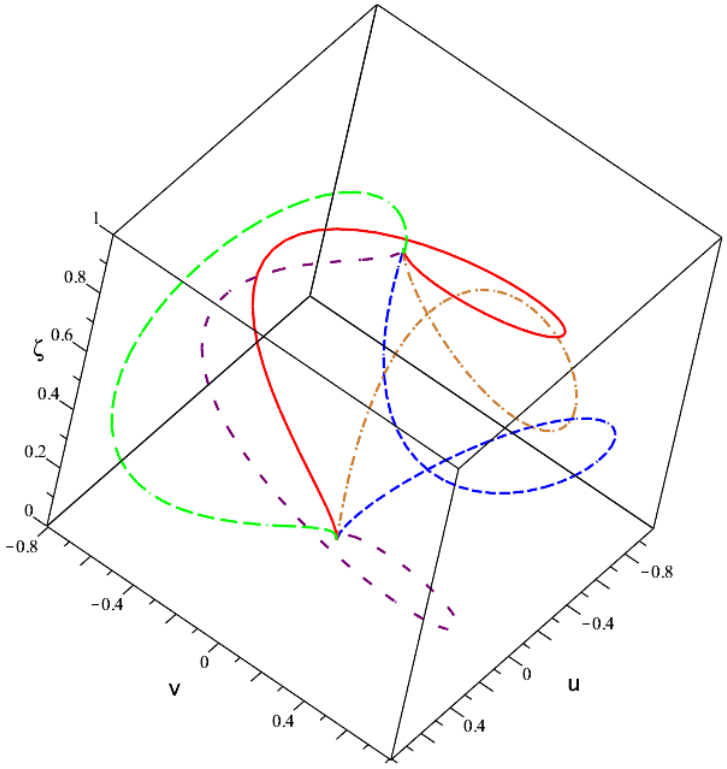

Figure 4.50 Radial Deflections with Different Ratios of A_7 and A_8

Figure 4.51 is the same plot when looking downward from the top end of the drill-string.

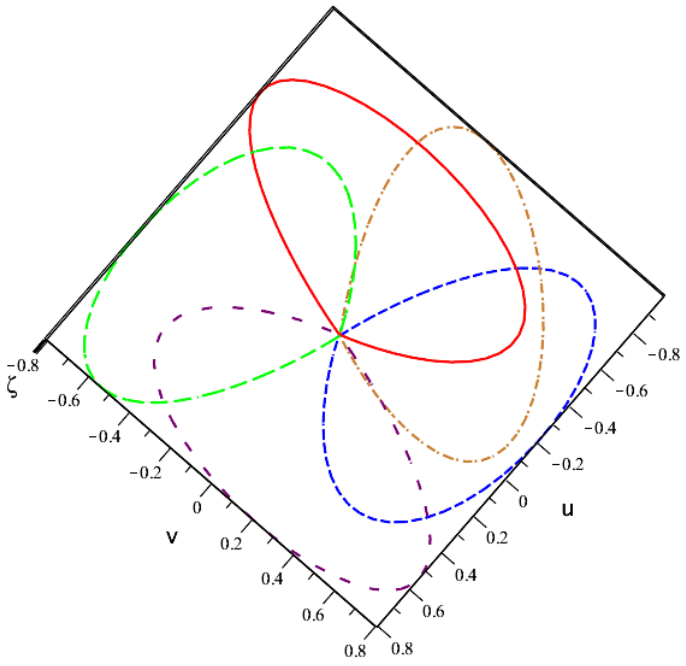

Figure 4.51 Vertical View of Radial Deflections with Different Ratios of A_7 and A_8

CHAPTER 5

COMSOL AND ABAQUS SIMULATION

5.1 Introduction

In former chapters, we have discussed the stability of a drill-string system for different loading cases with analytical and numerical methods. We know that there are some complex cases for which it is difficult, even impossible to find the analytical solutions. These cases include the loading conditions with the constant axial load, the constant end torque and whirling at same time, and all cases with the self-weight of the drill-string considered. So we need a method to validate the results from the Rayleigh-Ritz method and check the method's accuracy. Computer simulation has become an essential part of science and engineering and we choose it as our validating method for the problem. Today a broad spectrum of options for simulation is available. Researchers use everything from basic programming languages to various high-level packages implementing advanced methods. There are many commercial CAD/CAE software can help us with this problem. Two programs available on campus are COMSOL and ABAQUS. Attempts to use each of these to validate results obtained with the Rayleigh-Ritz method are described below.

5.2 COMSOL Simulation

COMSOL Multiphysics is a finite element analysis; solver and simulation software package for various physics and engineering applications, especially coupled phenomena, or multiphysics. COMSOL Multiphysics is an integrated environment for

solving systems of time-dependent or stationary second order in space partial differential equations in one, two, and three dimensions. Moreover, such equations may be coupled in an almost arbitrary way. COMSOL Multiphysics also offers an extensive interface to MATLAB and its toolboxes for a large variety of programming, preprocessing and post-processing possibilities. The packages are cross-platform (Windows, Mac, and Linux). In addition to conventional physics-based user interfaces, COMSOL Multiphysics also allows for entering coupled systems of partial differential equations (PDEs). The PDEs can be entered directly or using the so-called weak form. COMSOL provides a simulation environment that includes the possibility to add wide variety physical effects to the model. It is a flexible platform that allows even novice users to model all relevant physical aspects of their designs. Advanced users can go deeper and use their knowledge to develop customized solutions, applicable to their unique circumstances. Compatibility and adaptability are the most important characteristics of COMSOL.

We use COMSOL to simulate a drill-string buckling problem with a fixed-free boundary condition. The drill-string has a length of 100 m with a circular cross section which has a Radial of 0.1 m. The material of the drill-string is structural steel from the COMSOL library with the density of 7850 kg/m^3 and the Young's modulus of 200E9 Pa. A constant vertical load is applied at the top free end to cause the drill-string buckling. The analytical solution of the first critical buckling load is from equation $P_{cr} = \frac{\pi^2 EI}{(2L)^2}$ [57]. We have the first critical load of 3875.8 N for this problem. The simulating result from the COMSOL is 3526.3 N. There is a 9% of error between these two results. And we found that the

accuracy would be different when we use different shape of the cross section. Figure 5.1 is the diagram of the problem we study.

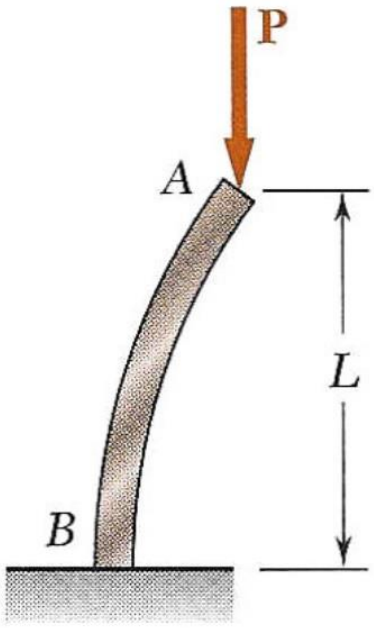

Figure 5.1 Buckling Drill-string with Fixed-free Boundary Conditions

Figure 5.2 is the simulation results from COMSOL for this problem. The difficulty we had is that when we tried to use different boundary conditions and loading conditions, COMSOL did not give us reasonable results as for this simple case. So we moved on to use ABAQUS as our simulation tool to solve our problem.

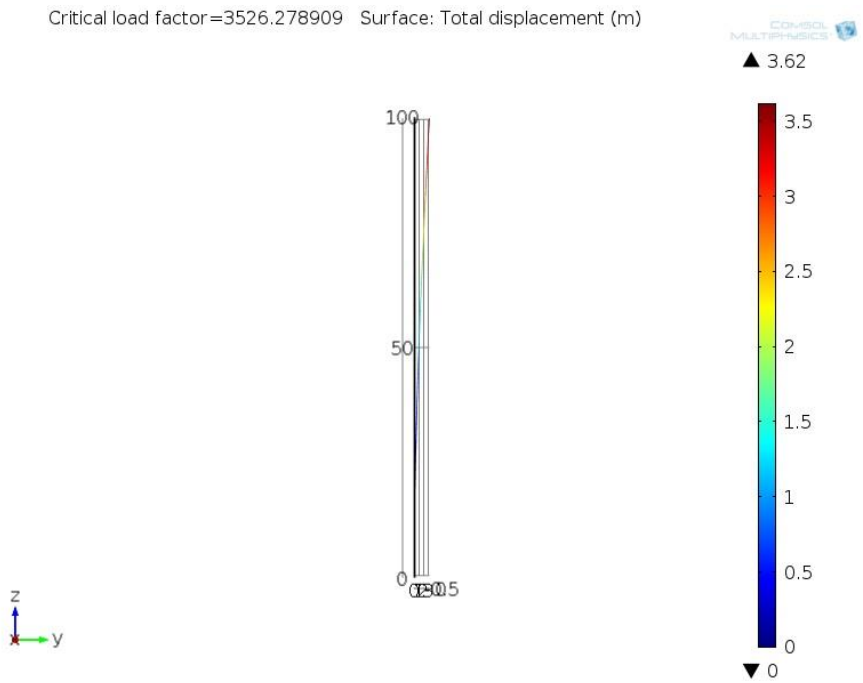

Figure 5.2 COMSOL Simulation Result with Fixed-free Boundary Conditions

5.3 ABAQUS

ABAQUS FEA is a software suite for the finite element analysis and computer-aided engineering. The ABAQUS suite of software for finite element analysis (FEA) is known for its high performance, quality and ability to solve many kinds of challenging simulations. ABAQUS is used in the automotive, aerospace, and industrial products industries. The product is popular with academic and research institutions due to the wide material modeling capability, and the program's ability to be customized. ABAQUS also provides a good collection of multiphysics capabilities, such as coupled acoustic-structural, piezoelectric, and structural-pore capabilities, making it attractive for production-level simulations where multiple fields need to be coupled.

The ABAQUS product suite consists of five core software products and we use ABAQUS/CAE to analyze our problem. It is a software application used for both the modeling and analysis of mechanical components and assemblies (pre-processing) and visualizing the finite element analysis result. ABAQUS/CAE provides a complete modeling and visualization environment for ABAQUS analysis products. With direct access to CAD models, advanced meshing and visualization, and with an exclusive view towards ABAQUS analysis products, ABAQUS/CAE is the modeling environment of choice for many ABAQUS users.

5.3.1 Buckling Drill-string for Fixed-Free Boundary Conditions

We use ABAQUS to simulate a drill-string buckling problem with a fixed-free boundary condition as shown in Figure 5.1 at first. The drill-string has a length of 45 m with a circular cross section which has a Radial of 0.05 m. T There is a critical length for a drill-string under gravity only. For the drill-string we used, it is 49.49 m as calculated by Mclachlan [18]. When we chose a length over this critical length, ABAQUS could not give a reasonable result. We did a lot work to figure out the reason but not success. That is why we use 45 m as our length of the drill-string. This could be a further topic for the next step. The material of the drill-string is structural steel with the density of 7850 kg/m^3 and the Young's modulus of 200E9 Pa. A constant vertical load is applied at the top free end to cause the drill-string buckling. The analytical solution of the first critical buckling load is from equation $P_{cr} = \frac{\pi^2 EI}{(2L)^2}$ and we have the first critical axial load of 1196.23 N for this problem. The simulated result from ABAQUS is 1196.2 N as shown in Figure 5.3. Two results from different methods are very close.

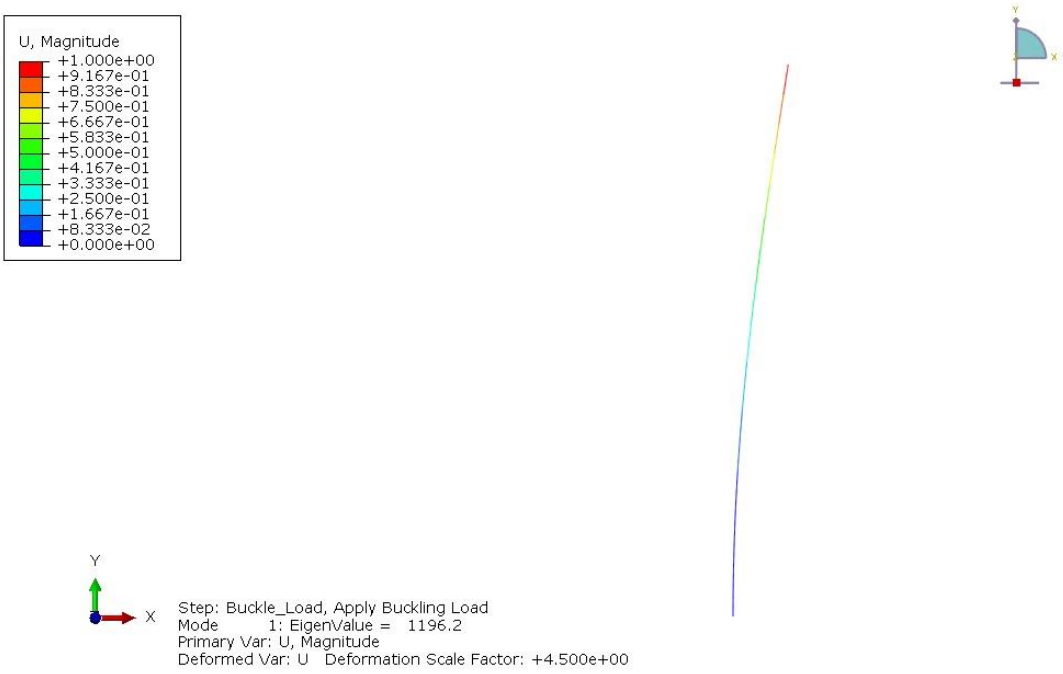

Figure 5.3 ABAQUS Simulation Result with Fixed-free Boundary Conditions

5.3.2 Buckling Drill-string for Fixed-Fixed Boundary Conditions

We use ABAQUS to simulate a drill-string buckling problem with a fixed-fixed boundary condition as these cases solved by the Rayleigh-Ritz method. The drill-string is the same as the one from the above case. A constant vertical load is applied at the top end to cause the drill-string buckling. The analytical solution of the first critical buckling load is from equation $P_{cr} = \frac{4\pi^2 EI}{L^2}$ [57] and we have the first critical axial load of 19139.68 N for this problem. The simulated result from the ABAQUS is 19140.0 N as shown in Figure 5.4. We can have the axial load parameter $\alpha = 39.487$ from its definition. Two results from different methods are very close.

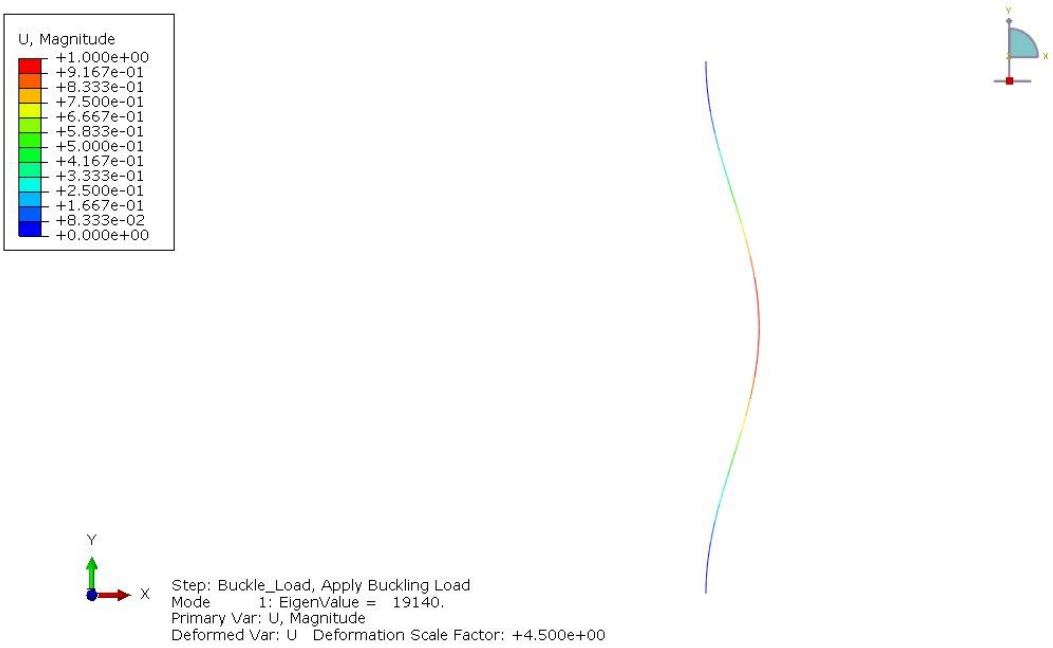

Figure 5.4 ABAQUS Simulation Result with Fixed-Fixed Boundary Conditions

5.3.3 Buckling Drill-string with Self-weight for Fixed-Fixed Boundary Conditions

When the self-weight of the drill-string is included in the system, the drill-string is under a variable axial load for each cross section. We use ABAQUS to analyze this case and got the first critical axial load 49848.6 N as shown in Figure 5.4. We can have the axial load parameter $\alpha = 39.487$ from its definition. The analytical solution for this case is not available and we only have the numerical solution from the Rayleigh-Ritz method. The comparison of these results is displayed in the next chapter.

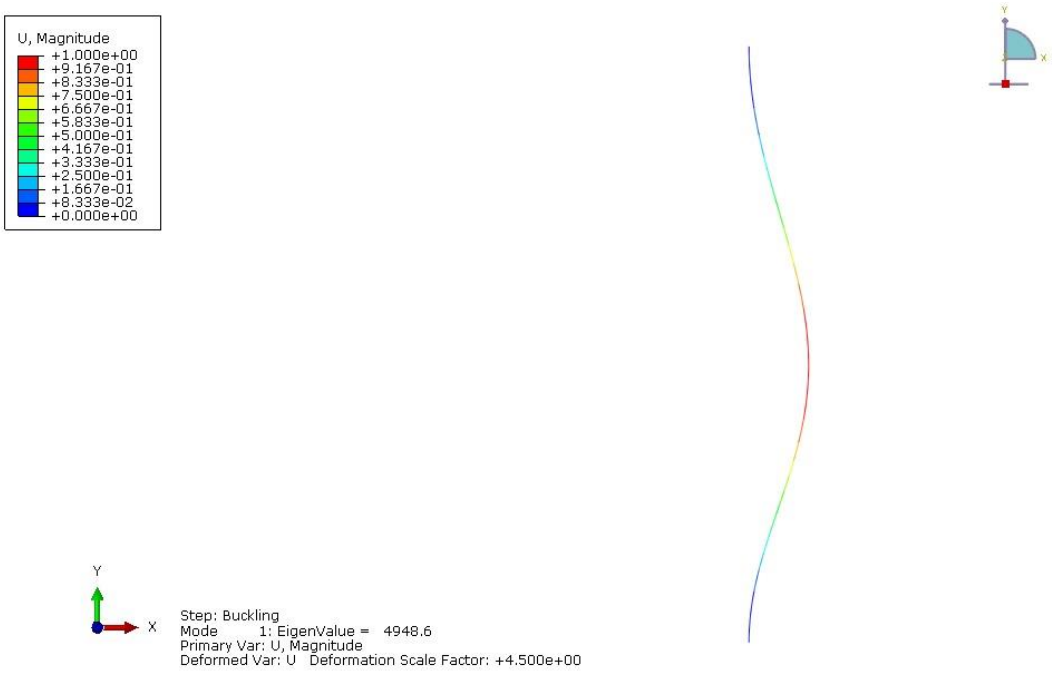

Figure 5. 5 ABAQUS Simulation Result with Self-weight Included

CHAPTER 6

VALIDATION OF RESULTS FROM DIFFERENT METHODS

6.1 Introduction

To demonstrate the validity and the accuracy of the Rayleigh-Ritz method detailed in previous chapters, comparisons of these results for different loading conditions from different methods are carried out here. These comparisons are conducted also with the purpose of better understanding the effects of different parameters on the stability of the drill-string. From these results, we also learn to recognize that including or neglecting the self-weight of the drill-string has a significant effect on the drill-string's stability.

6.2 Result Validation for Different Loading Cases

6.2.1 Constant Axial Load Only

For this case, we have three solutions from three methods. The first critical axial load parameter from the analytical solution is $\alpha = 4\,\pi^2$ and the one from the Rayleigh-Ritz method is $\alpha = 39.487$. The analytical solution of the first critical buckling load is from the equation $P_{cr} = \frac{\pi^2 EI}{(2L)^2}$ and we have the first critical load of 1196.23 N for this problem. The simulated result from ABAQUS is 1196.2 N. The critical loads from the three methods are very close and we could say that the error is negligible. And for this case, the deflection is obtained by setting the coefficient in front of the mode shape an arbitrary value. Comparing the mode shape can tell us the difference among them. Figure 6.1 shows the comparison of the mode shapes of three deflections from the three methods.

The red solid line is from the analytical method, the blue dashed line is from the Rayleigh-Ritz method and the green long-dashed line is from ABAQUS. From the figure, we see that two mode shapes from the analytical method and the Rayleigh-Ritz method are essentially the same while the one from ABAQUS is a little different from other two. It shows that the Rayleigh-Ritz method gives a slightly better result than that from ABAQUS. The maximum deflections are normalized to 1 and occur at the middle of the drill-string, which is $\zeta = 0.5$. The mode shapes are symmetric because the boundary conditions and the applied load are symmetric.

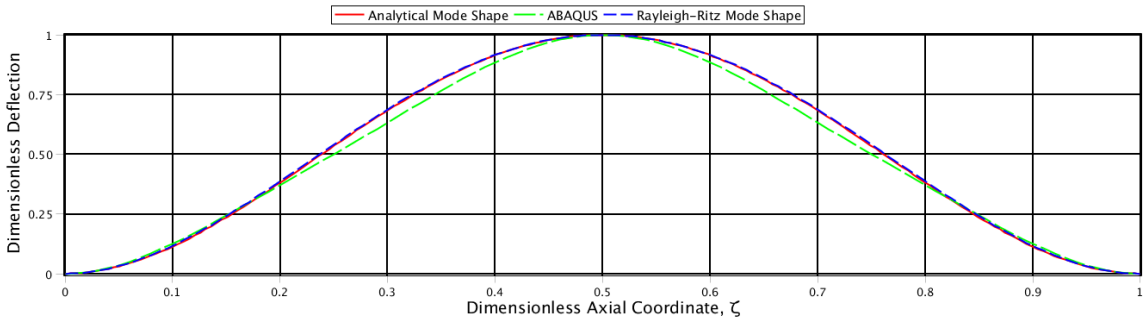

Figure 6.1 Comparison of Mode Shapes with Constant Axial Load Only

6.2.2 Constant Whirling Only

For this case, we have two solutions from two methods. The first critical whirling speed parameter from the analytical solution is $\beta = 500.564$ and the one from the Rayleigh-Ritz solution also is $\beta = 500.564$. The critical load parameters from the two methods are identical and we could say that the error is negligible. Figure 6.2 shows the comparison of the mode shapes from the two methods. The red solid line is from the analytical method and the blue dashed line is from the Rayleigh-Ritz method. From the figure, we

see that the two mode shapes are essentially the same. The maximum deflections are normalized to 1 and both occur at the middle of the drill-string, which is $\zeta = 0.5$. The mode shapes are symmetric because the boundary conditions and the effect of whirling to the drill-string are symmetric.

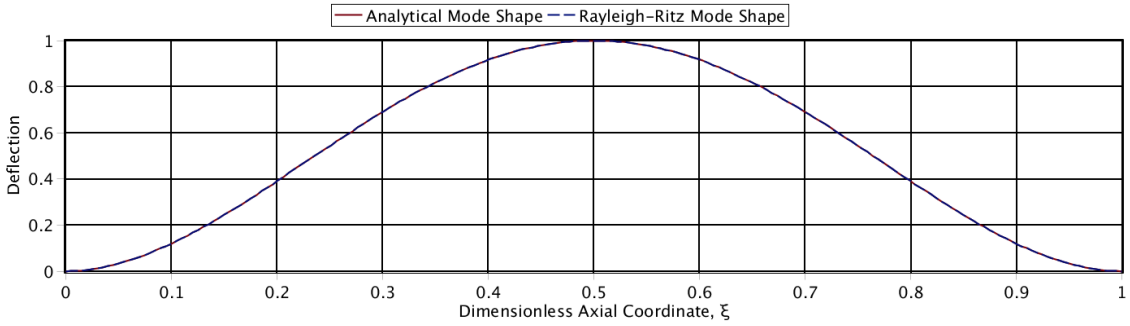

Figure 6.2 Comparison of Mode Shapes with Constant Whirling Only

6.2.3 Constant End Torque Only

For this case, we have two solutions from two methods. The first critical end torque parameter from the analytical solution is $\lambda = 8.987$ and the one from the Rayleigh-Ritz solution also is $\lambda = 8.987$. The critical end torques from the two different methods are identical and we could say that the error is negligible. Figure 6.3 shows the comparison of the first function of the mode shapes from the two methods. The red solid line is from the analytical method and the blue dashed line is from the Rayleigh-Ritz method.

The comparison of the second function of the mode shapes from the two methods is shown in Figure 6.4. The red solid line is from the analytical method and the blue dashed line is from the Rayleigh-Ritz method. From the figures, we see that two mode shapes are a little different.

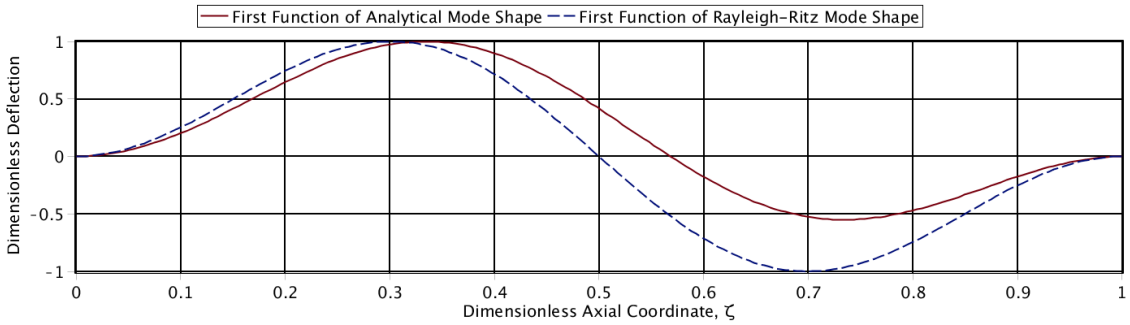

Figure 6.3 Comparison of the First Function of the Mode Shapes with Constant End Torque Only

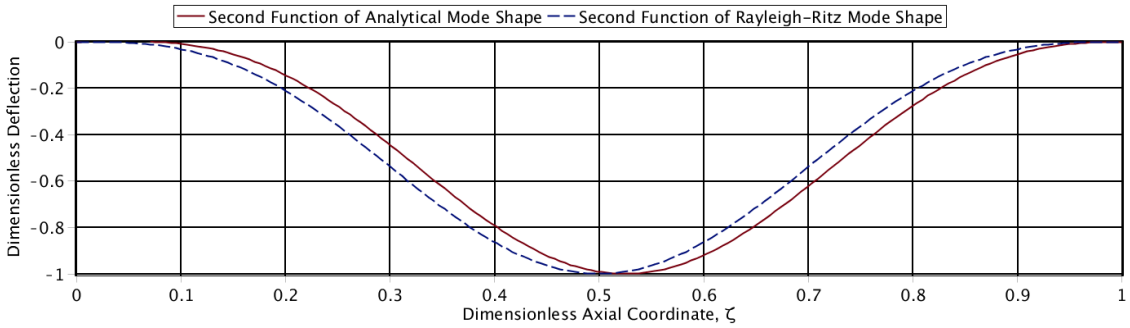

Figure 6.4 Comparison of the Second Mode Shapes with Constant End Torque Only

The maximum deflection is normalized to 1 but occur at different cross sections of the drill-string. For the first mode shape, it happens at $\zeta = 0.334$ from the analytical method, and $\zeta = 0.301$ for the Rayleigh-Ritz method. For the second mode shape, it happens at $\zeta = 0.524$ from the analytical method, and $\zeta = 0.500$ for the Rayleigh-Ritz method.

The comparisons of the deflections in the axis Ox and Oy from the two methods are shown in Figure 6.5.

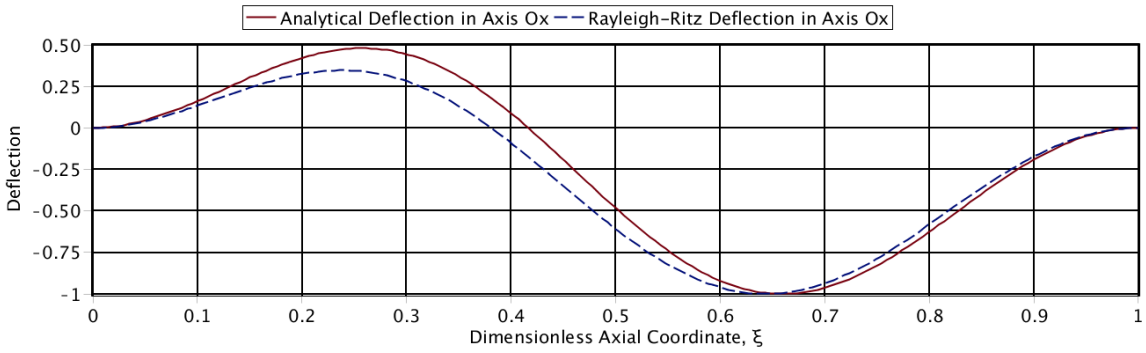

Figure 6.5 Comparison of the Deflection in the Axis Ox with Constant End Torque Only

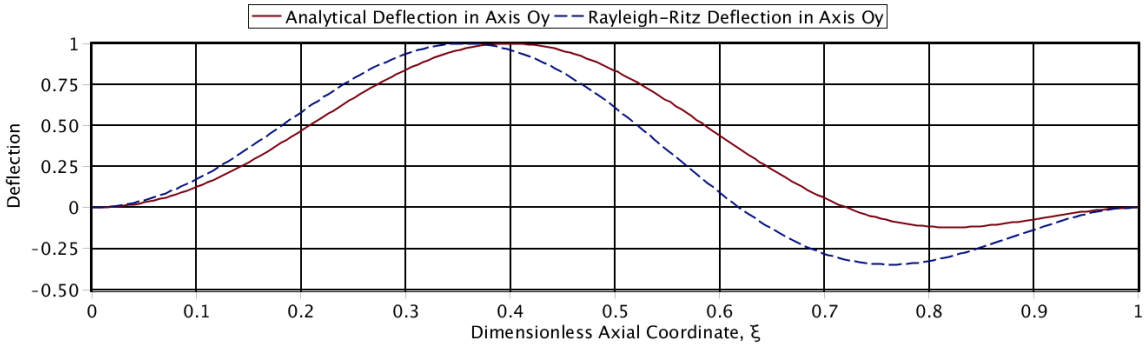

Figure 6.6 Comparison of the Deflection in the Axis Oy with Constant End Torque Only

From the figures, we see that two deflections are a little different. The maximum deflection is normalized to 1 but occur at different cross sections of the drill-string. For the deflection in the axis Ox, it happens at $\zeta = 0.659$ from the analytical method, and $\zeta = 0.643$ for the Rayleigh-Ritz method. For the deflection in the axis Oy, it happens at $\zeta = 0.400$ from the analytical method, and $\zeta = 0.357$ for the Rayleigh-Ritz method. But when we use different ratios of A_7 and A_8 for the two methods, we can have a better result for them. We use $A_7 = 1$ and $A_8 = 1.288$ for the analytical method and $A_7 =$

1 and $A_8 = 1$ for the Rayleigh-Ritz method. The comparison of the deflection in the axis Ox is shown in Figure 6.7.

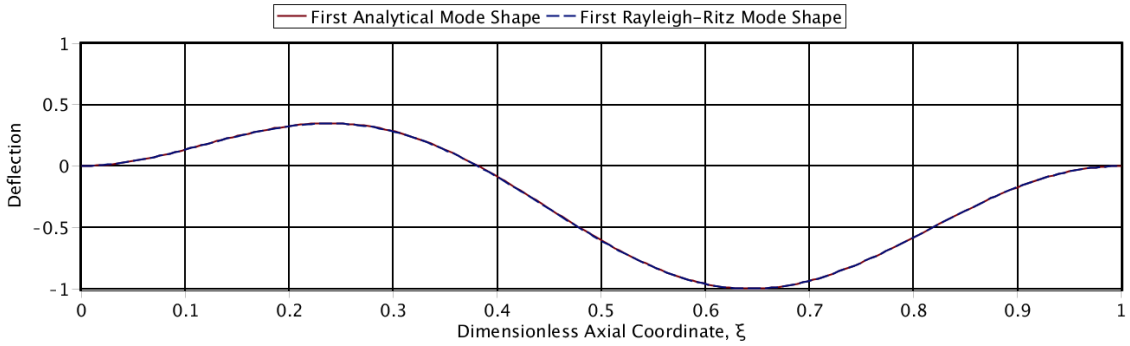

Figure 6.7 Comparison of the Deflection in the Axis Ox with Different Ratios of A_7 and A_8

The comparison of the deflection in the axis Oy is shown in Figure 6.8.

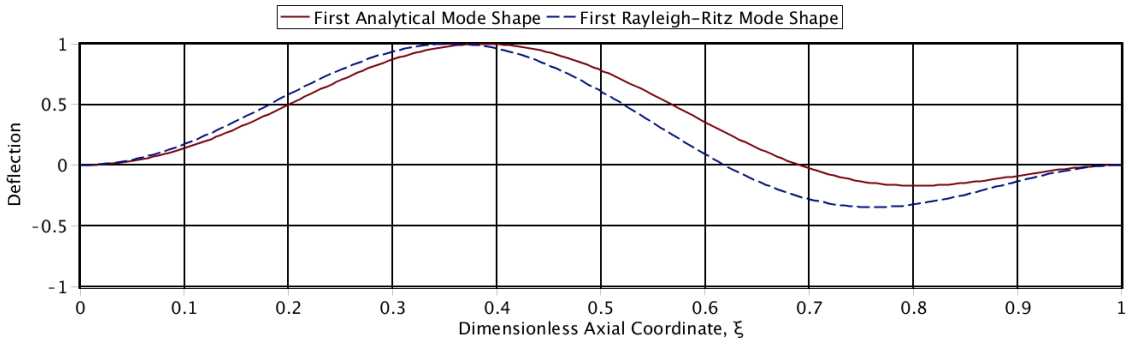

Figure 6.8 Comparison of the Deflection in the Axis Oy with Different Ratios of A_7 and A_8

From the figures, we can see that the deflections in the axis Ox from the two methods are very close and the deflections in the axis Oy from the two methods are still a little different but better than the former results. We can say that the different ratios of A_7 and A_8 used give us a better result.

6.2.4 Constant Axial Load and Whirling

When more than one load is applied to the system, critical combinations of loading parameters make the system unstable. For this case, the constant axial load is applied at the top end while the drill-string is whirling at a constant angular velocity. Choosing any arbitrary axial load, we can find a corresponding critical whirling speed above which the system is unstable. The maximum value of the critical axial load is the critical load in the absence of whirling, and vice versa. We have two solutions from two methods. The maximum first critical axial load parameter from the analytical solution is $\alpha = 4\,\pi^2$ and the one from the Rayleigh-Ritz solution also is $\alpha = 39.478$. The maximum first critical whirling speed parameter from the analytical solution is $\beta = 500.564$ and the one from the Rayleigh-Ritz solution also is $\beta = 500.564$. Figure 6.9 shows the interaction of critical combinations of the axial load parameter and the whirling speed parameter.

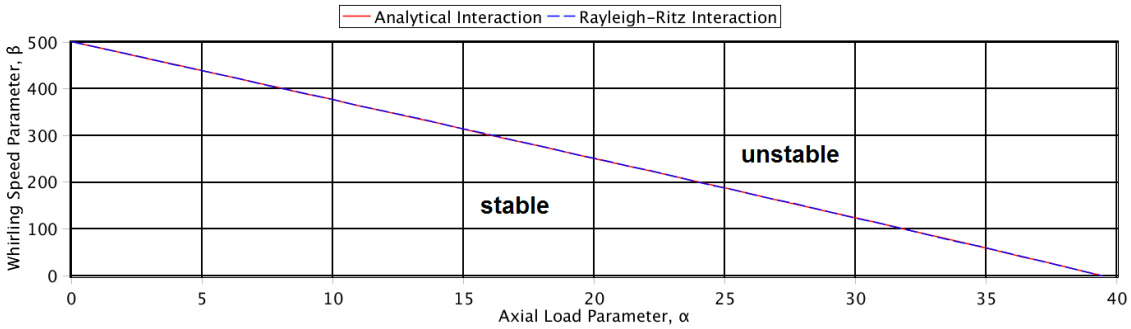

Figure 6.9 Comparison of Interaction of α and β

The red curve is the analytical solution and the blue one is the Rayleigh-Ritz solution. All combinations of the axial load and the whirling speed under the line make the drill-string stable, while it is unstable when they are above the line. The plot tells us that the results from the two methods are very close and the Rayleigh-Ritz energy method gives an

accurate result.

We choose a specific case with $\alpha = \pi^2, \beta = 378.367$ to compare the mode shapes for the two methods. Figure 6.10 shows the comparison of the mode shapes from the two methods.

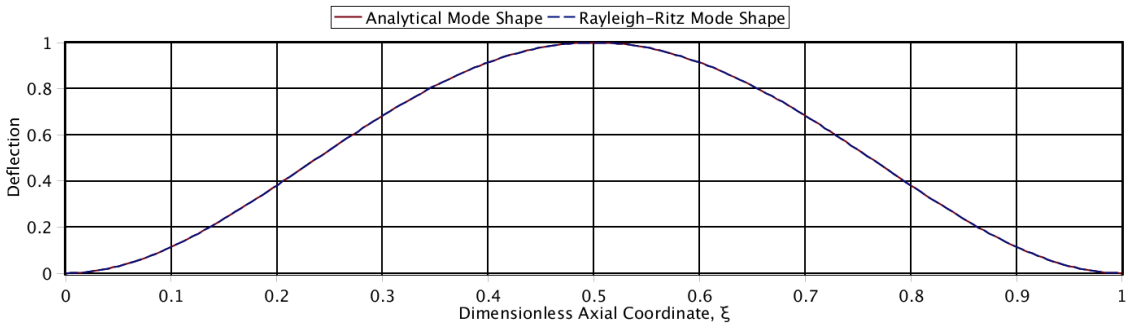

Figure 6.10 Comparison of Mode Shapes from Two Methods

The red solid line is from the analytical method and the blue dashed line is from the Rayleigh-Ritz method. From the figure, we see that the two mode shapes are essentially the same. The maximum deflections are normalized to 1 and both happed at the middle of the drill-string, which is $\xi = 0.5$. The mode shapes are symmetric because the boundary conditions and the applied load are symmetric. The effect of whirling also is symmetric to the drill-string. We can say that the Rayleigh-Ritz method gives an accurate result for this case.

6.2.5 Constant Axial Load and End Torque

For this case, the constant axial load and the end torque are applied at the top end at the same time. Choosing any arbitrary axial load, we can find a corresponding critical end torque which makes the drill-string stable. The maximum value of the critical axial load

is the critical load in the absence of end torque, and vice versa. The maximum first critical axial load parameter from the analytical solution is $\alpha = 4\,\pi^2$ and the one from the Rayleigh-Ritz solution also is $\alpha = 39.478$. The maximum first critical end torque parameter from the analytical solution is $\lambda = 8.987$ and the one from the Rayleigh-Ritz solution also is $\lambda = 8.987$. The critical loads from the two different methods are identical and we could say that the error is negligible. Figure 6.11 shows the interaction of critical combinations of the axial load parameter and the end torque parameter. The red curve is the analytical solution and the blue one is the Rayleigh-Ritz solution. All combinations of the axial load and the end torque under the line make the drill-string stable, while it is unstable when they are above the line. The plot tells us that the results from the two methods are very close and the Rayleigh-Ritz energy method gives an accurate result.

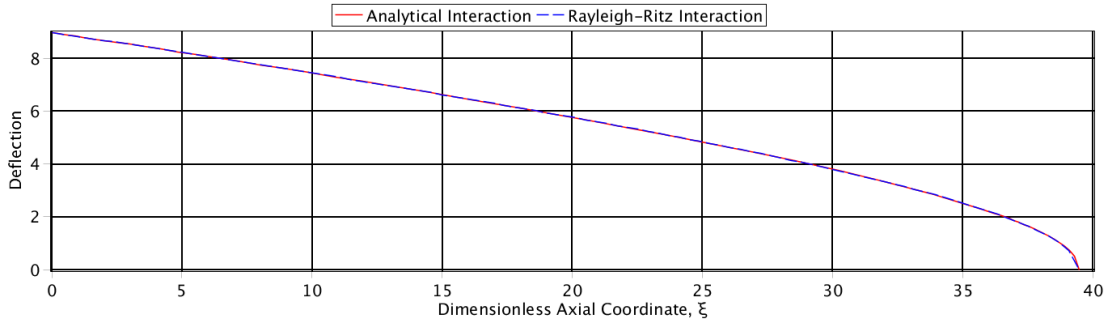

Figure 6.11 Comparison of Interaction of α and λ

We choose a specific case with $\alpha = \pi^2, \lambda = 7.472$ to compare the mode shapes for the two methods. Figure 6.12 shows the comparison of the first function of the mode shapes from the two methods. The red solid line is from the analytical method and the blue dashed line is from the Rayleigh-Ritz method.

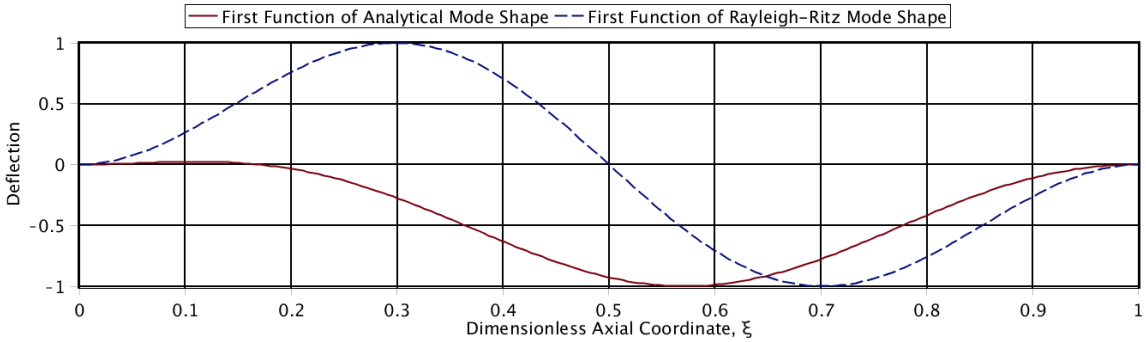

Figure 6.12 Comparison of the First Function of the Mode Shapes with $\alpha = \pi^2, \lambda = 7.472$

The comparison of the second function of the mode shapes from the two methods is shown in Figure 6.13. The red solid line is from the analytical method and the blue dashed line is from the Rayleigh-Ritz method. From the figures, we see that two mode shapes are a little different. The maximum deflection is normalized to 1 but occur at different cross sections of the drill-string.

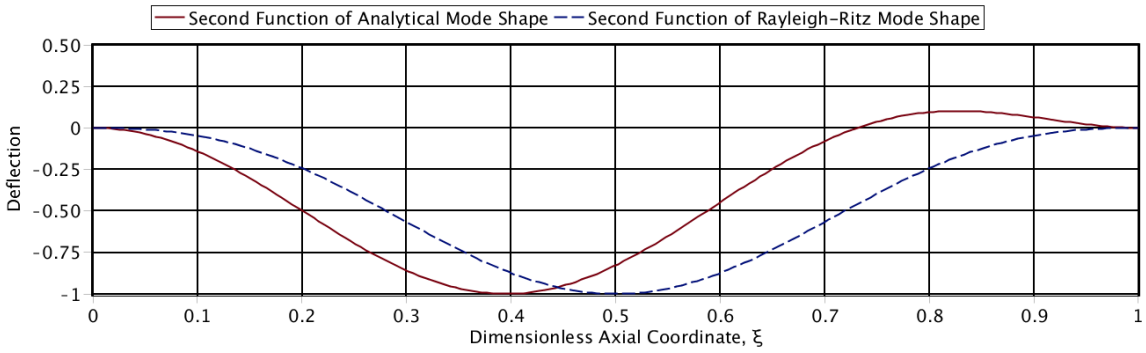

Figure 6.13 Comparison of the Second Mode Shapes with $\alpha = \pi^2, \lambda = 7.472$

The comparisons of the deflections in the axis $0x$ and $0y$ from the two methods are shown in Figure 6.14 and Figure 6.15.

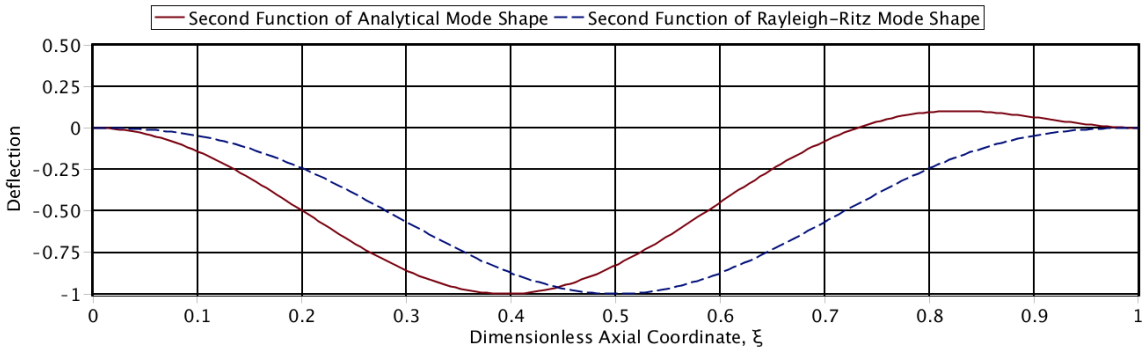

Figure 6.14 Comparison of the Deflection in the Axis Ox with $\alpha = \pi^2, \lambda = 7.472$

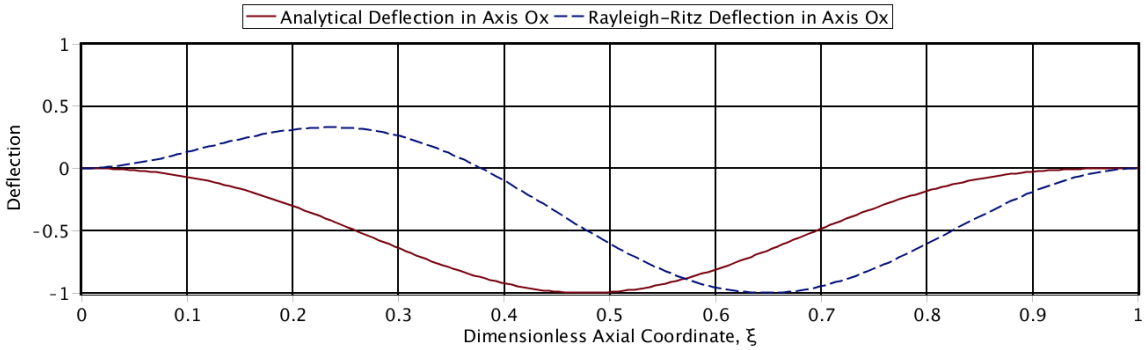

Figure 6.15 Comparison of the Deflection in the Axis Oy with $\alpha = \pi^2, \lambda = 7.472$

From the figures, we see that two deflections are different. The maximum deflection is normalized to 1 but occur at different cross sections of the drill-string. But when we use different ratios of A_7 and A_8 for the two methods, we can have a better result for them. We use $A_7 = 1$ and $A_8 = 0.365$ for the analytical method and $A_7 = 1$ and $A_8 = 1$ for the Rayleigh-Ritz method. The comparison of the deflection in the axis Ox is shown in Figure 6.16.

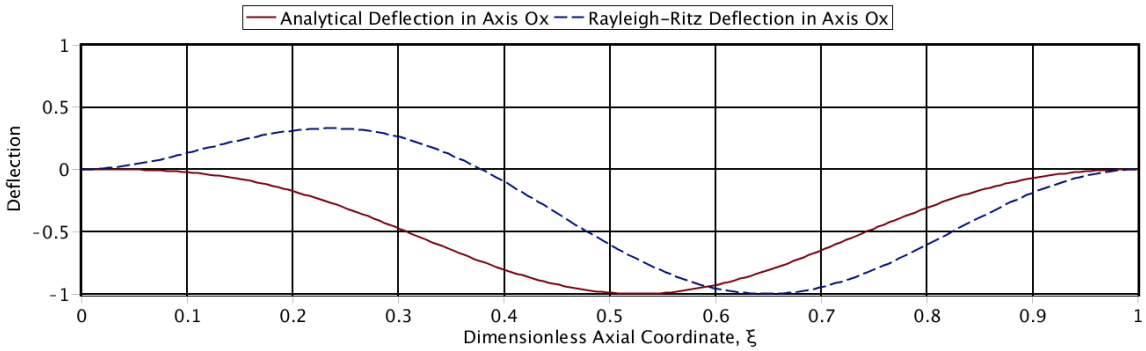

Figure 6.16 Comparison of the Deflection in the Axis Ox with Different Ratios of A_7 and A_8

The comparison of the deflection in the axis Oy is shown in Figure 6.17.

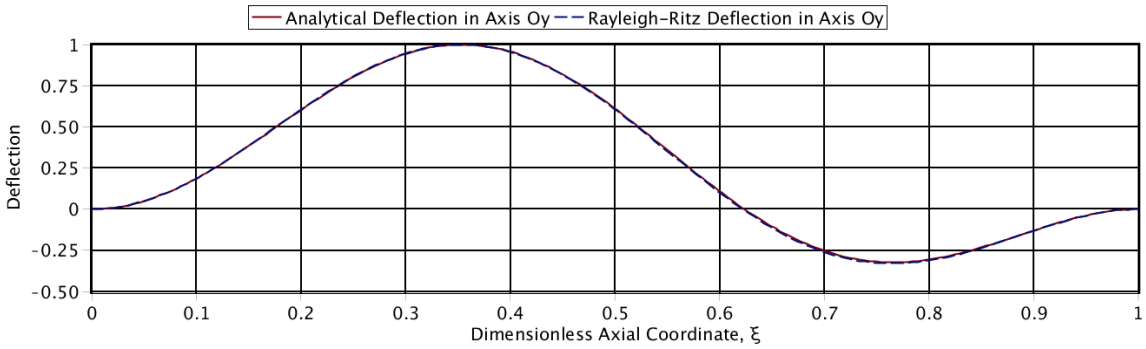

Figure 6.17 Comparison of the Deflection in the Axis Oy with Different Ratios of A_7 and A_8

From the figures, we can see that the deflections in the axis Oy from the two methods are very close and the deflections in the axis Ox from the two methods are still a little different but better than the former results. We can say that the different ratios of A_7 and A_8 used give us a better result.

6.2.6 Hook Load and Self-weight

When the self-weight of the drill-string is included in the system, it significantly changes the performance of the drill-string. We use ABAQUS to validate the results from the Rayleigh-Ritz method for the case with the hook load and the self-weight. For this case, the weight of the drill-string is included and the performance is very different.

Because we know the drill-string used in ABAQUS, the self-weight parameter is 56.12 calculated by the equation $\varphi = \frac{mgL^3}{EI}$. Then we can find the axial load parameter $\alpha = 10.187$. The critical axial load is 4938.576 N calculated by the equation $\alpha = \frac{PL^2}{EI}$. The critical axial load from ABAQUS simulation is 4948.6 N. the error is 0.2%, which is very good. Figure 6.11 is the comparison of mode shapes from the two methods.

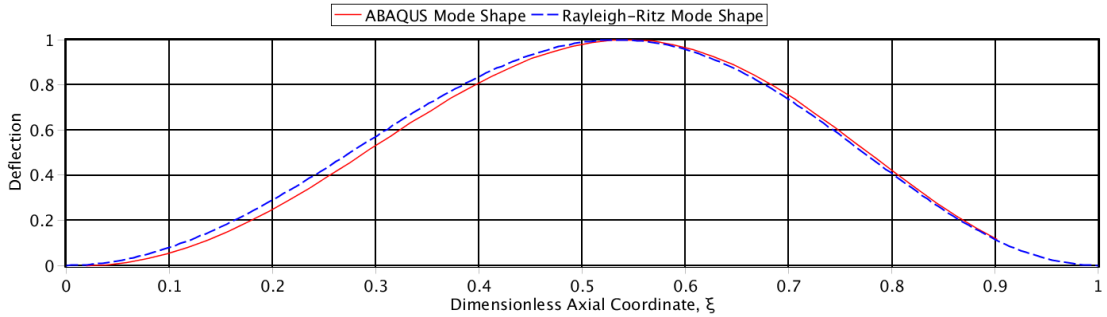

Figure 6.18 Comparison of Mode Shapes with $\alpha = 10.187$ and $\varphi = 56.120$

The maximum deflections were normalized to 1 and not happed at the middle of the drill-string because of the gravity. For Rayleigh-Ritz energy method, the maximum deflection happed at $\zeta = 0.534$. For ABAQUS simulation method, the maximum deflection happed at $\xi = 0.532$. The red curve is the Rayleigh-Ritz solution and the blue one is the ABAQUS simulation solution as shown in Figure. From the figure, we can say that the

mode shapes are very close from two different methods and the Rayleigh-Ritz energy method gives a very good result for this case.

CHAPTER 7

CONCLUSIONS AND RECOMMENDATIONS

7.1 Introduction

The goal of this dissertation is to provide insights into the stability of a drill-string. Various types of vibrations appear in a rotary drill-string system and limit the performance of this system. Moreover, more than one type of vibration is present at the same time and complex loading conditions make the system harder to understand. In this dissertation, we address the steady-state stability analysis of a drill-string with different analyzing methods and find the effects of different loads.

For this purpose, we have built a mathematical model of a drill-string with MAPLE to describe its steady state. The boundary conditions for the drill-string are fixed at both ends, but the top end can slide in the axial direction. Analytical methods, the Rayleigh-Ritz energy method and CAE software are used to calculate the critical load values and mode shapes for different loading conditions. Results are compared among different methods and validate that the Rayleigh-Ritz energy method is accurate and efficient.

In this chapter we present general conclusions of this dissertation and recommendations for further research.

7.2 Conclusions

The system has analytical solutions for some simple cases. When different loads are applied at the same time, analytical solutions do not exist, which requires us to use numerical methods to solve the problem. The Rayleigh-Ritz energy method and

commercial software are used for these cases. As a result, several conclusions, as summarized in the next section, can be drawn.

1. When there is a constant axial load applied only at the ends of the drill-string, an analytical solution and a Rayleigh-Ritz solution can be found. The critical load and the mode shape from the two methods are very close, which shows the accuracy and correctness of the Rayleigh-Ritz method.

2. When the only load is the inertial load resulting from whirling around the original vertical axis, there are an analytical solution and a Rayleigh-Ritz solution. The critical load and the mode shape from the two methods are very close, which shows the method works good for this case.

3. When there is only an end torque applied to the drill-string, we have an analytical solution and a Rayleigh-Ritz solution. The critical loads from two methods are very close but the mode shapes are a little different. When we use different ratios of the two coefficients for the two methods, we can have a closer result from the two methods.

4. When a constant axial load is applied to the drill-string while whirling, the analytical method and the Rayleigh-Ritz method still give solutions which agree very well, which shows the method works well for this case.

5. When the drill-string is loaded with a constant axial load and an end torque, the analytical method and the Rayleigh-Ritz method give the critical combinations of loads which agree very well but there is a little difference between the mode shapes.

6. When the drill-string is loaded with a constant axial load and an end torque while whirling, there is no analytical solution because of the complexity of loading conditions. We get the reasonable results from the Rayleigh-Ritz method.

7. When the self-weight of the drill-string is included in the system, no analytical solution is available. Commercial software COMSOL and ABAQUS are used to validate the Rayleigh-Ritz method. The results with the case of the self-weight only and the case of the self-weight and a hook load agree well with the Rayleigh-Ritz energy method.

8. When the hook load and the end torque are applied to a drill-string with self-weight included while whirling, the motion is a very complex. We have not solved this case with ABAQUS but the Rayleigh-Ritz method gives a reasonable result.

7.3 Recommendations

A good understanding of the vibrations and the interaction between them in a rotary drilling system is very important. The collection of measurement data of the rotary drilling system is very expensive and time consuming. The knowledge obtained here provides an improved understanding of the effects of different parameters on the stability of a drill-string. Moreover, based on this knowledge, various control strategies can be designed to improve the performance of the drilling process and prevent the occurrence of component failures during the process.

This research indicates that further work needs to be done in the following problems. Further research should lead towards an improved understanding of various vibrations in

the drilling system and can support the development of methods aiming at the improvement of the stability.

1. Use an independent numerical method to analyze loading cases that cannot be treated by COMSOL and ABAQUS. These two programs have very limited the ability to analyze stability of a drill-string. They were able to solve only a few of the many cases of interest.
2. Consider the contact force from the borehole wall with different loads and parameters present. Real drill-strings are enclosed in solid-walled boreholes that limit their lateral motion and showed significantly affect stability under most conditions.
3. Investigate the influence of the drilling fluid on the stability of the drill-string. Real drill-strings have drilling fluid (mud) streamed continuously both inside and outside the string. This may have a significant effect on stability.

LIST OF REFERENCES

1. Jansen, J.D., *Nonlinear Dynamics of Oilwell Drillstrings*, in *Delft University of Technology*. 1993, Delft University of Technology: Delft University Press.

2. Preumont, A., *Twelve Lectures on Structural Dynamics*. 2013: Springer Netherlands.

3. Finnie, I. and J.J. Bailey, *An Experimental Study of Drill-String Vibration.* Journal of Manufacturing Science and Engineering, 1960. **82**(2): p. 129-135.

4. Cunningham, R.A., *Analysis of Downhole Measurements of Drill String Forces and Motions.* Journal of Manufacturing Science and Engineering, 1968. **90**(2): p. 208-216.

5. Deily, F.H., et al., *Downhole Measurements of Drill String Forces and Motions.* Journal of Manufacturing Science and Engineering, 1968. **90**(2): p. 217-225.

6. Greenhill, A.G., *On the Strength of Shafting When Exposed Both to Torsion and to End Thrust.* Proceedings of the Institution of Mechanical Engineers, 1883. **34**(1): p. 182-225.

7. Capelushnikov, M., *Why Holes Go Crooked in Drilling.* World Petroleum, 1930: p. 191.

8. Clark, L.V.W., *A Theoretical Examination of Straight and Directed Drilling Techniques.* Institute of Petroleum Technilogists, 1936. **22**: p. 140.

9. Woods, H. and A. Lubinski, *Charts Solve Hole-Deviation Problems—and Help Determine Most Economical Hole Size.* The Oil and Gas Journal, 1954. **53**(4): p. 84.

10. Woods, H. and A. Lubinski, *Practical Chart for Solving Problems on Hole Deviation.* Drilling and Production Practice, 1954.

11. Woods, H. and A. Lubinski, *Use of Stabilizers in Controlling Hole Deviation.* Drilling and Production Practice, 1955.

12. Woods, H. and A. Lubinski, *Use of Stablizers in Drill Collar String.* OGJ, 1955: p. 215.

13. Rollins, H.M. and W.S. Beachman, *New Straight Hole Drilling Tools in Use in West Texas.* Petroleum Engineer, 1952. **B-90**.

14. Lubinski, A., *A Study of the Buckling ofRotary Drilling Strings.* Drilling and Production Practice, 1950.

15. Rollins, H.M., *Studies of Straight-hole Drilling Practices 1952 to 1956.* API Drilling and Production Practices, 1956: p. 37.

16. Ziegler, H., *Principles of Structural Stability*. 1968: Waltham, Mass., Blaisdell Pub. Co.

17. Timoshenko, S., *Theory of Elastic Stability*. 1961, New York: McGraw-Hill.

18. Mclachlan, N.W., *Bessel Function for Engineers*. 1955: Clarendon Press.

19. Tan, X. and P. Digby, *Buckling of Drill String under the Action of Gravity and Axial Thrust.* International journal of solids and structures, 1993. **30**(19): p. 2675-2691.

20. Tan, X. and B. Forsman, *Buckling of Slender String in Cylindrical Tube under Axial Load: Experiments and Theoretical Analysis.* Experimental mechanics, 1995. **35**(1): p. 55-60.

21. Chen, J.-S. and H.-C. Li, *On an Elastic Rod Inside a Slender Tube under End Twisting Moment.* Journal of Applied Mechanics, 2011. **78**(4): p. 041009.

22. Coomer, J., et al., *A Non-linear Eigenvalue Problem Associated with Inextensible Whirling Strings.* Journal of sound and vibration, 2001. **239**(5): p. 969-982.

23. Virgin, L.N., *Vibration of Axially Loaded Structures*. 2007, New York: Cambridge University Press.

24. Dareing, D. and B.J. Livesay, *Longitudinal and Angular Drill-string Vibrations with Damping.* Journal of Manufacturing Science and Engineering, 1968. **90**(4): p. 671-679.

25. Johancsik, C., D. Friesen, and R. Dawson, *Torque and Drag in Directional Wells - Prediction and Measurement.* Journal of Petroleum Technology, 1984. **36**(7): p. 987-992.

26. Gulyaev, V., et al., *Quasistatic Critical States of Strings for Deep Drilling.* Strength of materials, 2006. **38**(5): p. 527-534.

27. Gulyaev, V., et al., *Quasistatic Bifurcation States of Super-deep Vertical Drill Strings.* Journal of mining science, 2010. **46**(5): p. 546-553.

28. Gulyaev, V.I., et al., *Stability of the Equilibrium of Rotating Drillstrings.* International Applied Mechanics, 2006. **42**(6): p. 692-698.

29. Gulyaev, V.I., et al., *Effect of the Length of a Rotating Drillstring on the Stability of Its Quasistatic Equilibrium.* International Applied Mechanics, 2007. **43**(9): p. 1017-1023.

30. Gulyayev, V., et al., *The Buckling of Elongated Rotating Drill Strings.* Journal of petroleum Science and Engineering, 2009. **67**(3): p. 140-148.

31. Tucker, R.W., *A Simple Cosserat Model for the Dynamics of Drill-strings*. 2001. p. 8.

32. Tucker, R.W., R.S. Tung, and C. Wang, *Nonlinear Flexural Excitations and Drill-String Dynamics.* Extracta Mathematicae, 1999. **14**(2): p. 217-246.

33. Tucker, R.W. and C. Wang, *An Integrated Model for Drill-string Dynamics.* Journal of Sound and Vibration, 1999. **224**(1): p. 123-165.

34. Tucker, R.W. and C. Wang, *Torsional Vibration Control and Cosserat Dynamics of a Drill-Rig Assembly*. Meccanica, 2003. **38**: p. 143-159.

35. Yigit, A.S. and A.P. Christoforou, *Coupled Axial and Transverse Vibrations of Oilwell Drillstrings.* Journal of Sound and Vibration, 1996. **195**(4): p. 617-627.

36. Yigit, A.S. and A.P. Christoforou, *Couples Torsional and Bending Vibrations of Drillstrings Subject to Impact with Friction.* Journal of Sound and Vibration, 1998. **215**(1): p. 167-181.

37. Yigit, A.S. and A.P. Christoforou, *Coupled Torsional and Bending Vibrations of Actively Controlled Drillstrings.* Journal of Sound and Vibration, 2000. **234**(1): p. 67-83.

38. Zare, J., S.J. Hashemi, and G. Rashed, *Finite Element Analysis of Drillstring Lateral Vibration.* Scientific Research and Essays, 2011. **6**(13): p. 2682-2694.

39. Khulief, Y. and H. Al-Naser, *Finite Element Dynamic Analysis of Drillstrings.* Finite elements in analysis and design, 2005. **41**(13): p. 1270-1288.

40. 陈敏, et al., *用能量法研究深直井管柱最大转速与正弦屈曲时临界轴向力间的关系.* 探矿工程: 岩土钻掘工程, 2006. **32**(12): p. 40-42.

41. 孟祥龙, et al., *轴力作用下钻柱稳定性分析.* 中国科技论文在线, 2010. **5**(11): p. 868-870.

42. Al-Hiddabi, S., B. Samanta, and A. Seibi, *Non-linear Control of Torsional and Bending Vibrations of Oilwell Drillstrings.* Journal of sound and vibration, 2003. **265**(2): p. 401-415.

43. Dunayevsky, V.A., F. Abbassian, and A. Judzis, *Dynamic Stability of Drillstrings under Fluctuating Weight on Bit.* SPE Drilling and Completion, 1993(June): p. 84-92.

44. Hakimi, H. and S. Moradi, *Drillstring Vibration Analysis Using Differential Quadrature Method.* Journal of Petroleum Science and Engineering, 2010. **70**(3): p. 235-242.

45. Liao, C.-M., et al., *Drill-string Dynamics: Reduced-order Models and Experimental Studies.* Journal of Vibration and Acoustics, 2011. **133**(4): p. 041008.

46. Palmov, V.A., E. Brommundt, and A.K. Belyaev, *Stability Analysis of Drillstring Rotation.* Dynamics and Stability of Systems, 1995. **10**(2): p. 99-110.

47. Shyu, R.-J., *Bending Vibration of Rotationg Drill Strings*, in *Ocean Engineering at the Massachusetts Institute of Technology*. 1989, MIT.

48. Alamo, F.C. and H.I. Weber. *Dynamics of Beams Using a Geometrically Exact Elastic Rod Approach*. in *8th Biennial ASME Conference on Engineering Systems Design and Analysis*. 2006. Torino, Italy: ASME.

49. Heisig, G., J. Sancho, and J.D. Macpherson. *Downhole Diagnosis of Drillstring Dynamics Data Provides New Level Drilling Process Control to Driiller*. in *Annual Technical Conference and Exhibition*. 1998. New Orleans, Louisiana.

50. Voronov, S.A., et al., *Influence of Torsional Motion on the Axial Vibrations of a Drilling Tool.* Journal of Computational and Nonlinear Dynamics, 2007. **2**: p. 58-64.

51. Huang, T. and D.W. Dareing, *Buckling and Lateral Vibration of Drill Pipe.* Journal of Engineering for Industry, 1968: p. 613-619.

52. Qin Qian, L.W., Qiao Ni, *Vibration and stability of vertical upward-fluid-conveying pipe immersed in rigid cylindrical channel.* Acta Mechanica Solida Sinica, 2008. **21**(5).

53. Schmalhorst, B., et al. *Drilling Dynamics in the Presence of Mud Flow*. in *IADC/SPE Drilling Conference*. 2000. New Orleans, Louisiana.

54. Santos, H., J. Placido, and C. Wolter. *Consequences and Relevance of Drillstring Vibration on Wellbore Stability*. in *SPE/IADC drilling conference*. 1999.

55. Curtis, H.D., *Fundamentals of Aircraft Structural Analysis*. 1997: Irwin Times Mirror Higher Education Group, London, Chicago.

56. Temple, G.F.J., W.G. Bickley, and J.W.S.B. Rayleigh, *Rayleigh's Principle and Its Applications to Engineering*. 1933: Milford.

57. Simitses, G. and D. Hodges, *Fundamentals of Structural Stability*. 2006, Elsevier. 480.

VITA

Liangming Pan was born in Zhejiang, China. He received his Bachelor degree in Mechanical Engineering and master degree in Automotive Engineering at Tongji University in China. Then, he worked as a product engineer at Shanghai Volkswagen Automotive over one year. In 2008, he began to pursue his master degree in Biomedical Engineering at the University of Tennessee, Knoxville. Then he started work with Dr. J. A. M. Boulet for his PhD degree in Mechanical Engineering in 2010. His research interest includes vibration and noise level analysis and stability analysis of a drill-string.